

MAY 2016

M.Sc. in Civil Engineering

BASHDAR OMER

**HASAN KALYONCU UNIVERSITY
GRADUATE SCHOOL OF
NATURAL & APPLIED SCIENCES**

**A CASE STUDY ON THE EFFECTS OF EARTHQUAKE
CHARACTERISTICS ON LANDSLIDE STABILIZATION PILES**

**M. Sc. THESIS
IN
CIVIL ENGINEERING**

**BY
BASHDAR OMER**

MAY 2016

**A Case Study on the Effects of Earthquake Characteristics on
Landslide Stabilization Piles**

M.Sc. Thesis

in

Civil Engineering

Hasan Kalyoncu University

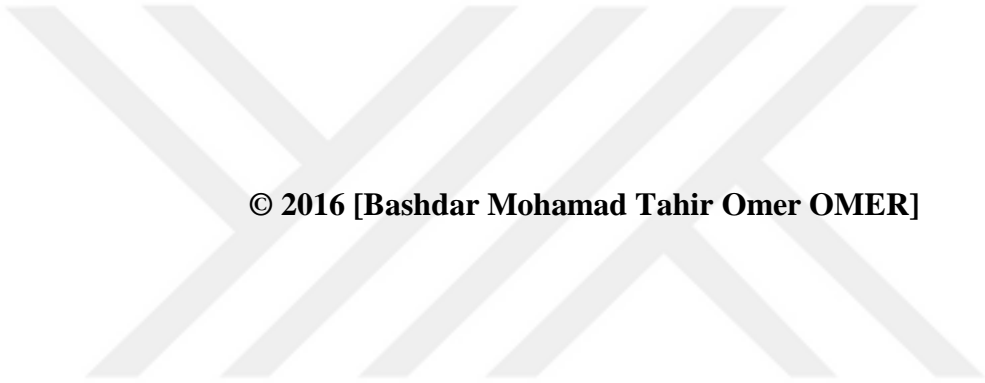
Supervisor

Assist. Prof. Dr. Volkan KALPAKCI

by

Bashdar OMER

May 2016



© 2016 [Bashdar Mohamad Tahir Omer OMER]

REPUBLIC OF TURKEY
HASAN KALYONCU UNIVERSITY
GRADUATE SCHOOL OF NATURAL & APPLIED SCIENCES
CIVIL ENGINEERING DEPARTMENT

Name of the thesis: A case study on the effects of earthquake characteristics on landslide stabilization piles

Name of the student: Bashdar Mohamad Tahir Omer OMER

Exam date: 27.5.2016

Approval of the Graduate School of Natural and Applied Sciences


Prof. Dr. Mehmet KARPUCU

Director

I certify that this thesis satisfies all the requirements as a thesis for the degree of Master of Science.


Assist. Prof. Dr. Şafak TERCAN

Head of Civil Engineering Department

This is to certify that we have read this thesis and that in our opinion it is fully adequate, in scope and quality, as a thesis for the degree of Master of Science.


Assist. Prof. Dr. Volkan KALPAKCI

Supervisor

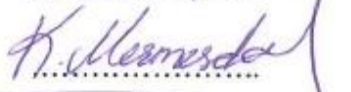
Examining Committee Members

Signature

Assist. Prof. Dr. Dia Eddin NASSANI

Assist. Prof. Dr. Kasım MERMERDAŞ

Assist. Prof. Dr. Volkan KALPAKCI


.....

.....

.....

I hereby declare that all information in this document has been obtained and presented in accordance with academic rules and ethical conduct. I also declare that, as required by these rules and conduct, I have fully cited and referenced all material and results that are not original to this work.



Bashdar OMER

ABSTRACT

A CASE STUDY ON THE EFFECTS OF EARTHQUAKE CHARACTERISTICS ON LANDSLIDE STABILIZATION PILES

OMER, Bashdar Mohamad Tahir Omer

M.Sc. in Civil Engineering

Supervisor: Assist. Prof. Dr. Volkan KALPAKCI

May 2016, 89 pages

In this study, effect of earthquake characteristics on landslide stabilization piles in the meaning of the pile axial loads, shear forces and bending moments are investigated through finite element analyses. A real landslide area located very close to the North Anatolian fault in the western part of the Black Sea region of Turkey was selected to be analyzed. A detailed site investigation program was executed including boreholes, inclinometer readings, site and laboratory tests the results of which were utilized throughout the study. Three different earthquake records, all scaled to the same maximum acceleration but having different predominant frequencies were applied to the models in time domain and the results were compared with each other. The results have revealed that the pile axial loads were not affected significantly for utilized earthquake records, but the change in the shear forces and bending moments were tremendous which may change the pile design significantly. The most critical results were obtained for the earthquake record with lowest predominant frequency which is attributed to the higher magnitudes of dynamic displacements as compared to others due to its low frequency content.

Key Words: Finite element, case study, pile, landslide

ÖZET

DEPREM ÖZELLİKLERİNİN HEYELAN ÖNLEME KAZIKLARINA ETKİSİ ÜZERİNE BİR VAKA ANALİZİ

OMER, Bashdar Mohamad Tahir Omer

Yüksek Lisans Tezi, İnşaat Mühendisliği Bölümü

Tez Yöneticisi: Yrd. Doç. Dr. Volkan KALPAKCI

Mayıs 2016, 89 sayfa

Bu çalışmada; deprem özelliklerinin heyelan önleme kazıklarına etki eden eksenel yük, kesme kuvveti ve eğilme momentlerine etkisi sonlu elemanlar yöntemi ile analiz edilerek incelenmiştir. Analizler için, Türkiye'nin Batı Karadeniz bölgesinde Kuzey Anadolu fay hattına yakın gerçek bir heyelan sahası seçilmiştir. Sahada, sondaj ve inklinometre okumaları ile saha ve laboratuvar deneylerini içeren kapsamlı bir çalışma yürütülmüş ve bu çalışmanın sonuçları analizlerde kullanılmıştır. Analizlerde, aynı maksimum ivmeye ölçeklenmiş fakat farklı hakim frekanslara sahip üç farklı deprem kaydı zaman uzayında modellere uygulanmış ve sonuçlar birbirleri ile karşılaştırılmıştır. Sonuçta, heyelan önleme kazıkları üzerine etki eden eksenel kuvvetlerin analiz edilen deprem kayıtları için önemli bir farklılık göstermediği, fakat kesme kuvvetleri ve eğilme momentlerinin kazık tasarımını ciddi şekilde etkileyecek mertebelerde değiştiği görülmüştür. Analizler sonucunda en kritik sonuçlar, en düşük hakim frekansa hakim deprem kaydı için elde edilmiş olup bu sonuç bahsi geçen deprem kaydının diğer kayıtlara oranla düşük frekans içeriğinin fazla olması ve dolayısıyla daha yüksek dinamik deplasmanlara sahip olmasıyla ilişkilendirilmiştir.

Anahtar Kelimeler: Sonlu elemanlar, vaka analizi, kazık, heyelan



To My Parents

ACKNOWLEDGEMENTS

To begin with I would like to thank the “ALLAH” for the virtues of this blessing for implanting the soul of endurance and faith in myself to complete this study.

It is a pleasure to express my deepest gratitude to my supervisor Assist. Prof. Dr. Volkan KALPAKCI for his kind supervision, continuous encouragement, valuable enthusiastic and unfailing advice throughout the present study.

Special thanks are reserved for Assist. Prof. Dr. Dia Eddin NASSANI and Assist. Prof. Dr. Kasım MERMERDAŞ For serving on the committee and their contributions and suggestions to improve the quality of the thesis.

It is my pleasure to express thanks to my family and friends for their support, encouragement and contribution they have made for my research to be successful.

Finally, I would like to thank my dearest friend Ahmed Aulla for his encouragement and help.

TABLE OF CONTENTS

ABSTRACT.....	V
ÖZET.....	VI
ACKNOWLEDGEMENTS.....	VIII
TABLE OF CONTENTS.....	IX
LIST OF FIGURES.....	XII
LIST OF TABLES.....	XV
LIST OF SYMBOLS/ABBREVIATIONS.....	XVI
CHAPTER 1.....	1
INTRODUCTION.....	1
1.1 General.....	1
1.2 Research Objective.....	2
1.3 Thesis Organization.....	2
CHAPTER 2.....	4
LITERATURE REVIEW.....	4
2.1 Introduction.....	4
2.2 Slope Stability Analyses.....	4
2.2.1 Limit Equilibrium Methods.....	5
2.2.1.1 The Ordinary Method.....	6
2.2.1.2 Bishop's Method.....	7
2.2.1.3 Janbu's Method.....	8
2.2.1.4 Lowe - Karafiath's Method.....	9
2.2.1.5 Corps of Engineers Method.....	9

2.2.1.6 Sarma Method	9
2.2.1.7 Morgenstern - Price Method	10
2.2.1.8 Spencer's Method.....	10
2.2.2 Finite Element Method	14
2.3 Types of Slope Failure Modes.....	14
2.3.1 Short Term Stability.....	15
2.3.2 Long Term Stability	15
2.4 Peak and Residual Strengths	16
2.5 Back Analysis of Slope Failure	17
2.5.1 Back Calculating Average Shear Strength.....	17
2.5.2 Back Calculating Shear Strength Parameters Based on Slip Surface Geometry	17
2.5.3 Limitation and Problems of Back Analysis	18
2.5.4 Back Analysis Methods	19
2.6 Factors Affecting Slope Stability Analysis	19
2.6.1 Failure Plane Geometry	20
2.6.2 Non Homogeneity of Soil Layers	20
2.6.3 Tension Crack	20
2.6.4 Dynamic Loading	20
2.6.4.1 Pseudo-static Analysis Method.....	20
2.6.4.1.1 Empirical Method.....	22
2.6.4.1.2 Rigid Body Response Analysis Method.....	23
2.6.4.1.3 Elastic Response Analysis.....	24
2.6.4.2 Time-history Analysis Method	27
CHAPTER 3	30
MATERIALS AND METHODS	30
3.1 Description of Problem and Study Area.....	30

3.2 Material Properties	33
3.2.1 Back Analysis	35
3.2.2 Slope Stabilization	39
CHAPTER 4	45
ANALYSES AND RESULTS	45
4.1 Earthquake Records.....	45
4.2 Finite Element Analyses.....	51
4.3 Results and Discussions	53
CHAPTER 5	57
CONCLUSIONS.....	57
5.1 Limit Equilibrium Analyses	57
5.2 Finite Element Analyses.....	58
5.3 Discussions and Conclusions	58
REFERENCES.....	60
APPENDICES	66
Appendix A Pile Axial Force Envelope Diagrams	66
Appendix B Pile Shear Force Envelope Diagrams	74
Appendix C Pile Bending Moment Envelope Diagrams	82

LIST OF FIGURES

Figure 2.1 Ordinary method of slices (Anderson and Richards, 1987)	6
Figure 2.2 Simplified Bishop Method (Anderson and Richards, 1987)	7
Figure 2.3 Correction factor for Janbu's simplified method (1973)	8
Figure 2.4 Forces on a slice for Spencer's method (Spencer, 1967).	11
Figure 2.5 Shear characteristics of over consolidated clay (Skempton, 1964).	15
Figure 2.6 Definitions of Peak and Residual Stress Envelopes (Skempton, 1985) ...	16
Figure 2.7 Critical circles for three different sets of shear strength parameters giving a factor of safety of 1 (Duncan et al., 2014).....	18
Figure 2.8 Pseudo-static Analysis Method (Melo and Sharma, 2004)	22
Figure 2.9 One dimensional shear slice theory (Seed and Martin, 1966).	24
Figure 2.10 El Centro, California, earthquake of 18 May, 1940, N-S component (Newmark, 1965).	28
Figure 3.1 Site location map of the studied area.	30
Figure 3.2 A general view of the studied area.	32
Figure 3.3 Damage at drainage lines due to landslide.	32
Figure 3.4 Movements at road level.....	33
Figure 3.5 Material Properties of Ulus Formation.	34
Figure 3.6 Studied cross sections on the landslide area	34
Figure 3.7 Results of back analysis.....	35
Figure 3.8 Back analysis result of section 1-1.	36
Figure 3.9 Back analysis result of section 2-2.	37
Figure 3.10 Back analysis result of section 3-3.	37
Figure 3.11 Back analysis result of section 4-4.	38
Figure 3.12 Back analysis result of section 5-5.	38
Figure 3.13 Back analysis result of section 6-6.	39
Figure 3.14 Earthquake zones of Turkey map.	40
Figure 3.15 Earthquake zones map of study area.	40
Figure 3.16 Section 1-1 after slope stabilization.....	41

Figure 3.17 Section 2-2 after slope stabilization.....	42
Figure 3.18 Section 3-3 after slope stabilization.....	42
Figure 3.19 Section 4-4 after slope stabilization.....	43
Figure 3.20 Section 5-5 after slope stabilization.....	43
Figure 3.21 Section 6-6 after slope stabilization.....	44
Figure 4.1 Time history data of Landers Earthquake.....	47
Figure 4.2 Time history data of Chalfant Valley Earthquake	48
Figure 4.3 Time history data of Loma Prieta Earthquake	49
Figure 4.4 Fourier amplitude spectrum of Landers earthquake	50
Figure 4.5 Fourier amplitude spectrum of Chalfant Valley earthquake.....	50
Figure 4.6 Fourier amplitude spectrum of Loma Prieta earthquake.	51
Figure 4.7 Finite element mesh of section 4-4.....	53
Figure 4.8 Pile Axial Forces	54
Figure 4.9 Pile Shear Forces	55
Figure 4.10 Pile Bending Moments	56
Figure A.1 Axial force diagram of Landers EQ for pile 1 (N = 5230 kN/m).	66
Figure A.2 Axial force diagram of C. Valley EQ for pile 1 (N = 4630 kN/m).....	66
Figure A.3 Axial force diagram of L. Prieta EQ for pile 1 (N = 4550 kN/m).	67
Figure A.4 Axial force diagram of Landers EQ for pile 2 (N = 1180 kN/m).	67
Figure A.5 Axial force diagram of C. Valley EQ for pile 2 (N = 1090 kN/m).....	68
Figure A.6 Axial force diagram of L. Prieta EQ for pile 2 (N = 848.98 kN/m).	68
Figure A.7 Axial force diagram of Landers EQ for pile 3 (N = 1820 kN/m).	69
Figure A.8 Axial force diagram of C. Valley EQ for pile 3 (N = 1780 kN/m).....	69
Figure A.9 Axial force diagram of L. Prieta EQ for pile 3 (N = 1630 kN/m).	70
Figure A.10 Axial force diagram of Landers EQ for pile 4 (N = 1610 kN/m).	70
Figure A.11 Axial force diagram of C. Valley EQ for pile 4 (N = 1450 kN/m).....	71
Figure A.12 Axial force diagram of L. Prieta EQ for pile 4 (N = 1180 kN/m).	71
Figure A.13 Axial force diagram of Landers EQ for pile 5 (N = 1450 kN/m).	72
Figure A.14 Axial force diagram of C. Valley EQ for pile 5 (N = 1270 kN/m).....	72
Figure A.15 Axial force diagram of L. Prieta EQ for pile 5 (N = 1070 kN/m).	73
Figure B.1 Shear force diag. of Landers EQ for pile 1 (V = 914.02 kN/m).	74
Figure B.2 Shear force diag. of C. Valley EQ for pile 1 (V = 652.37 kN/m).....	74
Figure B.3 Shear force diag. of L.Prieta Valley EQ for pile 1 (V = 621.01 kN/m)...	75
Figure B.4 Shear force diag. of Landers EQ for pile 2 (V = 1600 kN/m).	75

Figure B.5 Shear force diag. of C. Valley EQ for pile 2 ($V = 776.08$ kN/m).....	76
Figure B.6 Shear force diag. of L.Prieta Valley EQ for pile 2 ($V = 657.92$ kN/m)...	76
Figure B.7 Shear force diag. of Landers EQ for pile 3 ($V = 670.49$ kN/m).	77
Figure B.8 Shear force diag. of C. Valley EQ for pile 3 ($V = 530.95$ kN/m).....	77
Figure B.9 Shear force diag. of L. Prieta Valley EQ for pile 3 ($V = 510.34$ kN/m)..	78
Figure B.10 Shear force diag. of Landers EQ for pile 4 ($V = 295.97$ kN/m).	78
Figure B.11 Shear force diag. of C.Valley EQ for pile 4 ($V = 206.54$ kN/m).....	79
Figure B.12 Shear force diag. of L.Prieta Valley EQ for pile 4 ($V = 165.4$ kN/m)...	79
Figure B.13 Shear force diag. of Landers EQ for pile 5 ($V = 357.46$ kN/m).	80
Figure B.14 Shear force diag. of C. Valley EQ for pile 5 ($V = 311.53$ kN/m).....	80
Figure B.15 Shear force diag. of L. Prieta Valley EQ for pile 5 ($V = 242.3$ kN/m)..	81
Figure C.1 Bending moment diag. of Landers EQ for pile 1 ($M = 4390$ kNm/m). ...	82
Figure C.2 Bending moment diag. of C. Valley EQ for pile 1 ($M = 2360$ kNm/m)..	82
Figure C.3 Bending moment diag. of L. Prieta EQ for pile 1 ($M = 1930$ kNm/m). ..	83
Figure C.4 Bending moment diag. of Landers EQ for pile 2 ($M = 8290$ kNm/m). ...	83
Figure C.5 Bending moment diag. of C. Valley EQ for pile 2 ($M = 5320$ kNm/m)..	84
Figure C.6 Bending moment diag.of L.Prieta EQ for pile 2 ($M = 4730$ kNm/m).	84
Figure C.7 Bending moment diag. of Landers EQ for pile 3 ($M = 6170$ kNm/m). ...	85
Figure C.8 Bending moment diag. of C. Valley EQ for pile 3 ($M = 3910$ kNm/m)..	85
Figure C.9 Bending moment diag. of L. Prieta EQ for pile 3 ($M = 3700$ kNm/m). ...	86
Figure C.10 Bending moment diag. of Landers EQ for pile 4 ($M = 1060$ kNm/m)..	86
Figure C.11 Bending moment diag. of C.Valley EQ for pile 4 ($M = 660$ kNm/m)...	87
Figure C.12 Bending moment diag. of L. Prieta EQ for pile 4 ($M = 515.4$ kNm/m).	87
Figure C.13 Bending moment diag. of Landers EQ for pile 5 ($M = 542.5$ kNm/m).	88
Figure C.14 Bending moment diag. of C.Valley EQ for pile 5 ($M = 507$ kNm/m)...	88
Figure C.15 Bending moment diag. of L.Prieta EQ for pile 5 ($M = 421.2$ kNm/m).	89

LIST OF TABLES

Table 2.1 Summary of Limit Equilibrium methods for Slope stability analysis (Duncan et al., 2014).....	13
Table 2.2 Horizontal seismic coefficient values recommended by different references (Melo and Sharma, 2004).....	23
Table 3.1 Results of shear strength parameters of cross sections by back analysis... 36	
Table 3.2 Calculated FOS under dynamic loading after slope stabilization.....	41
Table 4.1 Earthquake ground motion properties and locations.....	46
Table 4.2 Material properties of the soil layers.....	52
Table 4.3 Material properties of the plates (Piles)	52
Table 4.4 Pile Axial Forces.....	54
Table 4.5 Pile Shear Forces.....	55
Table 4.6 Pile Bending Moments.....	56

LIST OF SYMBOLS/ABBREVIATIONS

J_0	Bassel function of the first type has order of zero
J_1	Bassel function of the first order
\ddot{u}	Acceleration
\dot{u}	Velocity
α_R and β_R	Rayleigh coefficient of damping matrix
ω_n	Natural frequency
c	Cohesion
c'	Effective cohesion
E	Elastic Modulus
EQ	Earthquake
f_0	Janbu correction factor
f_n	Natural frequency
FOS	Factor of safety
G	Shear modulus of material
GSI	Geological Strength Index
k_h	Horizontal pseudo-static coefficient
k_v	Vertical pseudo-static coefficient
l	Length of slice

P	Base normal force acting on shear surface
q_u	Unconfined compressive strength
S	Shear strength
S_m	Stress mobilized
V_s	Shear wave velocity
T	Shear force acting at the base of a slice
t	Time
u	Displacement
U	Pore water pressure
W	Weight of slices
ρ	Density of the material
ϕ'	Effective friction angle
ϕ	Internal friction angle
α	Angle between center of the slice & global horizontal base's tangent
γ	Unit weight of material

CHAPTER 1

INTRODUCTION

1.1 General

Slope instabilities are frequently observed worldwide in both natural and man-made slopes. A landslide or landslip is a geological event that includes a wide range of ground movements. Landslides happen when slope stability changes from a stable to unstable condition. Gravity action is the primary driving force for landslides under static loading. Landslides are treating human life, causing financial losses and ecological damage every year such that landslides are responsible on average for 1000 death and the financial losses are around 10-20 billion USD annually (Highland, 2004). A change of stability of any slope is dependent on a number of factors some of which may be listed as pore water pressure, erosion, earthquakes, earthwork, vibrations and blasting.

Earthquake forces are also responsible for slope instabilities, since a significant inertial force is applied to the soil mass in lateral direction during an earthquake. Approximately 20% of the registered landslides are triggered by seismic activity as discussed in Sigaran-Loria et al. (2007). Seismic slope stability analysis is one of main study objective of geotechnical engineering. There are many methods for analysis such as; pseudo-static method, time-history method and etc. (Zhou and Zuo, 2014). The slope instabilities under earthquake loading occur very suddenly and may have catastrophic results for human lives and infrastructure.

1.2 Research Objective

The slope instabilities are observed frequently in Turkey, especially in the Black Sea region. The slopes are steep and composed of mostly decomposed soils which are exposed to significant rain for most of the year. Also, some of these landslide areas are located very close to “North Anatolian Fault”.

A significant number of new roads are being constructed in this region and most of them are passing through landslide areas. These areas are mostly in seismically active regions. Only pseudo-static method is suggested in the design guide of “T.C. General Directorate of Highways” for seismic analysis of landslides. However, this method only gives a general factor of safety value based on force and/or moment equilibrium but does not provide any data about deformation of the soil mass and forces acting on structural members. The current general practice is to find an earthquake record which had occurred close to the investigation site and scale it according to the maximum acceleration value suggested in Turkish Earthquake Code (TEC, 2007). But every earthquake record has different characteristics and these characteristics may affect the results significantly.

The main objective of this research was to investigate the effects of earthquake characteristics on behavior of landslide stabilization piles using three different earthquake records scaled to the same maximum acceleration. For this purpose, a real landslide area in western part of the Black Sea region was studied. The landslide geometry and mechanism were determined through limit equilibrium analyses using Slide 6.0 software. Then, the dynamic finite element analyses were done by Plaxis software in time domain.

1.3 Thesis Organization

The thesis is divided into five chapters. Chapter 1 contains general introduction, which introduces the theses hypothesis and clarify purpose of the study and thesis outline. Chapter 2 describes two main methods for analysis of slopes, which are limit equilibrium method and finite element method. Most of the currently utilized limit equilibrium methods such as; Bishop method, Janbu corrected method and etc. are described in detail in this chapter together with the principles of back analysis, peak and residual strength concepts. Chapter 3 includes description of the problem and

study area, determination of material properties by back analysis and stabilization of slope by piles based on pseudo-static method. Chapter 4, based on time history analyses using three different earthquake records by finite element method, covers results of axial, shear and bending moment of piles, discussion of results and comparison with each other. The results and the findings of the study are summarized in chapter 5.



CHAPTER 2

LITERATURE REVIEW

2.1 Introduction

This chapter provides a brief review of the two dimensional methods used for slope stability analysis. Slope stability analyses have two major methods which are limit equilibrium method and finite element method. Limit equilibrium methods are based on the force and moment equilibrium. They are more traditional and older methods since they do not require complex solution as in finite element method. These methods require information about the strength parameters of the soil (cohesion and angle of internal friction) and the geometrical properties of the slope. Factor of safety is defined as the ratio of resisting over driving, expressed in terms of forces and/or moments. In finite element method, deformations in the slope geometry can also be obtained in addition to the stability analyses.

2.2 Slope Stability Analyses

Slope stability analysis is a major task to compute factor of safety of a particular slope in given physical and geological conditions. In a stable slope resisting forces in the slope must be greater than the forces causing the failure (Duncan et al., 2014).

Stability analysis is able:

- 1) to evaluate the safety of a structure in terms of its stability.
- 2) to find the critical failure surface and to know the shape of failure.
- 3) to understand and numerically assess the sensitivity of stability to its geologic parameters and climatic conditions.
- 4) to measure the movement of the slope.
- 5) to support in their design and assess remedial measures.

To analyze the stability of a slope there are several different methods available. At present time, no every one of the analysis methods is favored over others therefore

reliability of any solution is completely left to the engineer in charge (Albataineh, 2006). Based on the main procedure, methods are divided into two main groups; Limit Equilibrium Methods and Finite Element Methods.

Each of these methods are subdivided into two groups according to numbers of dimensions; two-dimensional and three-dimensional methods.

2.2.1 Limit Equilibrium Methods

Geotechnical engineer's uses limit equilibrium method because it provides factor of safety of the slope against failure. Engineering practitioner uses limit equilibrium method because it does not need complex input parameters, but neglect behavior of stress-strain and have not been giving information about deformations (RocScience, 2004). The limit equilibrium method provides only an assessment of the slope stability, but does not have any information to obtain the amount of movement of the slope. In the limit equilibrium method analyses have two important assumptions as presented in Griffiths and Lane (1999): i) the slope can be divided into slices and ii) the interslices force acting between each of it.

Slope stability analyses may be carried out by several limit equilibrium methods. The first method was presented in (Fellenius, 1936) for a circular slip surface as entitled the Ordinary method or Swedish approach. The first method concerning the interslice normal forces was developed by Bishop (1955), suggesting a non-linear equation to calculate factor of safety against failure. Janbu (1959) advanced a simplified method for non-circular failure surfaces, in which a potential sliding mass was divided to several vertical slices. The generalized procedure of slices at the same time was developed as a further progress of the simplified method by Janbu (1973) and after that, (Morgenstern-Price, 1965; Spencer, 1967; Sarma, 1973) and several others made contributions with different assumptions for the interslice forces. Chugh (1986) developed a procedure of general limit equilibrium extension, where Spencer and Morgenstern-Price methods considered both force and moment equilibrium conditions (Abramson et al., 2002). In the following part different methods developed in limit equilibrium analysis are reviewed, to mention the main differences in various methods.

2.2.1.1 The Ordinary Method

In Ordinary method moment equilibrium for a circular slip surface is checked for stability. In this method both the interslices normal and shear forces are neglected. The advantage of ordinary method is easiness in calculating the factor of safety. Researchers (Whitman and Bailey, 1967) have been presented that factor of safety calculated with this approach is from time to time as much as 60 percent conservative, comparing to more exact methods. For the slice has been shown in the Fig. 2.1, the Mohr-Coulomb failure principle is:

$$S = c' + (\sigma - U) \tan \varphi' \quad (2.1)$$

Using factor of safety equation like,

$$T = \frac{1}{FOS} (c'l + (p - Ul) \tan \varphi') \quad (2.2)$$

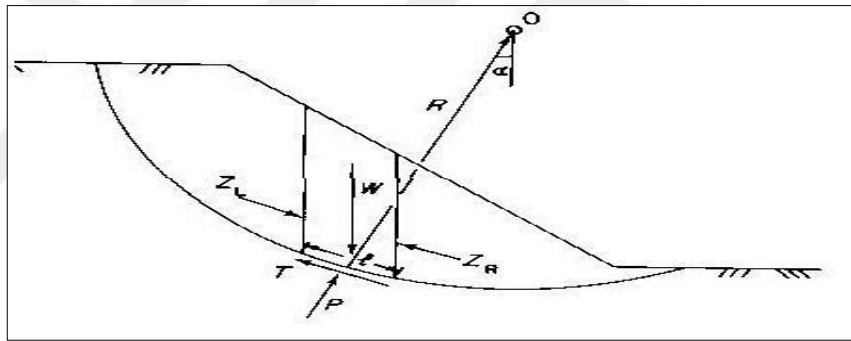


Figure 2.1 Ordinary method of slices (Anderson and Richards, 1987).

Neglecting the interslices force, creates normal forces on the base of each slice such as:

$$P = w \cos \alpha \quad (2.3)$$

Take a Moment's about the center of the failure slope equation will be:

$$\sum W R \sin \alpha = \sum T R \quad (2.4)$$

Finally,

$$FOS = \frac{\sum(c'l + (w \cos \alpha - ul) \tan \varphi')}{\sum W \sin \alpha} \quad (2.5)$$

2.2.1.2 Bishop's Method

Bishop method has been developed by Bishop in (1955), as an improvement to the method of slices which was developed by (Fellenius, 1936) and discussed in previous section. Bishop's simplified method is very common in practice for the circular shear surface. Generally factor of safety is calculated as the ratio of the total resisting moments to driving moments. This method neglects the interslice shear forces but, considers the interslice normal forces (Abramson et al., 2002). This procedure is commonly quick and gives a comparably accurate solution with finite element methods in five percent differences; therefore it is appropriate for hand calculations (Anderson and Richards, 1987). Bishop method determines the factor of safety for the circular rotation of a soil mass as revealed in Fig. 2.2.

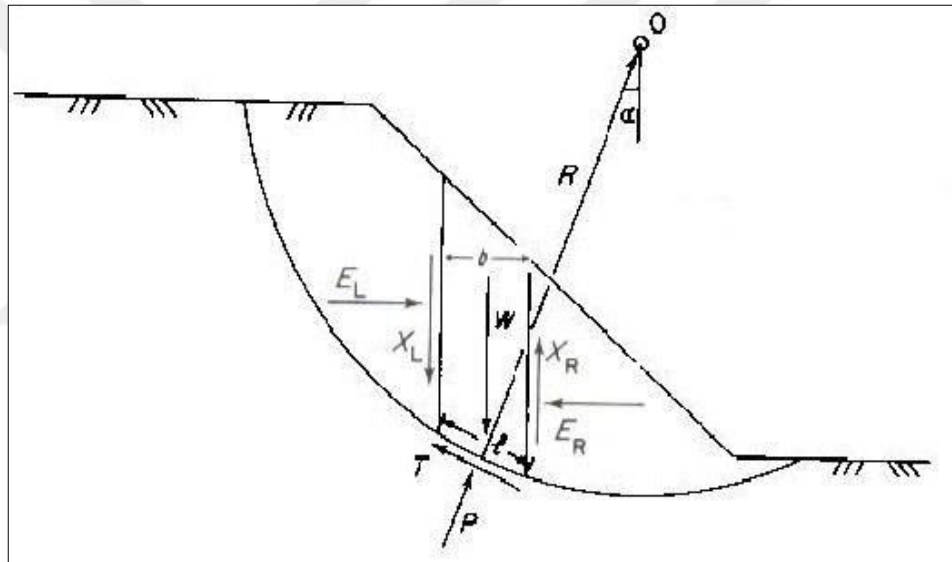


Figure 2.2 Simplified Bishop Method (Anderson and Richards, 1987).

While for the each slice have the base normal force of, P , is supposed to act on all base center. This force can be calculated by Equation 2.6.

$$P = \frac{\left[W - \frac{(c'l \sin \alpha - Ul \tan \phi' \sin \alpha)}{FOS} \right]}{m_\alpha} \quad (2.6)$$

where,

$$m_\alpha = \cos \alpha + \frac{(\sin \alpha \tan \phi')}{FOS} \quad (2.7)$$

Taking moment about center of circle gives the FOS as:

$$FOS = \frac{\sum \left[\frac{c' l \cos \alpha + (w - Ul \cos \alpha) \tan \phi'}{\cos \alpha + \frac{(\sin \alpha \tan \phi')}{FOS}} \right]}{\sum W \sin \alpha} \quad (2.8)$$

2.2.1.3 Janbu's Method

Janbu's simplified method is (Janbu, 1959) being based on a composite factor of safety and shear surface is determined by horizontal force equilibrium. This method neglects the shear forces, but considers interslice normal forces. Determination of base normal force (p) as in Bishop method is being referred above in equation (2.6). To calculate the initial factor of safety (F_0);

$$F_0 = \frac{\sum (C' L + (P - Ul) \tan \phi') \sec \alpha}{\sum W \tan \alpha} \quad (2.9)$$

The below given chart was suggested by Janbu (1973) to correct the calculated factor of safety values for the effect of interslice shear forces.

$$FOS = f_0 F_0 \quad (2.10)$$

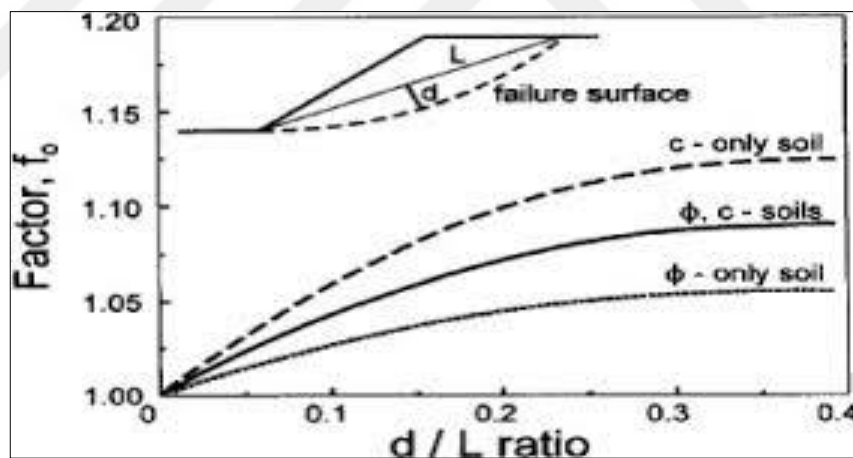


Figure 2.3 Correction factor for Janbu's simplified method (1973).

The depth to length ratio (d/L) of the failure surface is influenced to correction factor. The correction factor may increase the factor of safety by 5 -12% depending on the soil type (Abramson et al., 2002).

2.2.1.4 Lowe - Karafiath's Method

Lowe - Karafiath's method (1960) considers only the force equilibrium to calculate factor of safety. Shear and normal interslices force are taken into account. Lowe - Karafiath's method supposes the average slope of the surface inclination (β) and the base slice inclination (α) are equal to the interslice inclination force, i.e. $\theta = \frac{1}{2}(\beta + \alpha)$, where θ is the resultant force inclination of the interslice. So, the forces of interslice can be written as:

$$X = E \tan \theta \quad (2.11)$$

where,

X is interslice shear force

E is interslice normal force

θ is angle of inclination of interslice resultant force

2.2.1.5 Corps of Engineers Method

Method of the Corps of Engineers (1970) is similar to Lowe - Karafiath's method, with the exception of the interslice force inclination assumption. Consistent with this method, the angle of interslice resultant force may be assumed in two ways. First, it is assume that $\theta = \beta$, where β is angle of the slope. It means, the interslice forces are parallel to the ground surface. In the second assumption, θ assume to be equal to the mean slope angle between the entrance and exit points of the critical shear surface.

2.2.1.6 Sarma Method

Sarma (1973) method is an advanced approach for general blocks and non-vertical slices. This method uses both equilibrium force and moment equilibrium. Furthermore, interslice forces are expressed as a linear expression:

$$X = ch + E \tan \varphi \quad (2.12)$$

where,

h = height of slice.

2.2.1.7 Morgenstern - Price Method

Morgenstern - Price Method is another commonly used approach for analyzing general failure of surfaces. The method was firstly defined by (Morgenstern and Price, 1965). This approach includes much iteration and cannot be used easily without the assistance of a computer. It satisfies wholly static equilibrium necessities. Therefore, it is rigorous method, but the solution obtained must be checked for acceptability.

As said by Morgenstern-Price (1965), the force of interslice inclination can differ with a random function ($f(x)$) as:

$$T = f(x) \lambda E \quad (2.13)$$

where,

$f(x)$ = function of interslice force that varies continuously alongside the surface of slip,

λ = scale of factor of the function assumed.

The more slices are used for solution the more accurate the solution will become since $f(x)$ function will better define the relationship between the interslice forces.

2.2.1.8 Spencer's Method

This method has been developed by (Spencer, 1967). In this method, a trial and error procedure is suggested to calculate the factor of safety for a defined failure surface. The equations are expressed in terms of effective stress and both force and moment equilibrium is considered in the proposed method. In the Spencer method, the soil mass with in the surface of slip has been divided into vertical slices. In every slice, the sum of the moments of the forces and the resultant of the forces should both be zero. Safety factor is identified the total shear strength available (S) on the slip surface divided to the total stress mobilized (S_m) so as to sustain equilibrium.

$$F = \frac{S}{S_m} \quad (2.14)$$

A drawing of a slice with the forces acting upon is illustrated in Fig. 2.4. The force diagram is as follows:

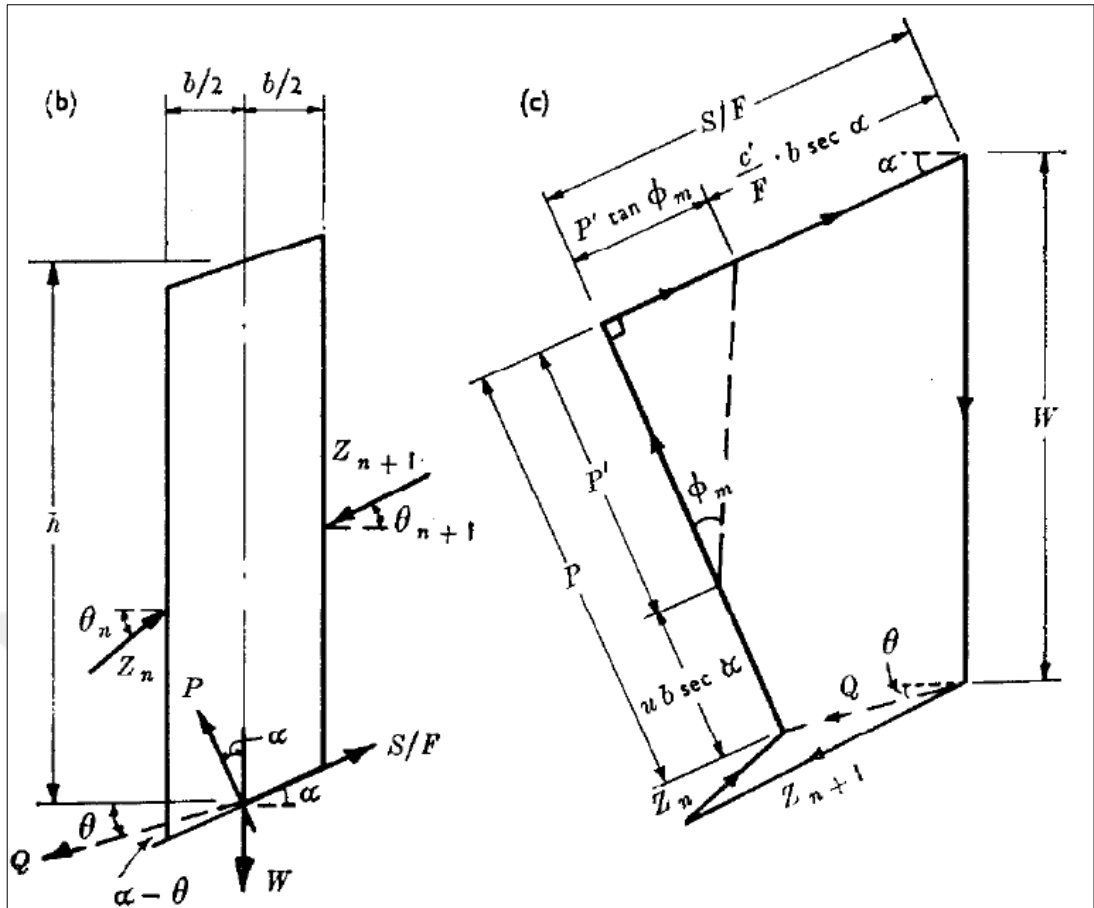


Figure 2.4 Forces on a slice for Spencer's method (Spencer, 1967).

The weight (W_i), (P) normal force to the base of slice (the force P' caused by the effective stress), ($Ub \cdot \sec \alpha$) created by pore pressure (U) on slice. So,

$$P = P' + Ub \cdot \sec \alpha \quad (2.15)$$

The mobilized shear force,

$$S_m = \frac{S}{F} \quad (2.16)$$

where,

$$S = c' b \sec \alpha + p' \tan \phi' \quad (2.17)$$

$$S_m = \frac{c' b \sec \alpha}{FOS} + \frac{p' \tan \phi'}{FOS} \quad (2.18)$$

The forces of interslice Z_n and Z_{n+1} ; from equilibrium, the resultant Q of these two forces must pass through the point of intersection of the three other forces.

By resolving the forces shown in Fig. 2.4 normal and parallel to the base of the slice, the resultant, Q_i of the later slice forces can be written as:

$$Q_i = \frac{\frac{c' b_i \sec \alpha_i}{FOS} + \frac{\tan \varphi'}{FOS} (W_i \cos \alpha_i - U_i b_i \sec \alpha_i) - W_i \sin \alpha_i}{\cos(\alpha_i - \theta_i) \left[1 + \frac{\tan \varphi'}{FOS} \tan(\alpha_i - \theta_i) \right]} \quad (2.19)$$

For force equilibrium of the entire mass, the sum of both vertical and the horizontal components of the interslice forces need to be zero.

$$\sum Q_i \cos \theta_i = 0 \quad (2.20)$$

$$\sum Q_i \sin \theta_i = 0 \quad (2.21)$$

Likewise, the sum of the moments of the interslice forces about the center rotation must be zero.

$$\sum [Q_i R \cos(\alpha_i - \theta_i)] = 0 \quad (2.22)$$

Meanwhile the slip surface is supposed to be circular,

$$\sum [Q \cos(\alpha_i - \theta_i)] = 0 \quad (2.23)$$

Considering the interslice forces are parallel,

$$\sum Q = 0 \quad (2.24)$$

The factor of safety values calculated by Bishop and Spencer method are so similar. Such that the difference was determined to not exceed around 1 % for most of the cases (Spencer, 1967).

Table 2.1 Summary of Limit Equilibrium methods for Slope stability analysis
(Duncan et al., 2014).

Methods	Accuracy and limitation
Ordinary Method of Slices (Fellenius, 1936)	<ul style="list-style-type: none"> - For flat slopes with high pore water pressure, it gives very low safety factor. - Used for circular slip surface - Assumes the soil is frictionless ($\phi = 0^0$)
Modified Swedish Method (Corps of Engineers 1970)	<ul style="list-style-type: none"> - Appropriate for all slip surfaces types. - Factor of safety greater than the other methods.
Bishop Modified Method (1955)	<ul style="list-style-type: none"> - Compared to the Ordinary method the factor of safety is different about 3-5 %. - Appropriate only for circular slip surfaces.
Janbu Simplified Method (1959) Janbu Corrected Method (1973)	<ul style="list-style-type: none"> - Accurate to every shape of slip surface. - Adequate for all equilibrium conditions.
Spencer Method (1967)	<ul style="list-style-type: none"> - Suitable for any shape of slip surface. - Adequate for all equilibrium conditions.
Morgenstern and Price Method (1965)	<ul style="list-style-type: none"> - Adequate for all equilibrium conditions. - Appropriate to every shape of failure.

2.2.2 Finite Element Method

Finite element method has been used since 1966 in analysis of slope stability problem (RocScience, 2004). In finite element method, it is not needed to make assumptions to obtain simplified closed form solutions but problem is solved in an iterative manner in a constructed mesh with the help of boundary conditions and approximation methods. In contrast to the limit equilibrium methods, finite element method includes much more complex and iterative solutions, so the utilization of method has increased since the last two decades with the advancements in computer technology.

In slope stability analysis finite element analysis has several advantages as compared to the limit equilibrium methods (Griffiths and Lane, 1999):

- No exact location or shapes are needed for the failure surface.
- No assumptions for interslice forces are needed.
- Finite element analysis is capable of calculating the deformations and,
- Finite element analysis can be used to analyze an ongoing failure.

The finite element method is a powerful alternative approach. In these analysis of slope stability method is precise and requires fewer assumptions concerning the mechanism of failure. In the finite element method irregular boundaries and flow lines and potential complex variation can be easily solved. The area to be analyzed is divided to elements; every element is jointed to another one together constructing the mesh for solution at nodes.

2.3 Types of Slope Failure Modes

In case of fine grained soils, the shear strength parameters of the soil will change in time. So, the stability of the slopes composed of the fine grained soils will be affected from this change. As a result, two types of failure modes are considered in such cases which are named as short-term and long-term stability for undrained and drained conditions respectively. There will be no such difference in the stability of slopes composed of coarse grained soils since the shear strength parameters of the soils are not subjected to change in time.

2.3.1 Short Term Stability

Short term stability is considered in case of undrained loading conditions for slopes containing fine grained soils. For example, in excavations shear stresses are produced that could cause failure in the undrained state. In the short term stability undrained shear strength (S_u) is used to define the shear strength of the soil. Based on laboratory observations and field analyses of soil samples the internal friction of angle of the soil is zero ($\phi = 0$), under undrained conditions the total stress method is sufficient for short term stability analysis especially in non-fissured clays. For over consolidated fissured clays, the $\phi = 0$ analysis can also be hired by taking into account reduced shear strength due to the magnitude and amount of fissuring in soils.

2.3.2 Long Term Stability

Long term stability is considered for drained loading conditions in slopes. Long term stability analysis for both non-fissured and over consolidated fissured clays is done in terms of effective stresses. Effective stress parameters, effective cohesion (c') and effective internal friction angle (ϕ') must be used to analyze the long term stability of slopes. In equilibrium pore water pressures and seepage conditions must be correctly taken into account. Skempton (1964) proposed the residual shear strength for long term slope analysis of over consolidated clays. Slow drained shear tests can be used to obtain the residual shear strength parameters. In Fig. 2.5 the shear strength characteristics of an over consolidated clay is given in terms of effective stress.

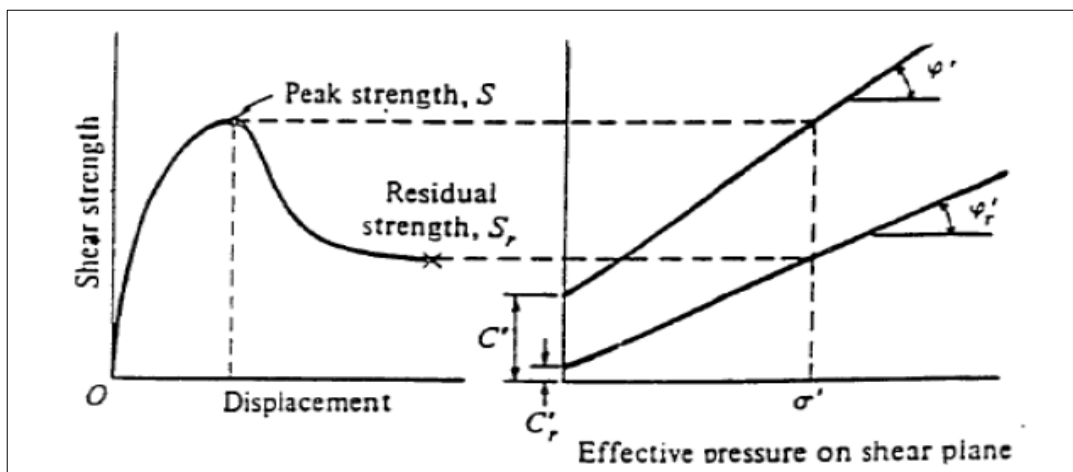


Figure 2.5 Shear characteristics of over consolidated clay (Skempton, 1964).

2.4 Peak and Residual Strengths

When a soil is exposed to shear strain, the shear stresses increase gradually up to a certain level. For any applied effective normal stress of the soil, the maximum shear resistance of the soil is known as the peak shear strength. Residual shear strength produced when soil is sheared beyond the peak shear strength value, decreases till a constant value is extended. The stress-strain curves and the corresponding failure envelopes for peak and residual states are illustrated in Fig. 2.6 for both normally and over consolidated soils.

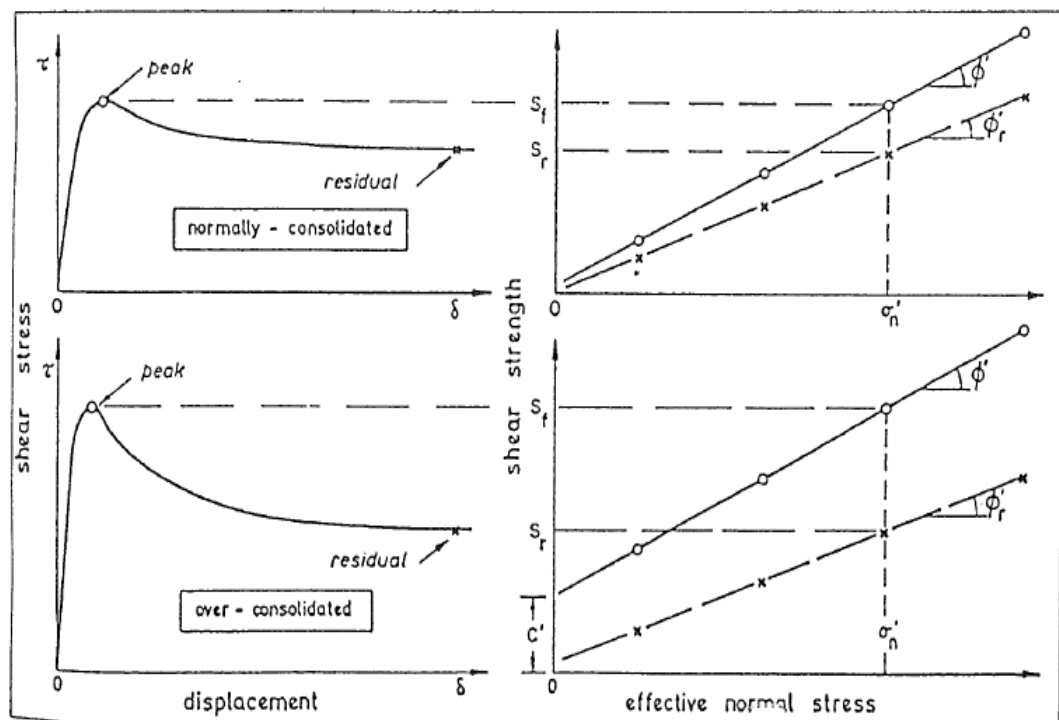


Figure 2.6 Definitions of Peak and Residual Stress Envelopes (Skempton, 1985).

The true residual strength can not be measured easily in many laboratory tests because the magnitudes of relative displacement that can be applied to the samples are limited for most of the test equipment. The resulting measured post peak strength is commonly referred to as the remolded strength, which falls at somewhere between the peak and residual strengths on the stress-strain curves presented in Fig.2.6.

2.5 Back Analysis of Slope Failure

Back analyses are used to identify the mechanism of the failure and shear strength parameters of soil along the failure surface. The slope has been failed, the safety factor at the time of failure is considered equal to one (i.e. resisting forces/moments equal to the driving forces/moments) (Cornforth, 2005). Usually, back analysis is one of the effective methods to afford an insight into the principal failure mechanism and expand the understanding as regards the factors controlling the stability of slopes (Ng et al., 2014).

One of the main advantages of back analysis is to consider the site effects like presence of cracks and preexisting shear plane which may not be determined by laboratory and field tests as discussed in (Duncan and Stark, 1992). As mentioned in (Deschamps and Yankey, 2006) back analysis is used commonly to understand the failure mechanisms of the slopes.

2.5.1 Back Calculating Average Shear Strength

The easiest method of back analysis is to compute the shear strength parameters from the known soil unit weight and slope geometry. In back analysis for undrained loading conditions, to get a factor of safety equal to one, the internal friction angle of soil assumed as zero and a suitable cohesion value is assumed. So, average shear strength parameters can be defined as a cohesion (c) with internal friction angle ($\phi = 0$). Assume that the slopes have been failed after a long time was formed of the slope. In this case, we use drained shear strength parameters and effective stresses to analyze stability of the slope (i.e. internal friction angle has a value). So, the friction angles that make the factor of safety equal to one should be determined for certain cohesion values.

2.5.2 Back Calculating Shear Strength Parameters Based on Slip Surface Geometry

For any given slope there are an unlimited number of shear strength parameters [cohesion (c , c') and friction angle (ϕ , ϕ')] that will produce factor of safety of one. Every such pair of shear strength values will produce a different slip surfaces. This is presented for an uncomplicated slope in Fig. 2.7, three pairs of shear strength parameters and corresponding critical circles have been revealed. Every single set

have a safety factor of unity, the critical slip surface is different for each of the analysis (Duncan et al., 2014).

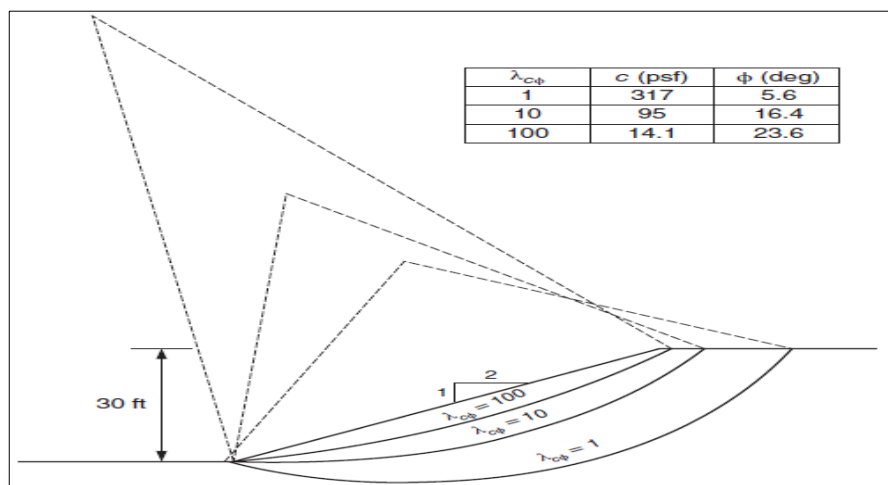


Figure 2.7 Critical circles for three different sets of shear strength parameters giving a factor of safety of 1 (Duncan et al., 2014).

2.5.3 Limitation and Problems of Back Analysis

Several studies have been conducted for use of the back-analysis method to determine the soil strength parameters. There are many publications that define limitations of back analyses (Leroueil and Tavenas, 1981; Azzouz et al., 1981; Leonards, 1982; Duncan and Stark, 1992; Gilbert et al., 1998; Tang et al., 1998; Stark and Eid, 1998).

Back analysis is a useful method for slope stability problems but one should be aware of its uncertainty and limitations (Gilbert et al., 1998) which are listed below:

- i. The exact geometry of the slope, comprising beneath surface stratigraphy and slip surface location, is rarely identified (Leonards, 1982).
- ii. Failure mechanisms, such as progressive failure are difficult to determine (Duncan and Stark 1992).
- iii. Pore water pressure data is normally sparse, if it is present at the whole thing (Chandler, 1977; Leroueil and Tavenas, 1981).
- iv. The shear strengths of the soil are being decreased significantly at the time of failure due to changes in pore water pressure or/and structures of the softening soil (Duncan et. al., 2014).

- v. There are several different demonstrations of strength of the soil, such as c and ϕ (Duncan and Stark, 1992) or linear as against nonlinear failure envelopes Chandler (1977), that possibly will create failure.
- vi. Back-calculated principles characterize only an average of the shear strength parameters that were mobilized on the failure surface; actual shear strength parameters may not be represented by average shear strength parameters at any point of failure surface.

2.5.4 Back Analysis Methods

Both deterministic methods (e.g., Wesley and Leelaratnam, 2001; Tiwari et al., 2005) and probabilistic methods (Luckman et al., 1987; Gilbert et al., 1998; Chowdhury et al., 2004) have been used to for back-analysis. The concepts behind deterministic and probabilistic back-analysis methods are not the same procedure. Even though deterministic back-analysis methods are going to find a set of parameters that would result in the slope failure, probabilistic back-analysis methods may finally determine many combinations of such parameters, but their relative possibilities are different, which can be measured by probability distributions (Zhang et al., 2010). In the deterministic method the safety factor is equal to one, to determine unique parameters for cohesion and internal friction angle of the soil (Jiang and Yamagami, 2008). Major advantages of probabilistic back-analysis is that it provides a logical way to incorporate information from other sources in the back-analysis and it is accomplished of back-analyzing various sets of slope stability parameters instantaneously (Zhang et al., 2010). One disadvantage of probabilistic approach generally it is not easy to implement as compared to the deterministic method.

If the input parameters in the probabilistic method are well characterized statistically, the obtained results will be realistic (Wang et al., 2013).

2.6 Factors Affecting Slope Stability Analysis

It is known there are many factors that affect slope stability analysis. The main factors may be listed as, failure plane geometry, soil non homogeneity of layers, tension cracks, dynamic loading or earthquakes, soil unit weight, loading conditions (i.e. undrained or drained), method of analysis and seepage flow. These major factors are briefly described based on (Fang, 1991).

2.6.1 Failure Plane Geometry

The geometry of the failure plane is very important in analyzing the problem. The failure may be circular and non-circular, deep or surficial and etc.

2.6.2 Non Homogeneity of Soil Layers

Depending upon the environmental condition of deposition and subsequent stress changes during geological history, soil strength parameters may be isotropic. On the other hand, most soils are anisotropic. This fact changes the stress state in slopes which is the main factor affecting the movements in the soil body.

2.6.3 Tension Crack

Tension cracks generally occur close the crest of a slope. The depth of crack generally decreases by decreasing the cohesion. The depth and location of a tension crack may become extremely important for the stability of a slope.

2.6.4 Dynamic Loading

The effect of dynamic loading, mostly earthquakes, on slope stability should also be considered. So the researchers after the 1960's have been started to study relationship between dynamic loading and slope stability, like (Seed and Goodman, 1964) considered the yield acceleration of slope in cohesionless soils.

2.6.4.1 Pseudo-static Analysis Method

The pseudo-static method is the most common practical procedure which is used for slope stability analysis under seismic loading. Pseudo-static analysis is used in earthquake engineering to analyze the seismic response of soil slopes and embankments. The idea was first developed by Terzaghi (1950), as discussed in (Jibson, 2011).

In a pseudo-static analysis, a limit equilibrium analysis is implemented in which the earthquake loading is denoted by equivalent horizontal and vertical forces (F_h and F_v) respectively (Cho, 2002). The pseudo-static forces are expressed as follows.

$$F_h = \frac{a_h W}{g} = k_h W \quad (2.25)$$

$$F_v = \frac{a_v W}{g} = k_v W \quad (2.26)$$

where,

W: the weight of the material above slip surface.

a_h , a_v : horizontal and vertical pseudo-static accelerations respectively.

In general formula of the plane surface, the safety factor under seismic loading has been expressed as given below:

$$FOS = \frac{\text{Resistance Force}}{\text{Driving Force}} = \frac{c_{ab} + [(W - F_v) \cos \beta - F_h \sin \beta] \tan \phi}{(W - F_v) \sin \beta + F_h \cos \beta} \quad (2.27)$$

Pseudo-static seismic coefficients are in horizontal and vertical (k_h and k_v), they are used to calculate the horizontal and vertical forces caused by a potential earthquake respectively, as illustrated in Fig. 2.7. These forces (horizontal and vertical forces) are added to overall equilibrium calculation for the every individual slices composing the surface of failure (Melo and Sharma, 2004).

In terms of Pseudo-static safety factor, the horizontal pseudo-static force has more effect in reduction of safety factor than vertical pseudo-static force. This is due to the fact that the vertical pseudo-static force reduces both the driving force and resisting force as seen in Eq.2.27. Generally, just the horizontal component of earthquake shaking is demonstrated since the influences of vertical forces are almost ignorable for most of the cases. (Kramer, 1996; Abramson et al., 2002; Jibson, 2011).

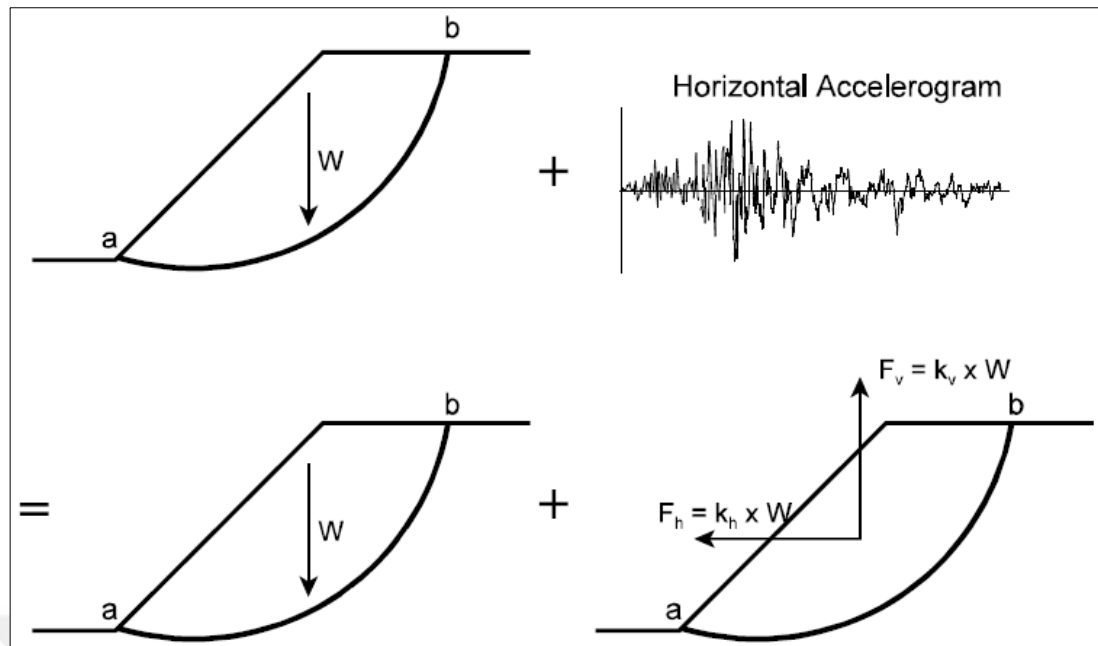


Figure 2.8 Pseudo-static Analysis Method (Melo and Sharma, 2004).

There are different methods for selection of suitable seismic coefficients some of which may be listed as: Empirical method, rigid body response method and elastic response analysis (Seed and Martin, 1966). The applicability of these methods will be illustrated in the following sections.

2.6.4.1.1 Empirical Method

Using empirical values for seismic coefficients is the most practiced way for pseudo-static analysis. Though, the selection of seismic coefficients analysis may be random (Melo and Sharma, 2004). As presented in Table 2.2, there are no exact rules to choose a suitable seismic coefficient for design of earth structures. Nevertheless, the designs guided generally recommend that the seismic coefficient should be based on the predictable level of acceleration within the failure mass and should correspond to some fraction of the estimated peak acceleration (Kramer, 1996).

Table 2.2 Horizontal seismic coefficient values recommended by different references
(Melo and Sharma, 2004).

Horizontal Seismic Coefficient, k_h	Description	
0.05 - 0.15	In the United States (Seed and Martin, 1966).	
0.12 - 0.25	In Japan (Numata, 1960).	
0.1	“severe” earthquakes	(Terzaghi, 1950)
0.2	“violent, destructive” earthquakes	
0.5	“catastrophic” earthquakes	
0.1 - 0.2	FOS \geq 1.15 (Seed, 1979)	
0.10	Major Earthquake, FOS > 1.0	(Corps of Engineers, 2003)
0.15	Great Earthquake, FOS > 1.0	
1/2 to 1/3 of PHA	FOS > 1.0 (Marcuson and Franklin, 1983).	
1/2 of PHA	FOS > 1.0 (Hynes-Griffin and Franklin, 1984).	
PHA = Peak Horizontal Acceleration, in g's.		

2.6.4.1.2 Rigid Body Response Analysis Method

If an earthfill structure is supposed to act as a rigid body, the acceleration will be uniform all over structure and will be equal to the ground acceleration. Hence, it is argued that the design seismic coefficient has to be equal to the maximum ground acceleration, but some limitation of the method such as: (i) All earth structures and slopes may not response in the same magnitude of to the same embankment of earthquake unless they have a rigid response and stiff. Accelerations acting on earth structures and slopes are being different than their own foundations due to the natural period and damping characteristics. (ii) The maximum acceleration acts during a very short time interval, also the deformation created by this maximum acceleration will be so small, but this act is assumed to act for unlimited period of time in this analysis method.

2.6.4.1.3 Elastic Response Analysis

This method is especially used for pseudo-static analysis of earthfill dams and slopes. Dynamic response has been developed by Mononobe et al. (1936) as cited by (Seed and Martin, 1966). For solution this approach is simplified by below listed assumptions:

- 1- Dam is a symmetrical triangular section.
- 2- It consists of uniform density and modulus of elasticity.
- 3- Width to height ratio of the dam is large thus, the bending deformation can be neglected.
- 4- Shear stress uniformly distributed in any horizontal plane.
- 5- Effect of water pressure as stored neglected and
- 6- Dam consist of horizontal slices connected by linearity and viscous damping.

Generally, supposing free vibration in the analysis also the damping is zero as illustrated in Fig. 2.8 at any depth (y) below the crest of the dam the force acting on a thin slice.

$$\frac{\partial^2 u}{\partial t^2} = \frac{G}{\rho} \left[\frac{\partial^2 u}{\partial y^2} + \frac{1}{y} \frac{\partial u}{\partial y} \right] \quad (2.28)$$

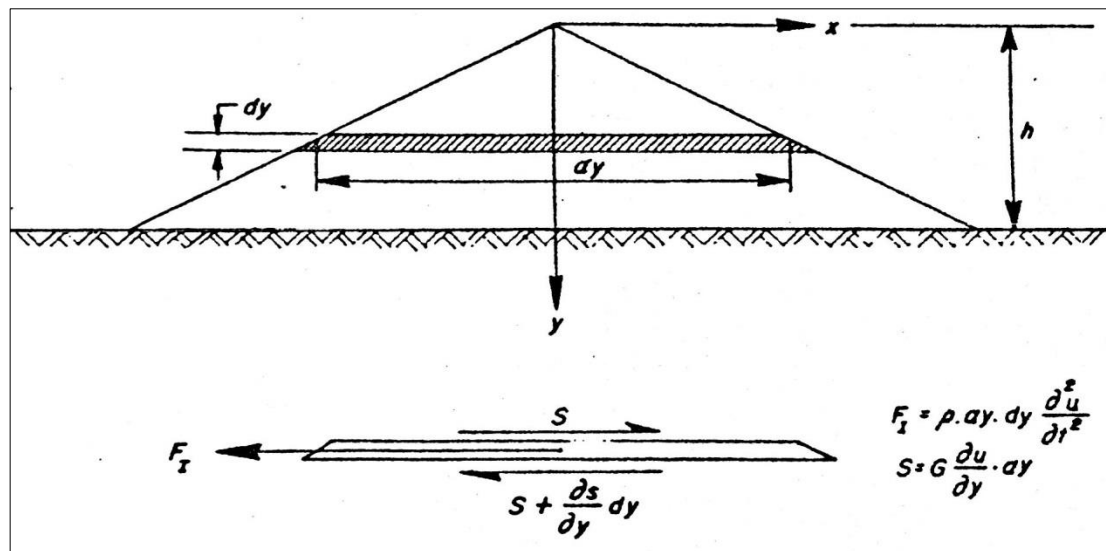


Figure 2.9 One dimensional shear slice theory (Seed and Martin, 1966).

Differential equation solution as shown below for the applicable boundary condition $y = h$, if $u = 0$ for all condition t . $y = 0$ if, $\frac{\partial u}{\partial y} = 0$ for all value of t .

$$u(y, t) = \sum_{n=1}^{n=\infty} [A_n \sin \omega_n t + B_n \cos \omega_n t] J_0 \left(\beta_n \frac{y}{h} \right) \quad (2.29)$$

where,

h: height of the dam

n: number of mode

β_n : the zero value of frequency equation $J_0 \left(\omega \sqrt{\frac{\rho}{G}} h \right) = 0$, when the $J_0 \left(\beta_n \frac{y}{h} \right)$ equal to the mode vibration for the n^{th} mode.

ω_n : natural frequency in the n^{th} mode of the dam equal $\frac{\beta_n}{h} \sqrt{\frac{G}{\rho}}$ (in rad/s).

A_n and B_n : constants defined by the initial conditions.

From the undamped natural frequency when, shear wave velocity of the dam

$V_s = \sqrt{\frac{G}{\rho}}$, so as to the natural frequency can be has written as:

$$\omega_n = \frac{\beta_n}{h} V_s \quad (2.30)$$

Random ground motion of the response of structure may be analyzed by supposing the ground motion as zero, the structure influence by acting of the force equal to the mass at any point times to the ground accelerations. Therefore, random horizontal ground motion is acted to the same dam with displacements, $u_g(t)$, velocities $\dot{u}_g(t)$ and accelerations $\ddot{u}_g(t)$, the motion's equation (zero damping) turn out to be as:

$$\frac{\partial^2 u}{\partial t^2} = \frac{G}{\rho} \left[\frac{\partial^2 u}{\partial t^2} + \frac{1}{y} \frac{\partial u}{\partial t} \right] = - \frac{\partial^2 u_g}{\partial t^2} \quad (2.31)$$

Individual of modes consist the whole response structure, every modes supposed to act separately. The over-all solution for this equation is as follow:

$$u(y, t) = \sum_{n=1}^{n=\infty} \frac{2 J_0 \left(\beta_n \frac{y}{h} \right)}{\omega_n \beta_n J_1 \left(\beta_n \right)} \int_0^t \ddot{u}_g \sin[\omega_n (t - \tau)] d\tau \quad (2.32)$$

But viscous damping forces are known to act the analysis, after that the damped response to the random ground motion, u_g , which might be induced during an earthquake, can be presented as follow

$$u(y, t) = \sum_{n=1}^{n=\infty} \frac{2 J_0 \left(\beta_n \frac{y}{h} \right)}{\omega_{dn} \beta_n J_0 \left(\beta_n \right)} \int_0^t \ddot{u}_g e^{-\lambda_n \omega_n (t-\tau)} \sin[\omega_{dn}(t - \tau)] dt \quad (2.33)$$

ω_{dn} : damped natural frequency in the n^{th} mode = $\sqrt{1 - \lambda_n^2} \approx \omega_n$ for a small value of λ_n

λ and λ_n : fraction of critical damping for the n^{th} mode

The overall and absolute acceleration, $\ddot{u}_a(y, t)$, acting on the dam at any time t , is given by,

$$\ddot{u}_a(y, t) = \ddot{u}(y, t) + \ddot{u}_g(t) \quad (2.34)$$

In the condition of zero damping (shown in Eq. 2.31) after normalizing the modes, that the modal influences to the absolute accelerations is obtained by;

$$\ddot{u}_{an}(y, t) = \omega_n^2 u_n(y, t) \quad (2.35)$$

The absolute acceleration at any height level (y), of the dam at time (t), is expressed by,

$$\ddot{u}_a(y, t) = \sum_{n=1}^{n=\infty} 2 \omega_n \frac{1}{\beta_n J_1(\beta_n)} J_0\left(\beta_n \frac{y}{h}\right) \int_0^t \ddot{u}_g e^{-\lambda_n \omega_n (t-\tau)} \sin[\omega_n (t - \tau)] d\tau \quad (2.36)$$

Although this equation is apparently cumbersome, its can express as simplified in the follow written

$$\ddot{u}_a(y, t) = \sum_{n=1}^{n=\infty} \ddot{u}_{an}(y, t) \quad (2.37)$$

where,

$$\ddot{u}_{an}(y, t) = \omega_n \phi_n(y) v_n(t) \quad (2.38)$$

so,

$$\omega_n = \frac{\beta_n}{h} \sqrt{\frac{G}{\rho}} \quad (2.39)$$

$$\phi_n(t) = \frac{2 J_0(\beta_n \frac{y}{h})}{\beta_n J_1(\beta_n)} \quad (2.40)$$

and

$$V_n(t) = \int_0^t \ddot{u}_g e^{-\lambda_n \omega_n (t-\tau)} \sin[\omega_n (t - \tau)] d\tau \quad (2.41)$$

The case that is analyzed in this thesis is part of highway project. So, the pseudo-static analyses are made using seismic coefficients recommended by “General Directorate of Highways”

2.6.4.2 Time-history Analysis Method

During earthquakes sudden ground displacement induces large inertia forces in the earth structure. The slopes of earth structures are exposed repetitive cyclic loadings during an earthquake. In the past, several cases were recorded that indicate severe damage or collapse and deformation of slope caused by vibration (Das and Ramana, 2011).

Time-history analysis is one of the comprehensive methods to analyze slope stability under earthquake loading (Chowdhury and Dasgupta, 2008). When an earthquake happens in the world all seismic monitoring stations record the wave signals. Based on this data, acceleration-time, velocity-time and displacement-time histories are obtained. Dynamic time-history analysis may be done with either linear elastic or inelastic material behavior assumptions (Chopra, 2011). For slope stability analysis, the finite element movement dynamic balance equation is expressed as follows (Zhou and Zuo, 2014):

$$M\ddot{u} + C\dot{u} + Ku = F \quad (2.42)$$

where,

M: Mass of matrix, the mass of the material consist of (soil + water + any constructions) is taken into account.

C: Damping of matrix.

K: Stiffness of matrix.

F: Load of vector ($ku = F$) relate to the static deformation.

The theory is defined on the bases of linear elasticity. The soil behavior can be both drained and undrained, the matrix C is defined as the damping ratio of the material, actually material damping is due to friction or by plasticity/viscosity. If the material is more plastic or viscous more vibration energy may be dissipated. The determination of material damping is difficult experimentally, but can be formulated as a function of mass and stiffness of matrices and expressed as (Brinkgreve, 2002):

$$C = \alpha_R M + \beta_R K \quad (2.43)$$

During an earthquake, the earth moves almost a random way in all directions for both horizontally and vertically. The acceleration-time history in north-south direction of El Centro, California earthquake (18 May 1940) is presented in Fig. 2.9, so exposed velocity and displacement value as calculated in the same direction. It can be seen from the figure maximum ground acceleration is around 0.32 g, the maximum ground velocity is 13.7 in/sec and the maximum ground displacement is 8.3 in (Newmark, 1965).

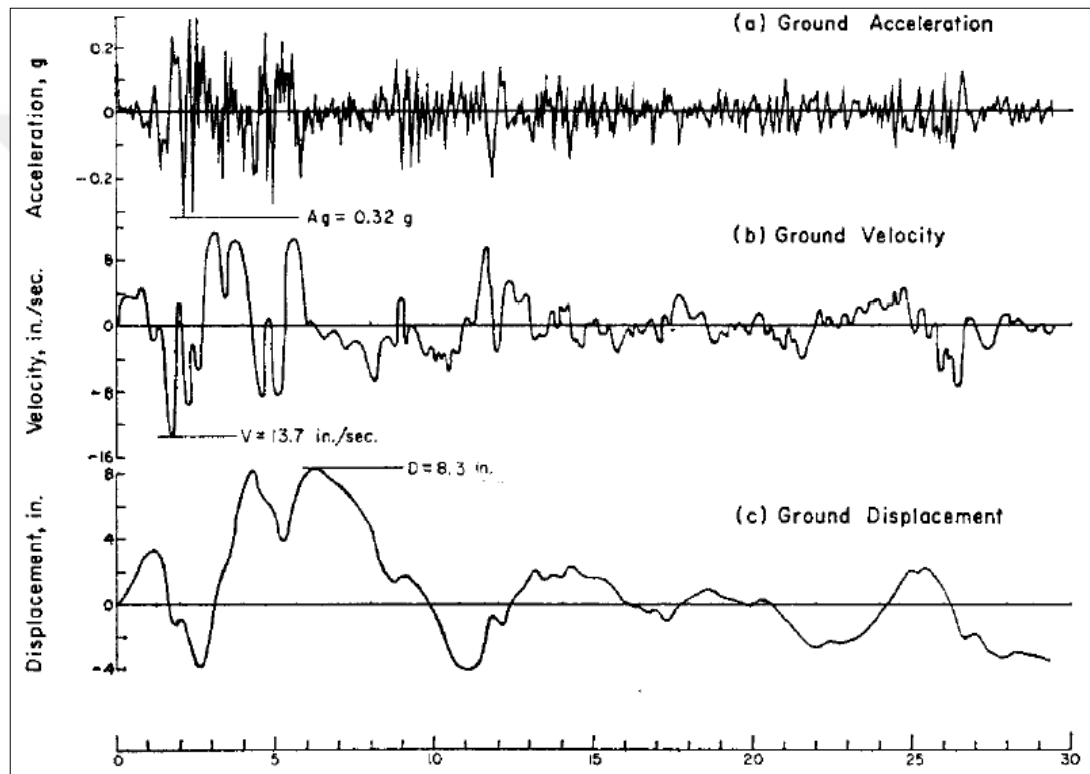


Figure 2.10 El Centro, California, earthquake of 18 May, 1940, N-S component (Newmark, 1965).

In considering the influence of an earthquake on an earth structure such as earthfill dam or slope. It is required to consider all the parts of the motion.(i.e. peak acceleration possibly is not significant in determining the response of a slope). Fig. 2.9 shows a low magnitude of acceleration for a long period, which induced large displacements. Thus the effect of velocities, ground displacement and differential displacement should be considered (Newmark, 1965).

Bouckovalas and Papadimitriou (2005) have been investigated the effects of slope geometry, main excitation frequency and duration, in addition to the dynamic soil properties on seismic ground motion in a parametric way. Siyahi and Arslan (2008) implemented the transient dynamic time history finite element simulations to study the performance of earthfill dams under seismic excitation. Sica et al. (2008) have been studied the influence of loading history on the seismic response of earthfill dams. Xueliang et al. (2015) studied effect of height of slope cause of changes the acceleration, displacement and velocity. With the increase of seismic peak acceleration, the dynamic response of slope is enhanced and the stability of slope declines. Koo et al., have presented a more rational method of using dynamic time history analyses to estimate the dynamic load prompted displacement in slopes. Moreover the benefit of the time history analysis could be giving the opportunity to the designer to evaluate the slope performance depleting realistic earthquake record and the soil is considered as having a non linear response.

CHAPTER 3

MATERIALS AND METHODS

In this chapter, the problem in the studied area is described in detail. Then, the material parameters for the soil layers are determined by either site/laboratory test results or back analysis. Finally, the required number of piles for slope stabilization under dynamic loading is determined according to the design guide of “Turkish General Directorate of Highways” solving the system by pseudo-static methods.

3.1 Description of Problem and Study Area

Study area is between Ulus and Bartın cities in the Bartın Province in western part of the black sea region in Turkey as shown in Fig. 3.1.



Figure 3.1 Site location map of the studied area.

A landslide occurred during a road construction (Fig. 3.2, Fig. 3.3 and Fig. 3.4). Site investigations were made to study the soil properties and landslide geometry. For this purpose a total of 28 boreholes were drilled and 12 inclinometers were inserted into the ground to measure the lateral displacements and determine the failure geometry.

The studies revealed that there was a big landslide at the site and it was continuous under static loading. There were mainly two different materials at the site. The bedrock was formed of “Ulus Formation” which is a mixture of relatively weak sandstones and claystones. The sliding mass was primarily composed of “Residual Ulus Formation” which is formed by decomposition of the bedrock. The thickness of this decomposed and weak layer changed between 6m – 32m at different parts of the study area.

The groundwater table was seen at 2.5m depth and followed the ground surface along the inclined surface. The inclinometer data showed that the sliding surface is very close to the contact of decomposed “Residual Ulus Formation” and “Ulus Formation” and mainly had a non-circular slip surface.

In this study, firstly the material properties of the soil layers were determined by evaluating site and laboratory test results and by back analysis. Then the necessary support system to stabilize the landslide according to the requirements of “Turkish General Directorate of Highways” was determined through limit equilibrium analyses. Then, the required support system was analyzed by different earthquake records scaled to the same maximum acceleration, to see the effect of earthquake characteristics on pile behavior.

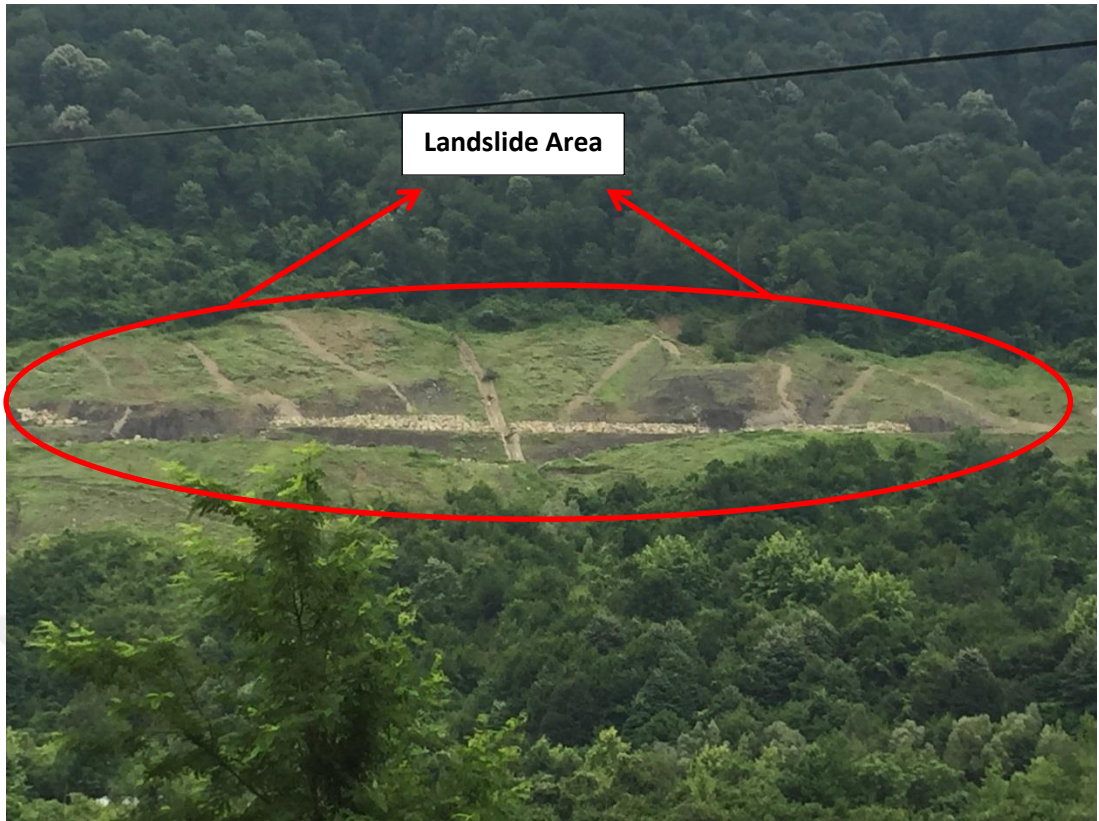


Figure 3.2 A general view of the studied area.



Figure 3.3 Damage at drainage lines due to landslide.



Figure 3.4 Movements at road level.

3.2 Material Properties

The material properties of the bedrock were determined through site and laboratory tests. The material had an average compressive strength of $q_u = 20$ MPa and GSI = 29. By these test results the strength and deformation parameters of the “Ulus Formation” were determined by “RocLab” software as (unit weight) $\gamma = 23$ kN/m³, (cohesion) $c = 185$ kPa, (internal friction angle) $\phi = 33^\circ$ and (elastic modulus) $E \approx 300000$ kPa (Fig. 3.5).

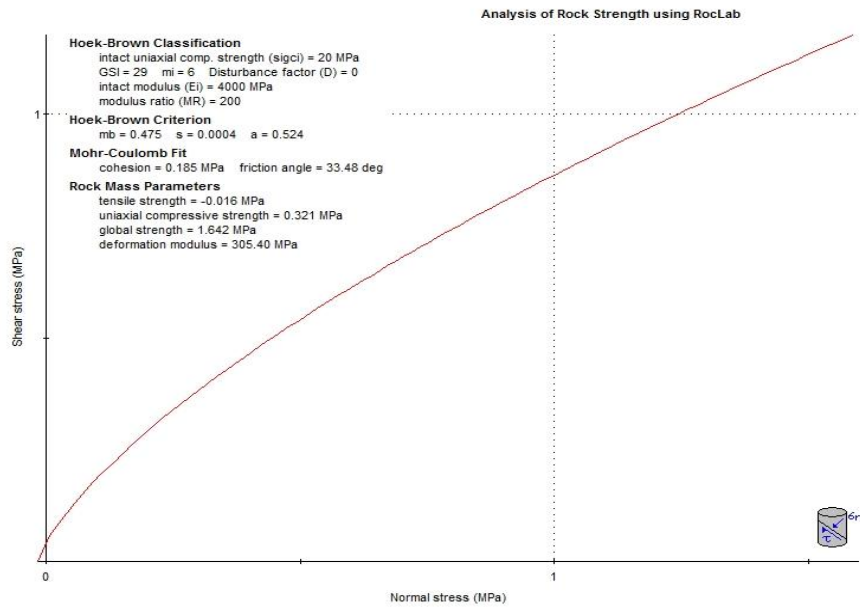


Figure 3.5 Material Properties of Ulus Formation.

The material properties of the sliding mass (Residual Ulus Formation) were hard to determine by site and/or laboratory tests since the material was so heterogeneous containing a wide range of soil particles as a mixture at different rates at different parts of the study area. As a result, it was decided to determine the material properties of this layer by back-analysis on six different cross sections using Slide software. The locations of these cross sections are showed in Fig.3.6.

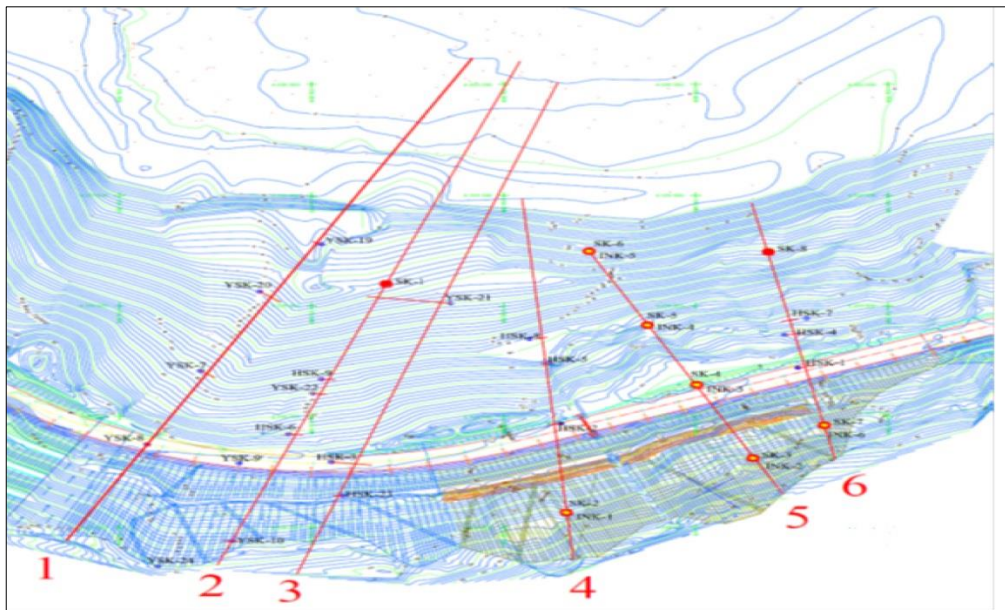


Figure 3.6 Studied cross sections on the landslide area.

3.2.1 Back Analysis

Back analysis is one of the tools to determine the material properties in sliding masses. “Slide 6.0” software was used in this part of the study. The “Mohr-Coulomb” strength parameters of the “Residual Ulus Formation” were investigated on six different cross sections. The sliding surfaces were determined by inclinometers. The non-circular slip surfaces were analyzed by corrected version of “Janbu” method which is known to give better results for non-circular failures.

The cohesion was changed between $c = 0 - 25$ kPa and the corresponding internal friction angle values (ϕ) were calculated which made the global factor of safety $FOS \leq 1.00$. After a trial & error procedure for each cross section the Mohr-Coulomb parameters pairs found for each cross section is plotted and given in Fig. 3.7. In this figure it can be clearly seen that, first three cross sections (1-1, 2-2 and 3-3) showed similar characteristics and the calculated material parameter coincided for $c = 10$ kPa. The section 4-4 is in the transition zone and has the most critical sliding thickness. The “Mohr-Coulomb” material pairs coincide well for $c = 5$ kPa for cross sections 5-5 and 6-6. So, the material parameters determined by back analysis are summarized in Table 3.1. The analysis sections are given between Fig. 3.8 – Fig. 3.13.

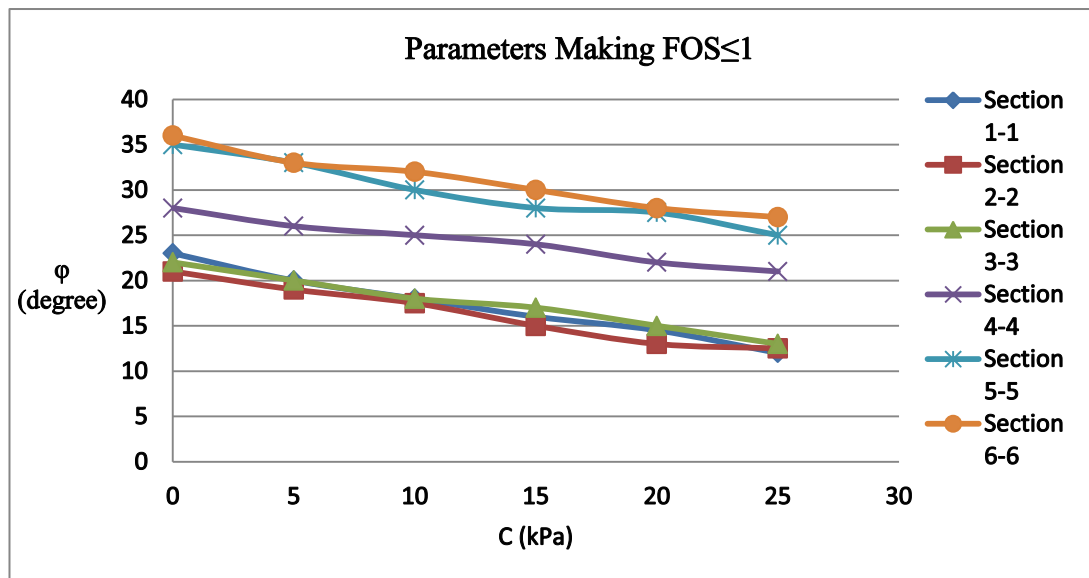


Figure 3.7 Results of back analysis.

Table 3.1 Results of shear strength parameters of cross sections by back analysis.

Cross sections	C (Cohesion) [kN/m ²]	φ (Int. fric. angle) [°]	γ (Unit weight) [kN/m ³]
Cross section 1-1	10	18	21
Cross section 2-2	10	18	21
Cross section 3-3	10	18	21
Cross section 4-4	5	26	21
Cross section 5-5	5	33	21
Cross section 6-6	5	33	21

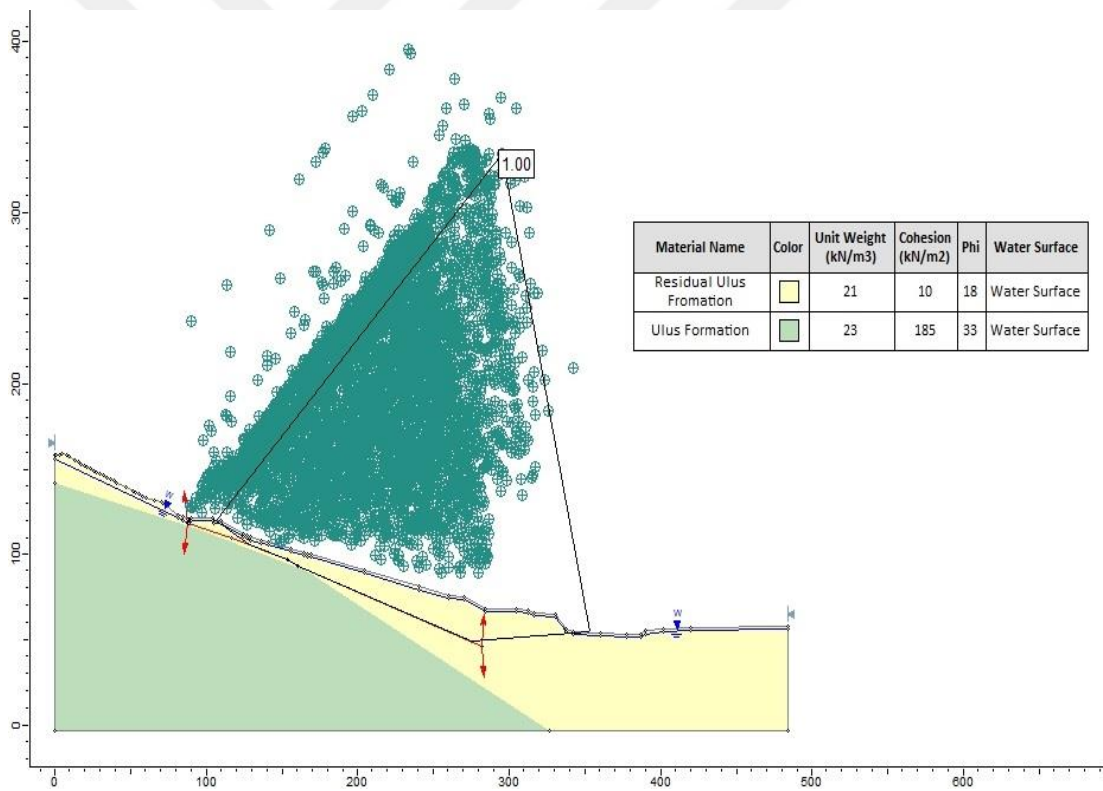


Figure 3.8 Back analysis result of section 1-1.

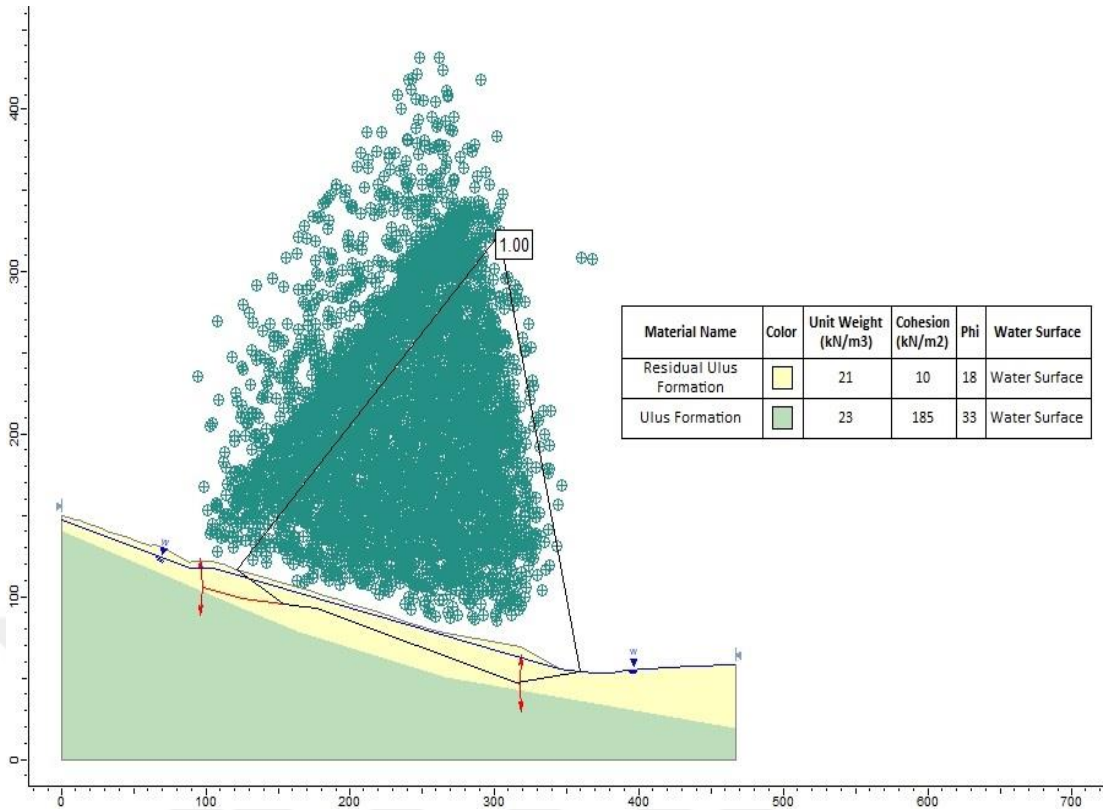


Figure 3.9 Back analysis result of section 2-2.

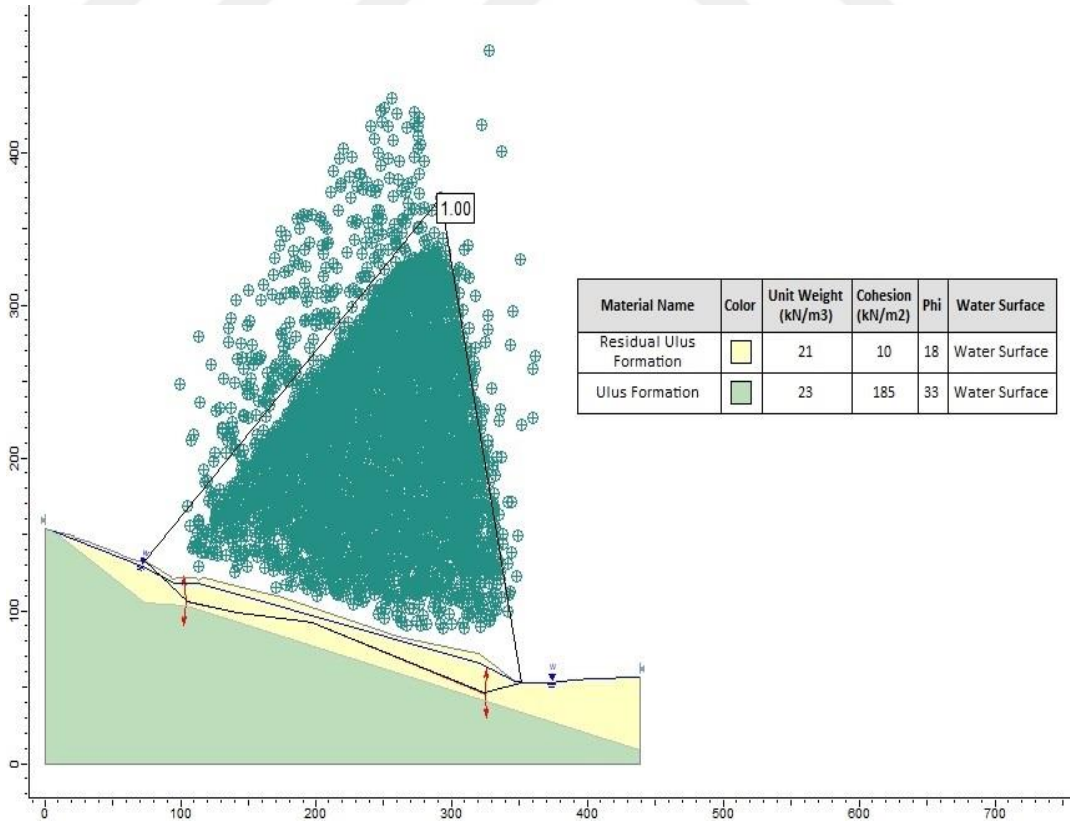


Figure 3.10 Back analysis result of section 3-3.

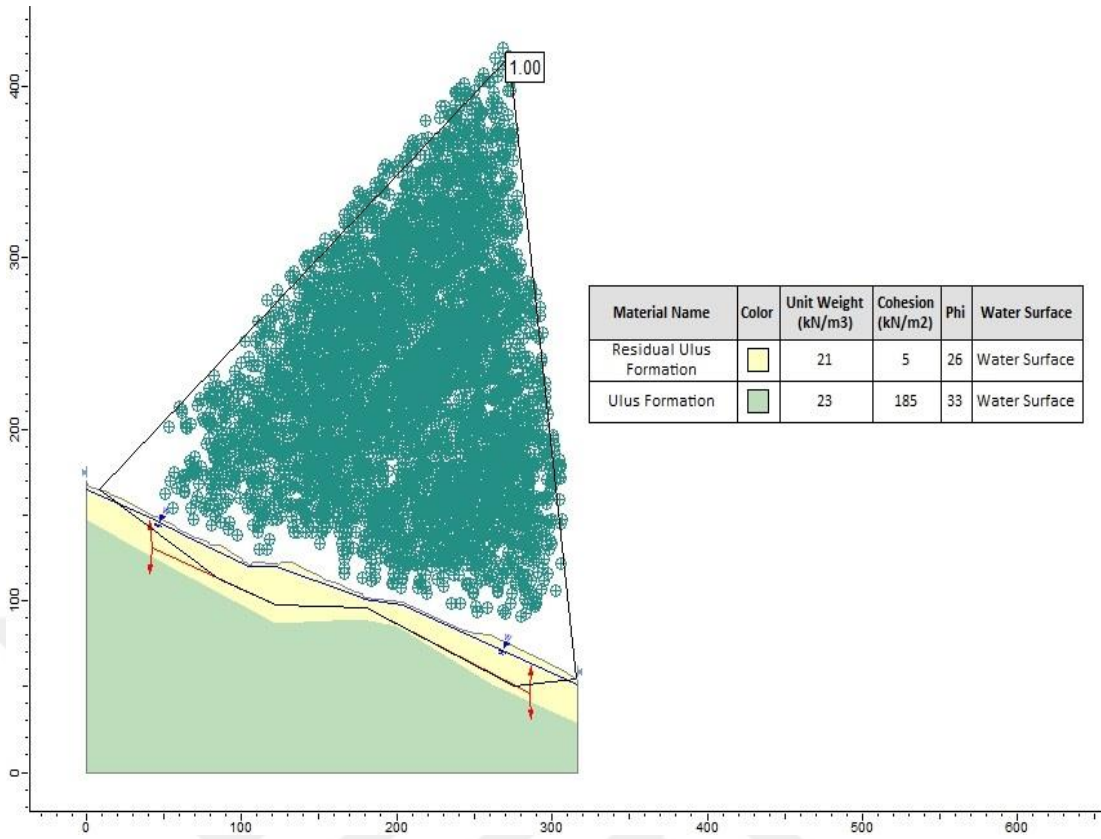


Figure 3.11 Back analysis result of section 4-4.

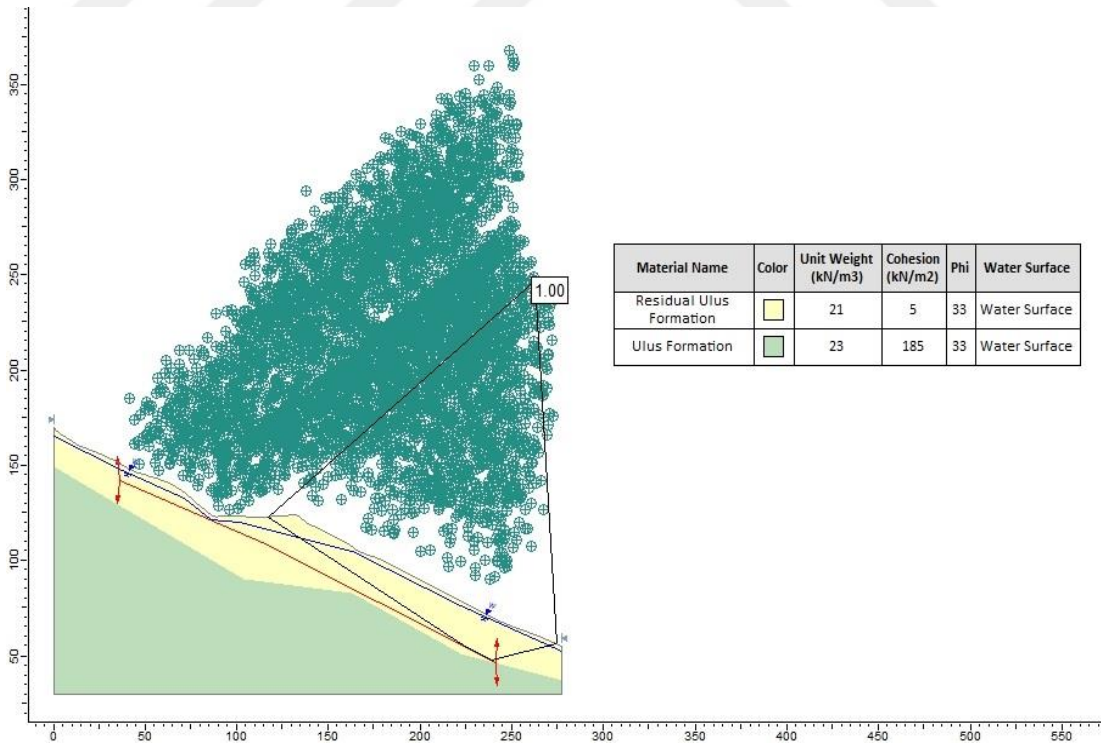


Figure 3.12 Back analysis result of section 5-5.

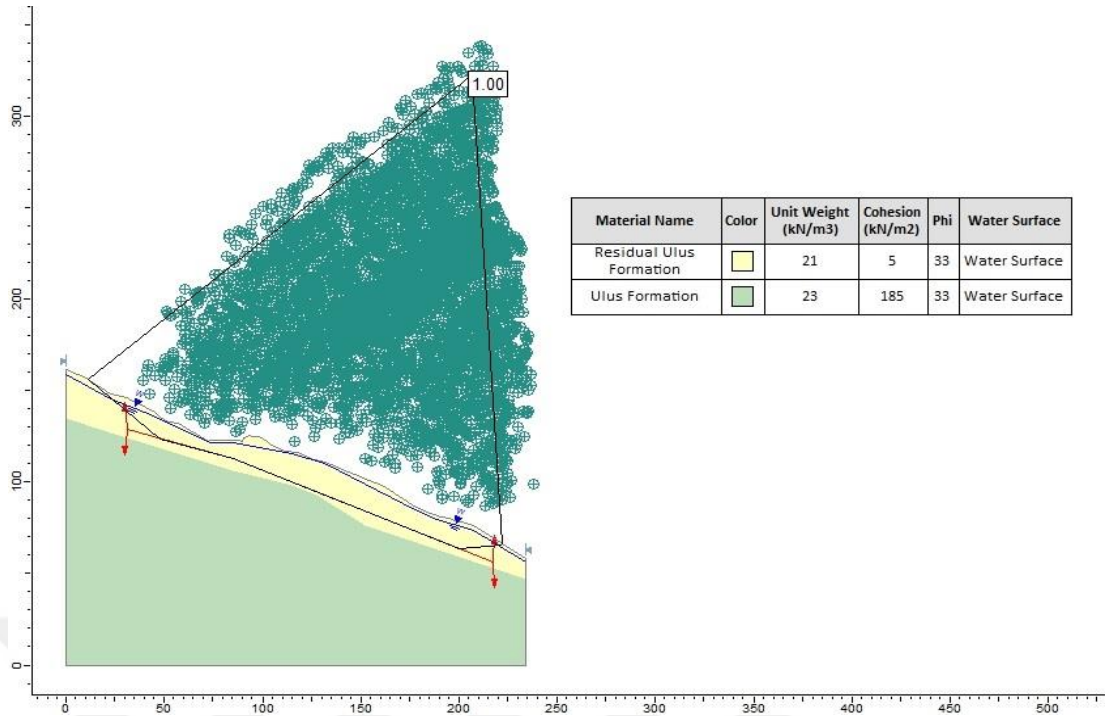


Figure 3.13 Back analysis result of section 6-6.

3.2.2 Slope Stabilization

Installation of piles is one of the methods used to improve the stability of slope, it is widely accepted and successful as described by several investigators (Poulos, 1995).

After determining the material parameters by back analysis, the necessary improvement for the area to stabilize landslide was determined by Slide software under dynamic loading according to the design guide of “Turkish General Directorate of Highways”. In this design guide, factor of safety is required to be $FOS \geq 1.10$ under dynamic loading.

The dynamic analyses at this stage were made by pseudo-static method. Seismic coefficient in Turkey changes between 0.05-0.2 values, recommended for design depending based on earthquake zone (Ozkan, 1998). In pseudo-static analysis the horizontal coefficient of acceleration was taken as $k_h = 0.2$ since the landslide area is in the first degree earthquake region according to Turkish Earthquake Code (TEC, 2007) as shown in Fig. 3.14 and Fig. 3.15.

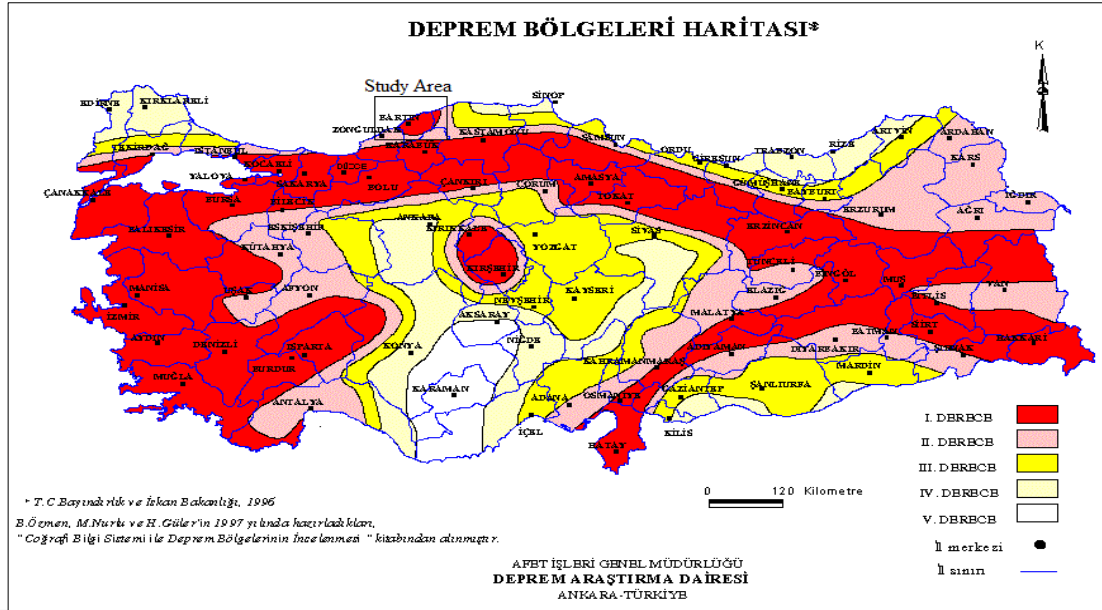


Figure 3.14 Earthquake zones of Turkey map.

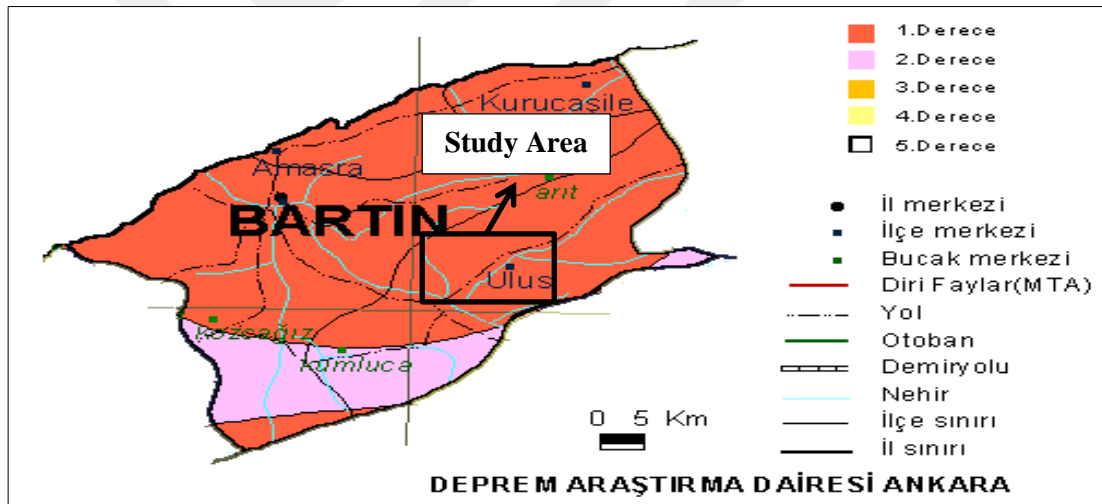


Figure 3.15 Earthquake zones map of study area.

In the slope stabilization analyses, the water table was different than the back analysis sections and taken to be constant after +105.00m elevation. Because, the back analysis had to model the current situation but the slope stabilization was made for long term conditions. A dam was being constructed at a very close distance to this site and level of dam lake will be at +105.00m elevation. So the water table had to be adopted to long term conditions. According to these analyses, to satisfy the requirement of “Turkish General Directorate of Highways”, 5 rows of piles were needed each of which had a diameter of $D = 1.20\text{m}$, length of $L = 40\text{m}$ and placed

center-to-center at 1.5m spacing in the third dimension. The results of the analyses are summarized in Table 3.2 and details are given in Fig. 3.16 – Fig. 3.21.

Table 3.2 Calculated FOS under dynamic loading after slope stabilization.

Cross Sections	Factor of Safety
Cross section 1-1	1.11
Cross section 2-2	1.11
Cross section 3-3	1.14
Cross section 4-4	1.11
Cross section 5-5	1.10
Cross section 6-6	1.10

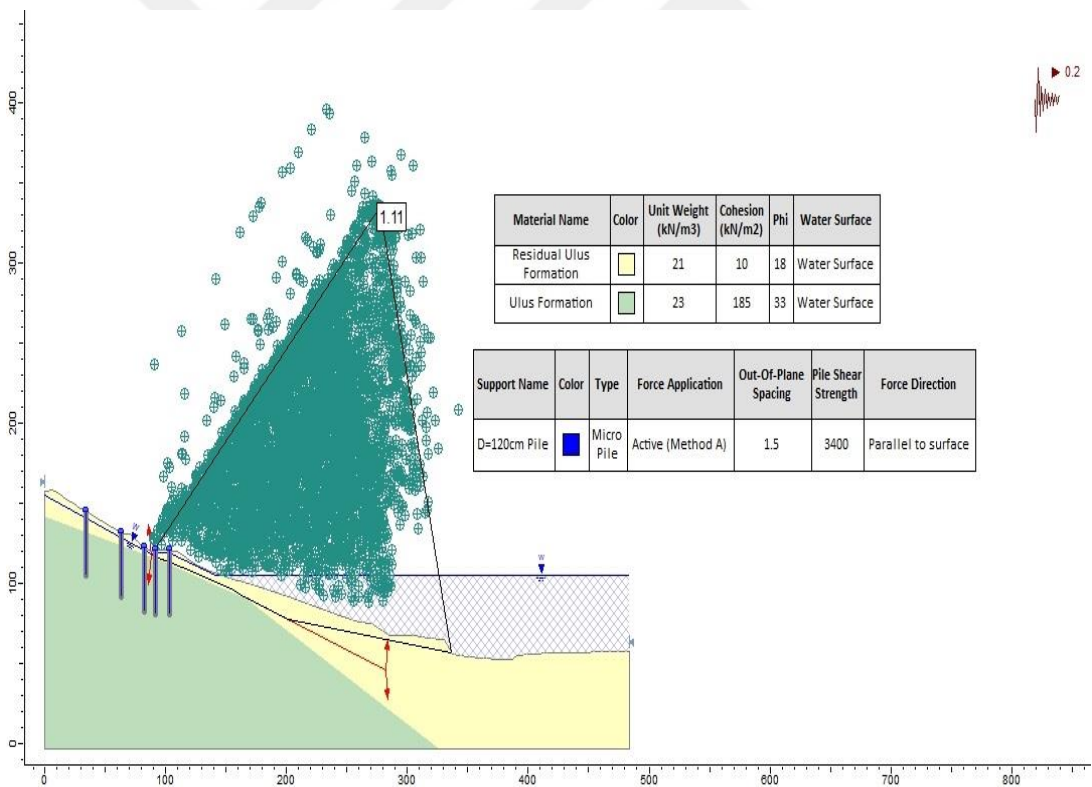


Figure 3.16 Section 1-1 after slope stabilization.

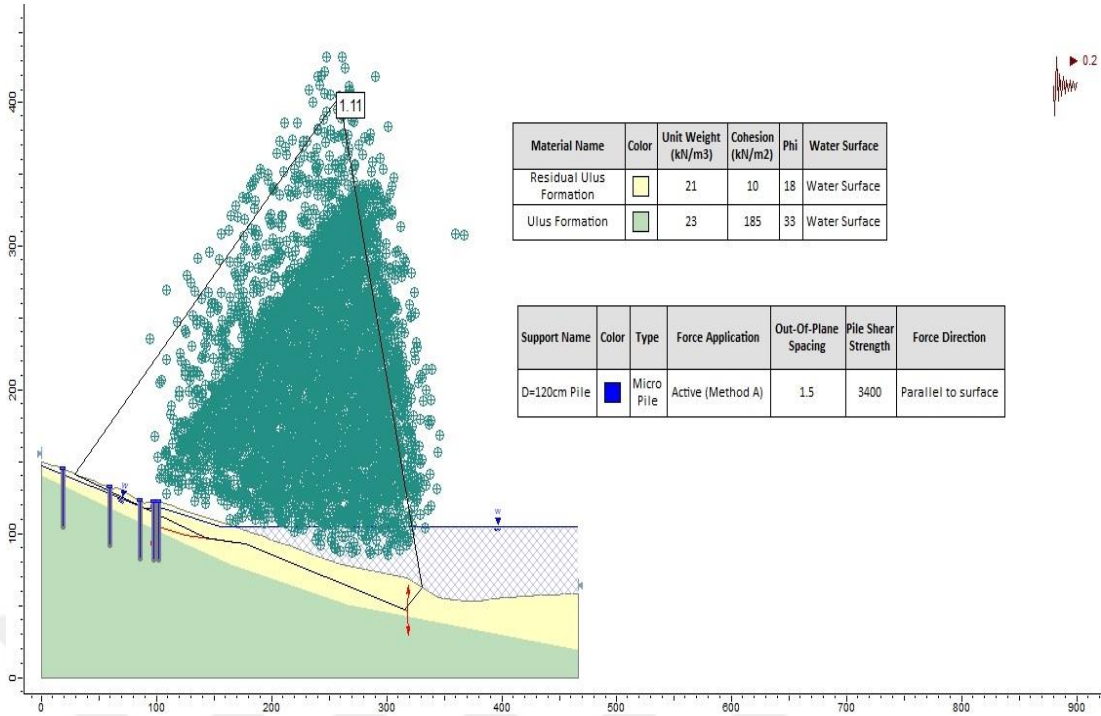


Figure 3.17 Section 2-2 after slope stabilization.

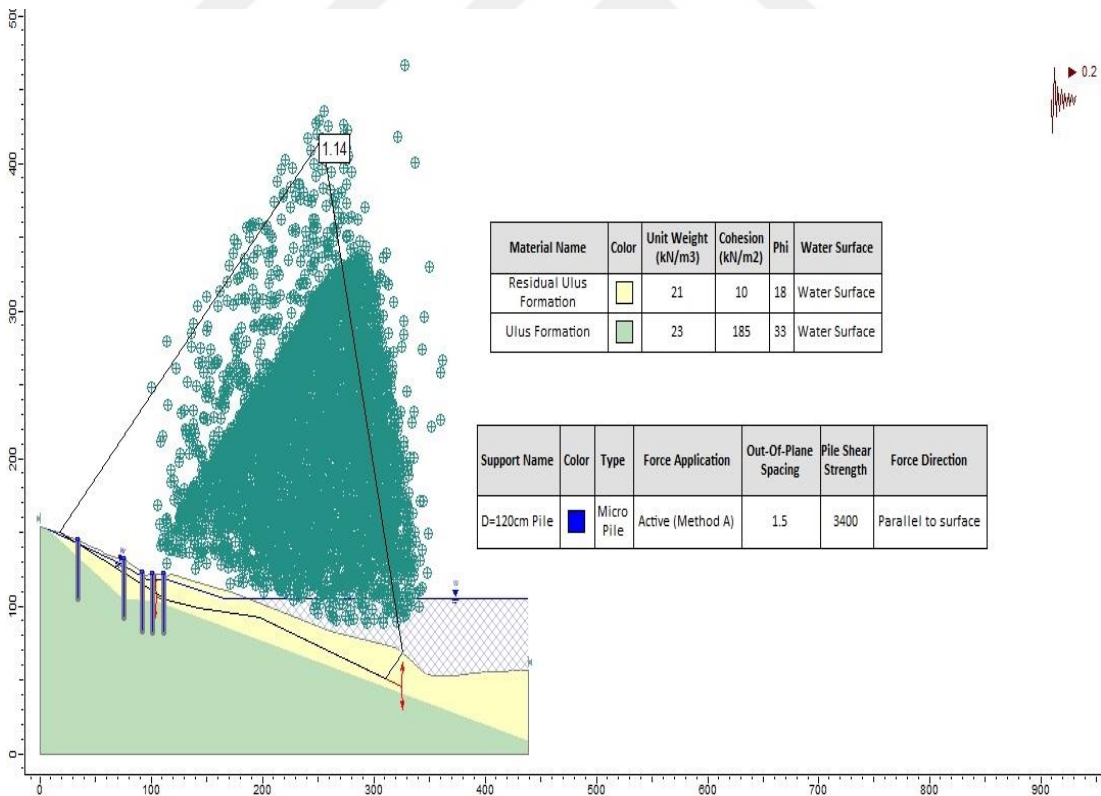


Figure 3.18 Section 3-3 after slope stabilization.

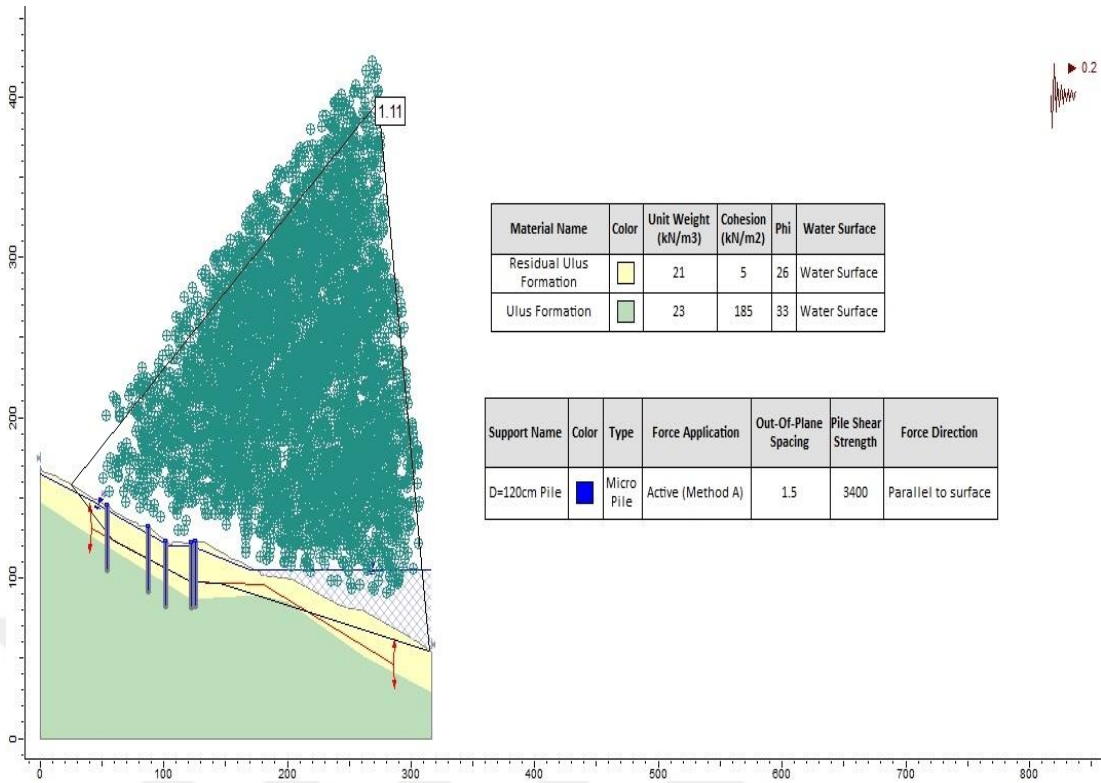


Figure 3.19 Section 4-4 after slope stabilization.

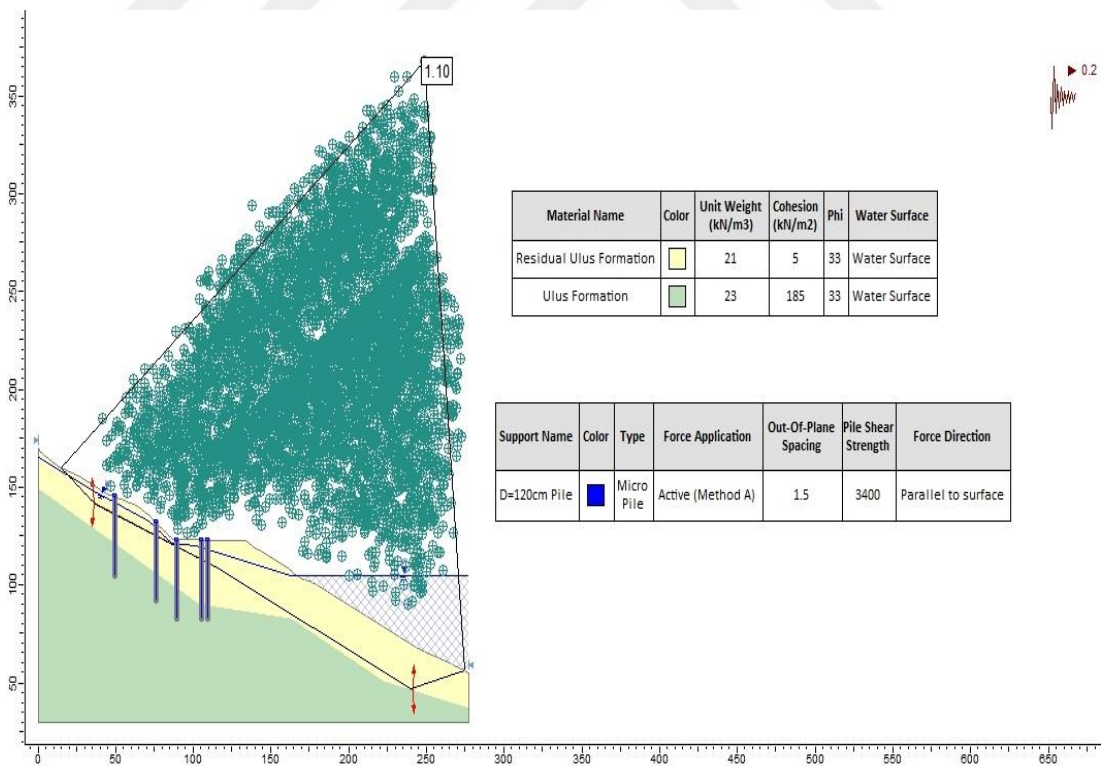


Figure 3.20 Section 5-5 after slope stabilization.

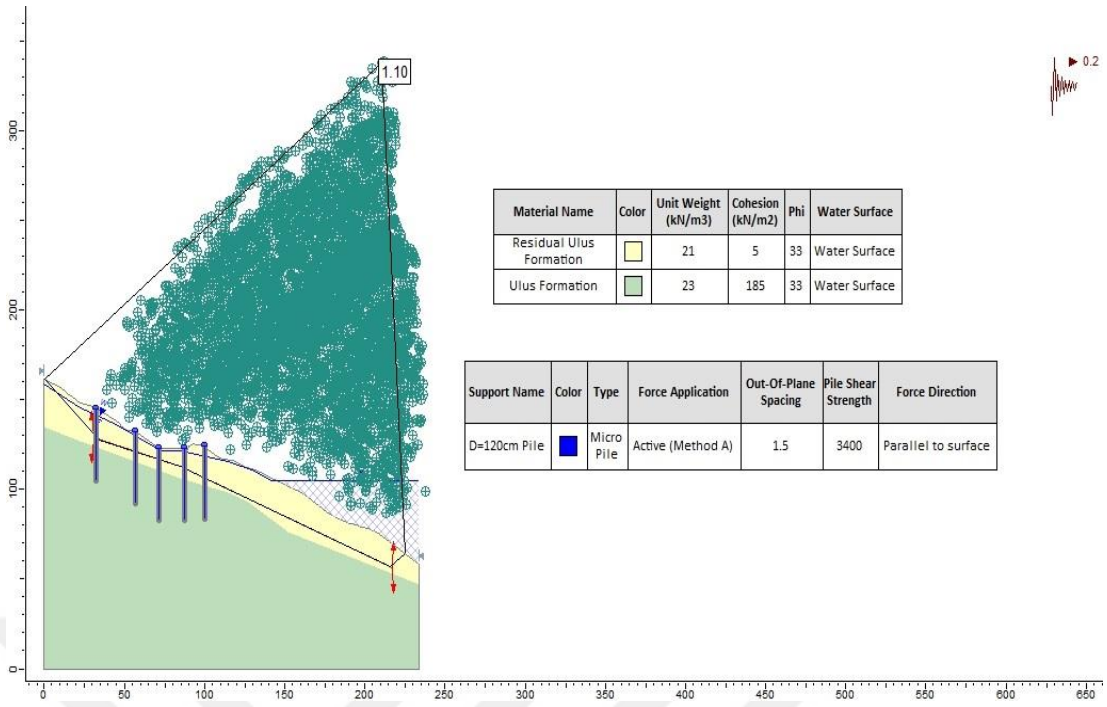


Figure 3.21 Section 6-6 after slope stabilization.

CHAPTER 4

ANALYSES AND RESULTS

4.1 Earthquake Records

In the previous chapter, the material parameters of the soil layers were determined and the analyses were continued by pseudo-static solutions to determine the necessary number of piles for slope stabilization according to the design guide of “Turkish General Directorate of Highways”. The results of these analyses had revealed that five rows of piles were needed to stabilize the analyzed slope to satisfy the requirements of the mentioned design guide.

In this design guide, the requirements are determined for pseudo-static analysis method. However, this method does not give any result for pile moment, shear and axial load which should be available for pile reinforcement detailing. For this purpose, time-history analysis by finite element method is mostly used in engineering applications. However, there is no guide for selection of the earthquake record. The only suggestion is for the maximum ground acceleration which is based on the earthquake regions described in TEC (2007). Any other earthquake characteristics are not considered during analyses and design. In this study, the effect of earthquake characteristics on pile behavior was investigated through time-history analyses by finite element method. Plaxis software was used in the analyses. The results were compared with each other.

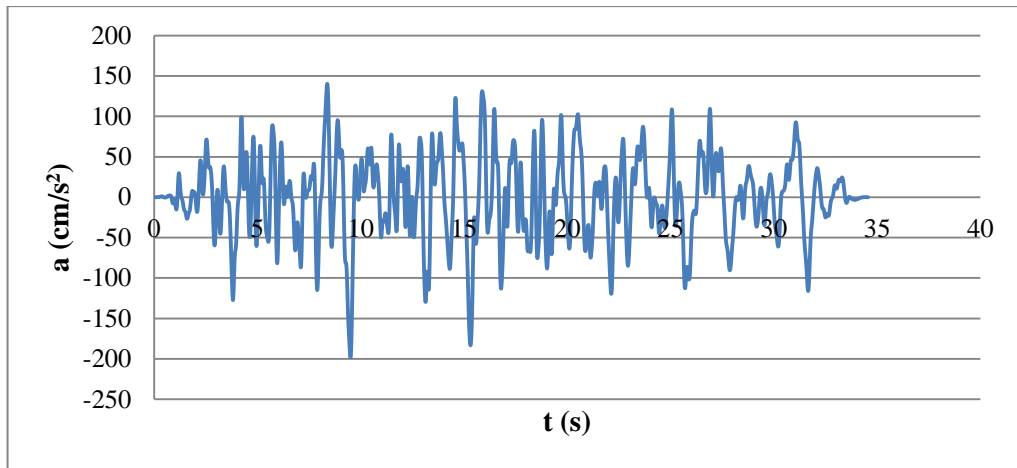
In this study, the section at the middle of the landslide area which has the thickest sliding mass (Section 4-4) was analyzed. Three different earthquake records which were generated by strike-slip faults were chosen. The records were selected in a way that the predominant frequency of the applied motion was approximately $f_n = 1, 2$ or 4Hz . The ground motion record of Landers earthquake was time scaled to make the $f_n = 1\text{Hz}$ by a time scale of $t_s = 0.75$. The motion data were acquired from the ground motion database of the “Pacific Earthquake Engineering Research Center, PEER”.

These data were originally filtered and baseline corrected. So, no other modification was applied to the original data. The list of the utilized ground motion records are given in Table 4.1.

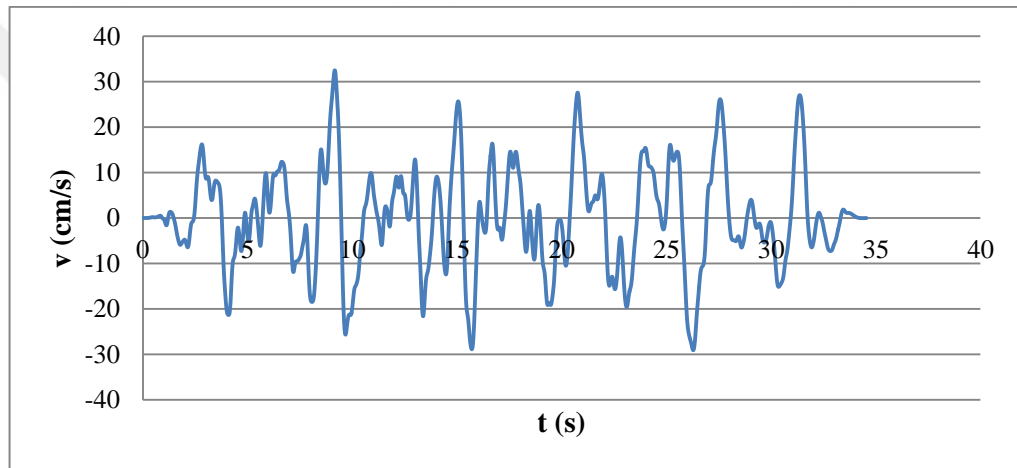
Table 4.1 Earthquake ground motion properties and locations.

Earthquake	Date	Station	Mechanism	f_n (Hz)
Landers	28.06.1992	Arcadia Av	Strike-Slip	1
Chalfant Valley	21.07.1986	Tinemaha Res	Strike-Slip	2
Loma Prieta	18.10.1989	Capitola	Strike-Slip	4

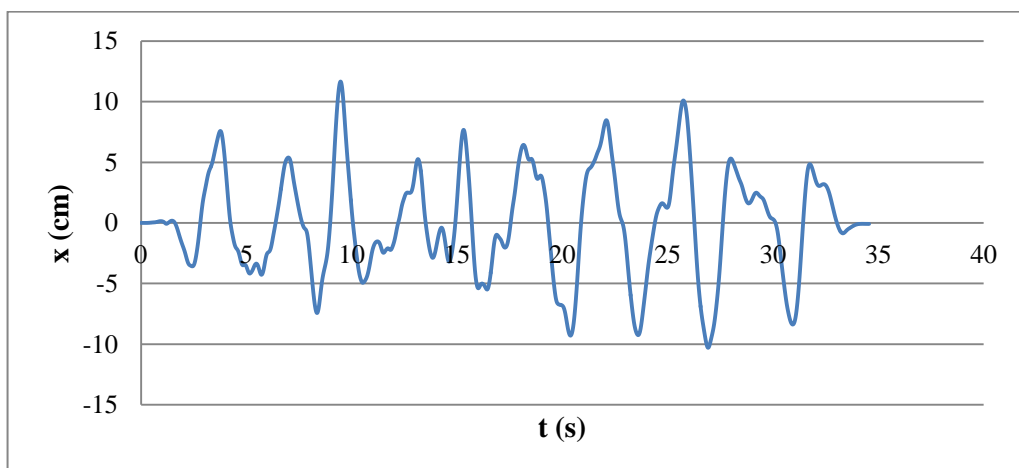
The earthquake records were all scaled to give a maximum horizontal acceleration of $a_{\max} = 0.2g$. The maximum acceleration was not taken as twice as much as the pseudo-static coefficient intentionally since the model dimensions and damping of the system were limited. The time histories and fourier amplitude spectra of the used motion records are given below in Fig. 4.1 – Fig. 4.6.



(a) Acceleration – Time history.

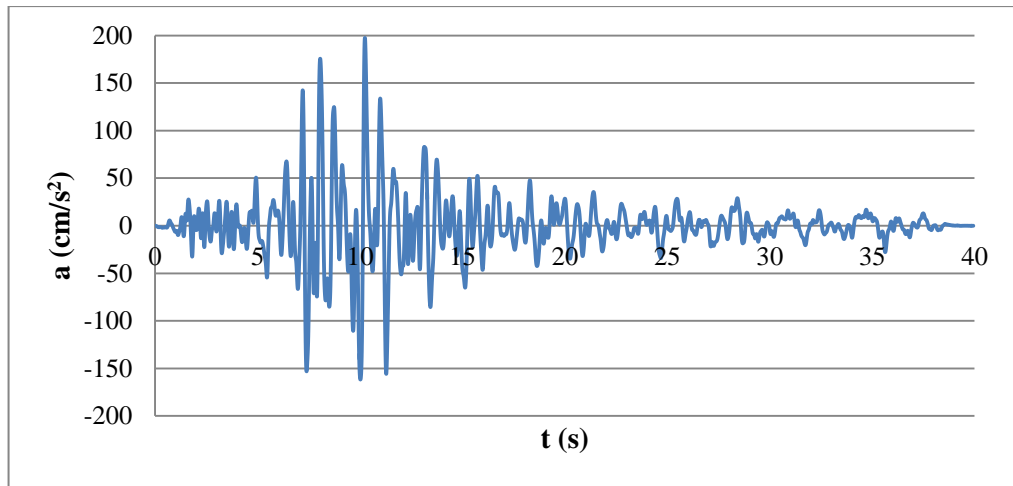


(b) Velocity – Time history.

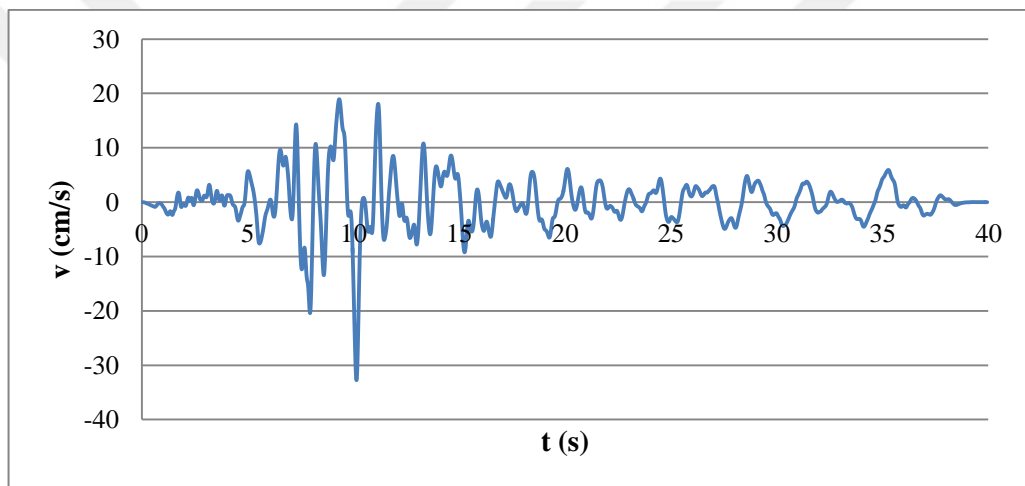


(c) Displacement – Time history.

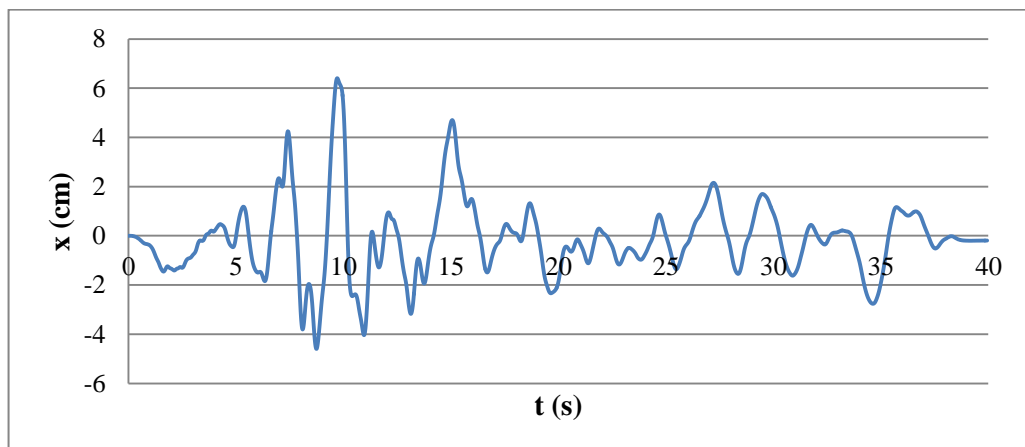
Figure 4.1 Time history data of Landers Earthquake.



(a) Acceleration – Time history.

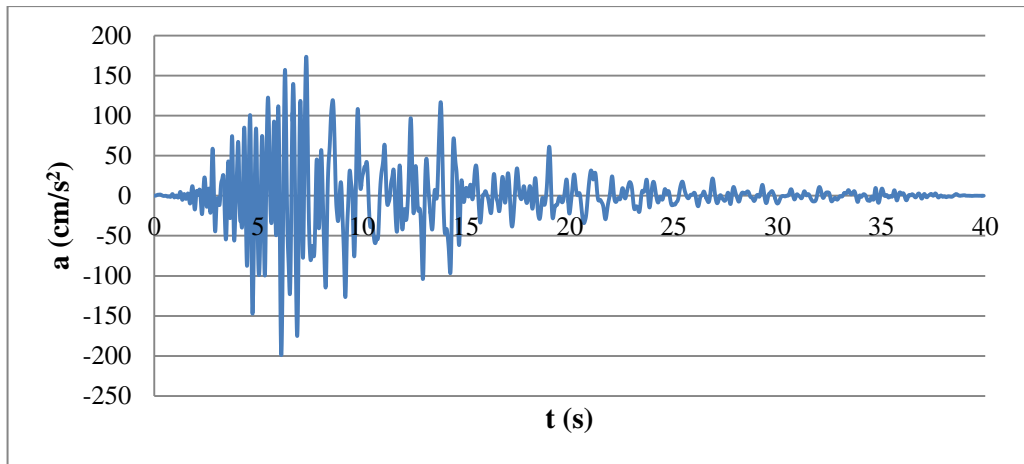


(b) Velocity – Time history.

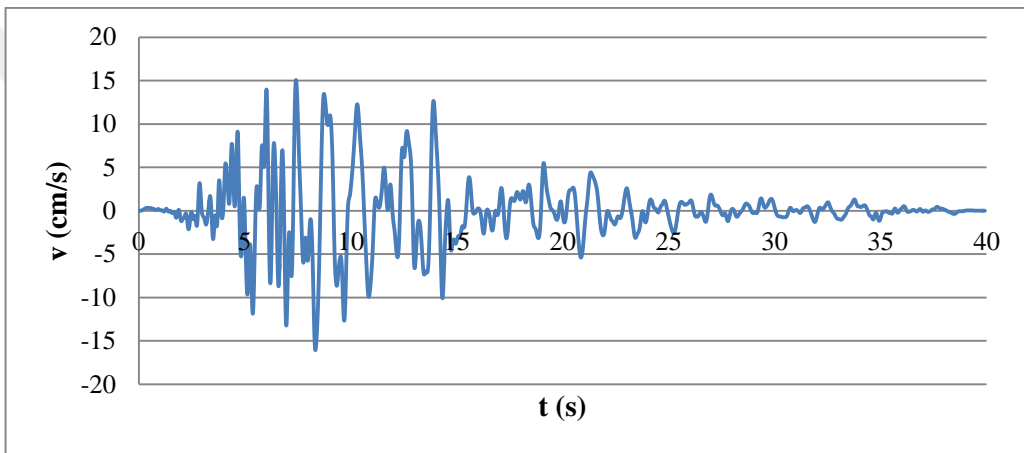


(c) Displacement – Time history.

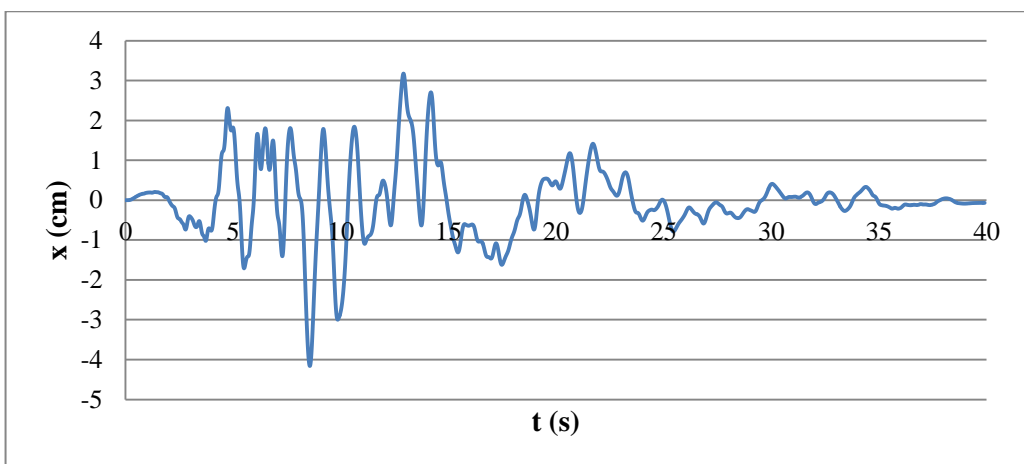
Figure 4.2 Time history data of Chalfant Valley Earthquake.



(a) Acceleration – Time history.



(b) Velocity – Time history.



(c) Displacement – Time history.

Figure 4.3 Time history data of Loma Prieta Earthquake.

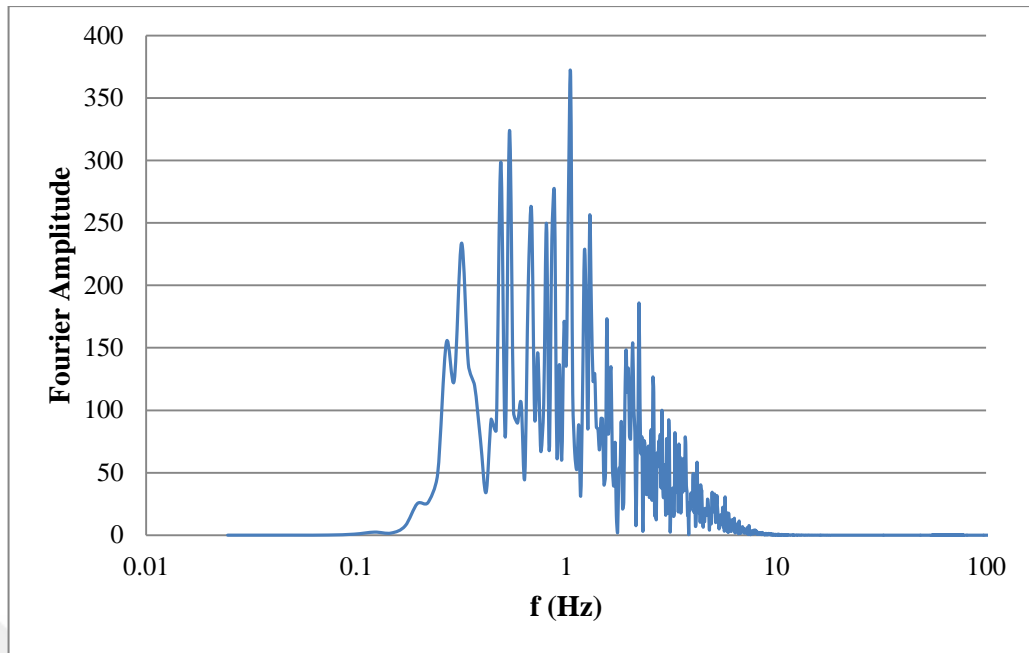


Figure 4.4 Fourier amplitude spectrum of Landers earthquake.

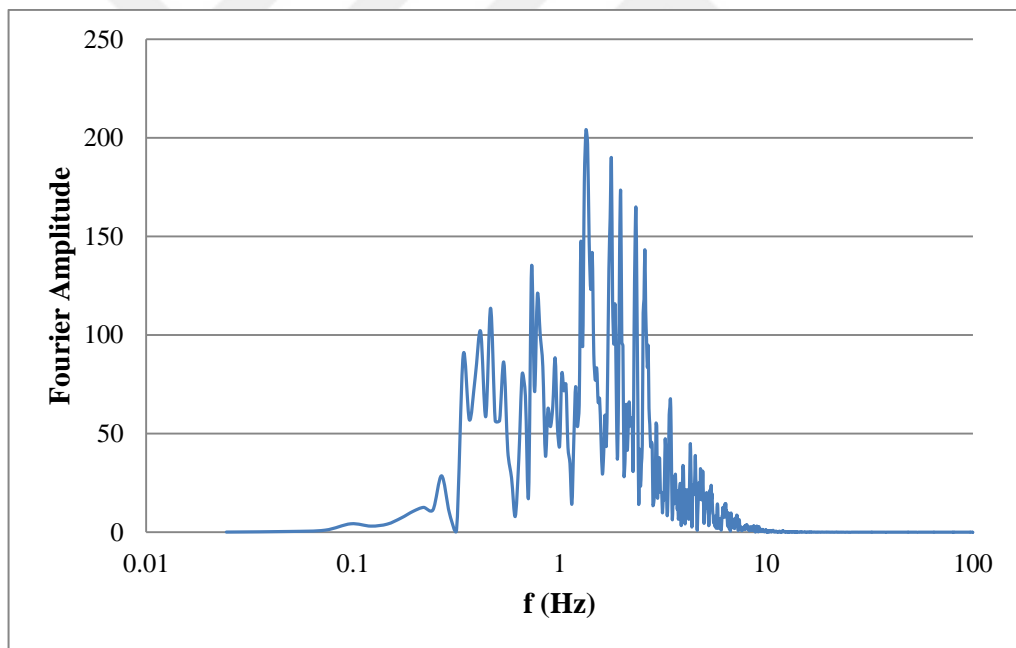


Figure 4.5 Fourier amplitude spectrum of Chalfant Valley earthquake.

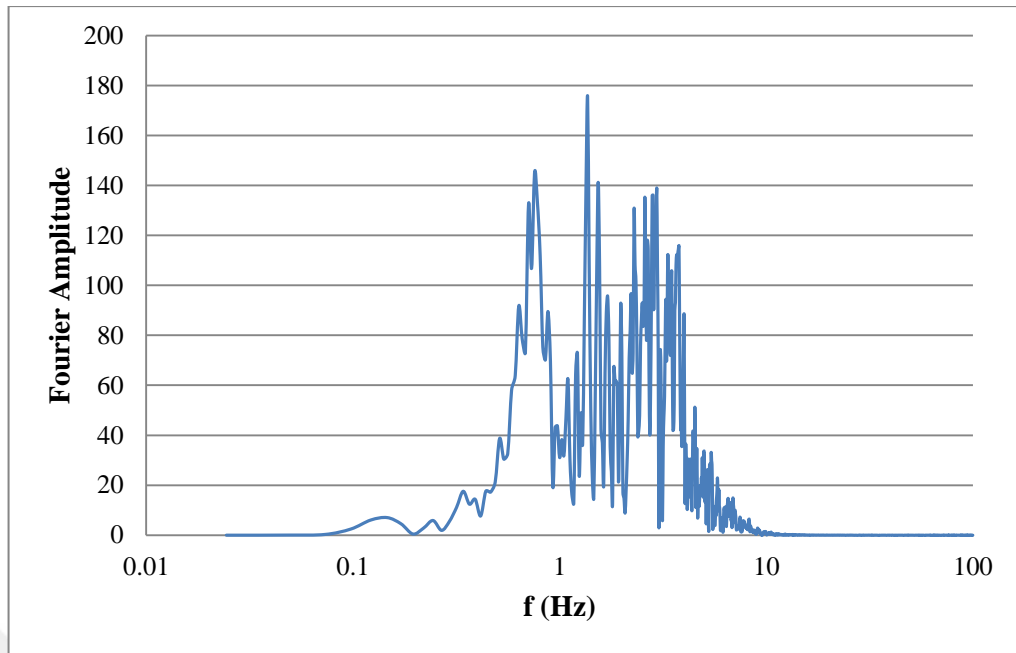


Figure 4.6 Fourier amplitude spectrum of Loma Prieta earthquake.

4.2 Finite Element Analyses

The section 4-4 is the critical cross section with the thickest sliding mass as mentioned before. This section was analyzed by finite element method using time history analysis. The model and mesh is given in Fig. 4.7. As it can be seen from this figure, the mesh is finer around the piles and gets coarser as gone from the piles through the boundaries. Basically, there are three materials which are “Residual Ulus Formation”, “Ulus Formation” and piles. The material properties used for these materials are given below in Table 4.2 and Table 4.3.

In the analyses, the initial case was modeled by gravity loading rather than “Ko procedure” since the ground is inclined. After this stage the piles were constructed and then the related earthquake record was applied to the model as time-history. This procedure was repeated for all analyses.

Table 4.2 Material properties of the soil layers.

Parameters	Name	Residual Ulus Formation	Ulus Formation	Units
Material model	-	Mohr-coulomb	Mohr-coulomb	-
Type of material behavior	-	Drained	Drained	-
Soil Unit weight	γ_{unsat}	21	23	kN/m ³
Soil Unit weight	γ_{sat}	21	23	kN/m ³
Young's modulus	E	$6 * 10^4$	$3 * 10^5$	kN/m ²
Poisson's ratio	ν	0.30	0.22	-
Cohesion	C	5	185	kN/m ²
Friction angle	ϕ	26	33	°
Psi	ψ	0	3	°
Interface strength	R_{int}	0.67	0.67	-

Table 4.3 Material properties of the plates (Piles).

Parameters	Name	Piles	Unit
Material type	-	Elastic	-
Normal stiffness	EA	$2.26 * 10^7$	kN/m
Flexural rigidity	EI	$2.04 * 10^6$	kNm ² /m
Weight	w	3.6	kN/m/m
Poisson's ratio	ν	0.2	-

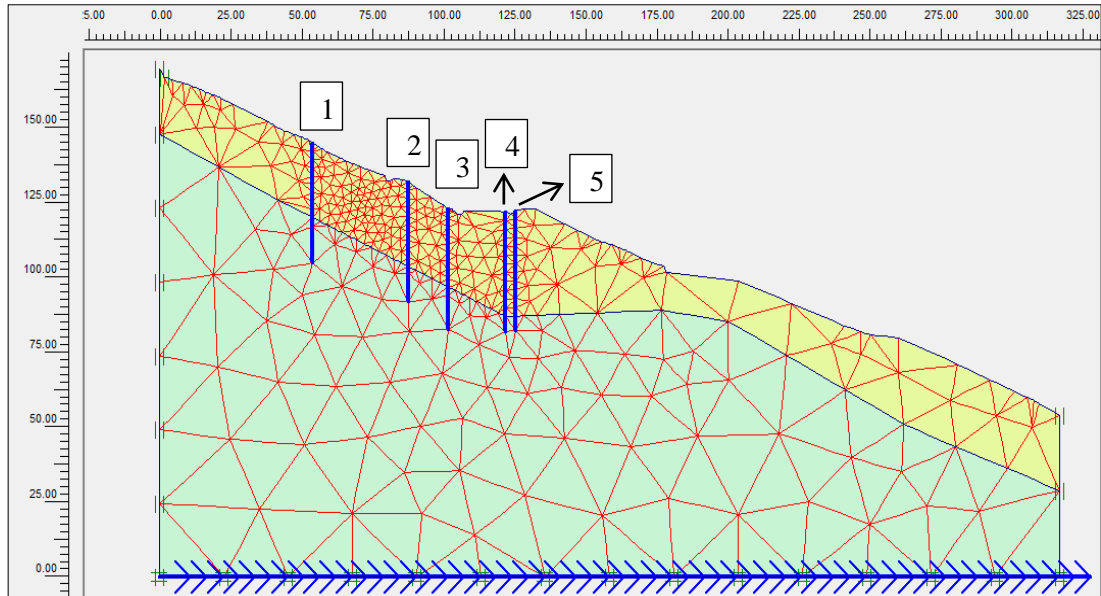


Figure 4.7 Finite element mesh of section 4-4.

4.3 Results and Discussions

The axial forces, shear forces and bending moments acting on 5 rows of piles were investigated separately. For each of these parameters the percent change between the maximum and minimum values calculated for different earthquakes were calculated. The values obtained from analysis are given in detail in Appendices A, B and C.

The axial forces calculated for different earthquake records were close to each other for all five rows of piles. The maximum change in axial force due to earthquake record for the same row of pile changed between 12% - 39%. Moreover, the axial forces were very high at the first row as compared to other rows which were more close to each other. The values are given in Table 4.4 and the data is plotted in Fig. 4.8.

Table 4.4 Pile Axial Forces.

Piles	Axial Forces (kN)			Maximum Change (%)
	Landers	Chalfant Valley	Loma Prieta	
1	7845	6945	6825	15
2	1770	1635	1274	39
3	2730	2670	2445	12
4	2415	2175	1770	36
5	2175	1905	1605	36

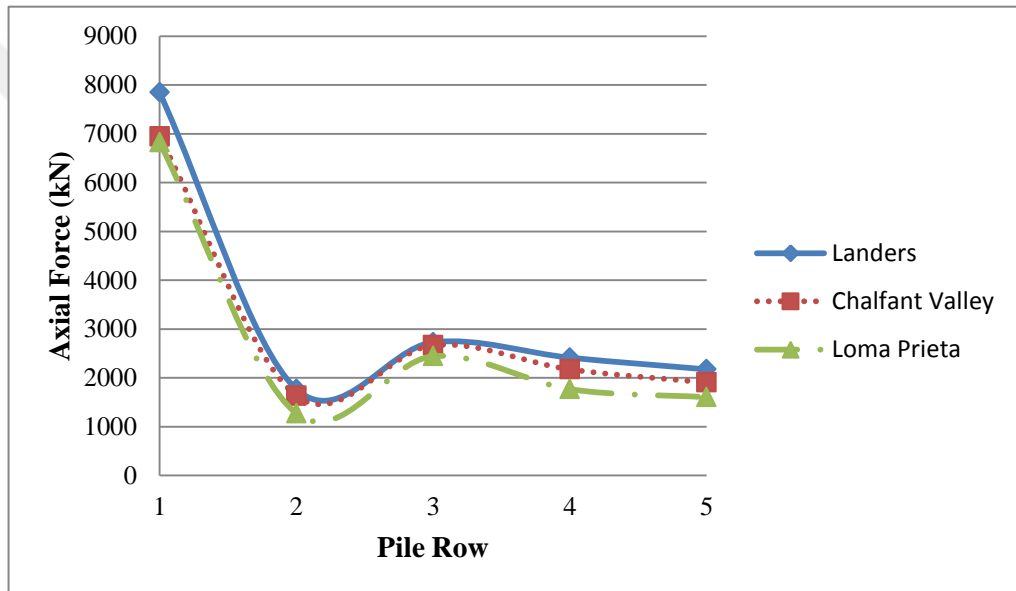


Figure 4.8 Pile Axial Forces.

The shear forces calculated for Chalfant Valley and Loma Prieta earthquakes were relatively close to each other as compared to the values obtained for Landers earthquake. The minimum values were obtained for Loma Prieta earthquake which has the highest predominant frequency and correspondingly the least dynamic displacements. The difference between minimum and maximum values was more critical for shear forces as compared to the axial forces which ranged between 31% - 143% with most of it in the 30% - 50% range. This showed that, the shear forces calculated for piles may vary significantly depending on the earthquake data used, which will change the design significantly. The values are given in Table 4.5 and the data is plotted in Fig. 4.9.

Table 4.5 Pile Shear Forces.

Piles	Shear Forces (kN)			Maximum Change (%)
	Landers	Chalfant Valley	Loma Prieta	
1	1371	979	931	47
2	2400	1164	987	143
3	1006	796	766	31
4	444	310	248	79
5	536	467	363	48

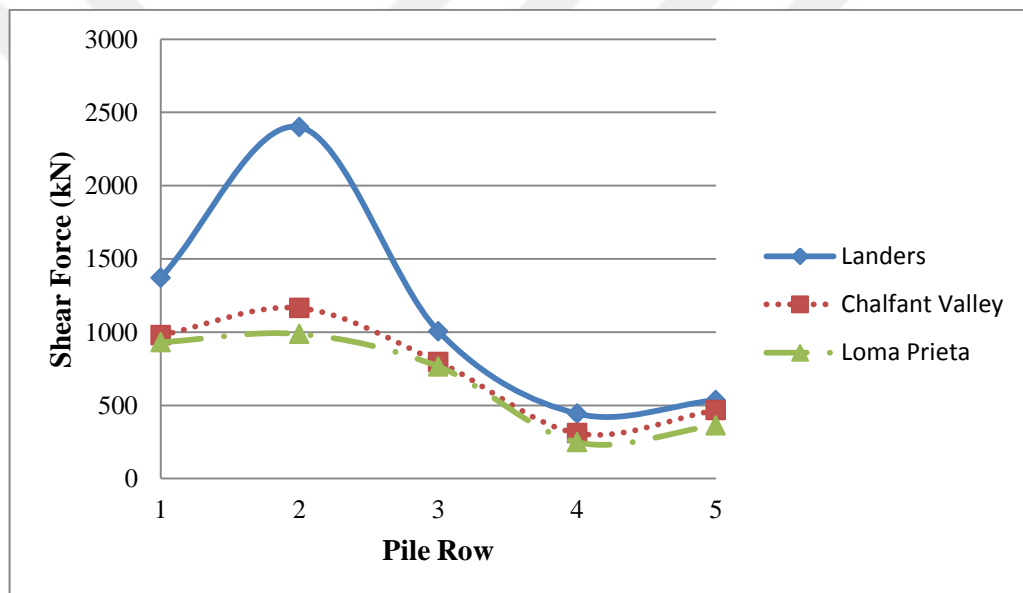


Figure 4.9 Pile Shear Forces.

Similar to the case in shear forces, bending moments calculated for Chalfant Valley and Loma Prieta earthquakes were relatively close to each other as compared to the values obtained for Landers earthquake. This is attributed to the relatively small displacements of Loma Prieta earthquake due to its higher frequency content. However, the differences in bending moments for different earthquake records were much critical as compared to the axial and shear forces which may lead to significant changes in the design. The percent change range was between 29% - 127% with most of them in the 70% - 100% band. The values are given in Table 4.6 and the data is plotted in Fig. 4.10.

Table 4.6 Pile Bending Moments.

Piles	Bending Moments (kNm)			Maximum Change (%)
	Landers	Chalfant Valley	Loma Prieta	
1	6585	3540	2895	127
2	12435	7980	7095	75
3	9255	5865	5550	67
4	1590	990	773	106
5	814	761	632	29

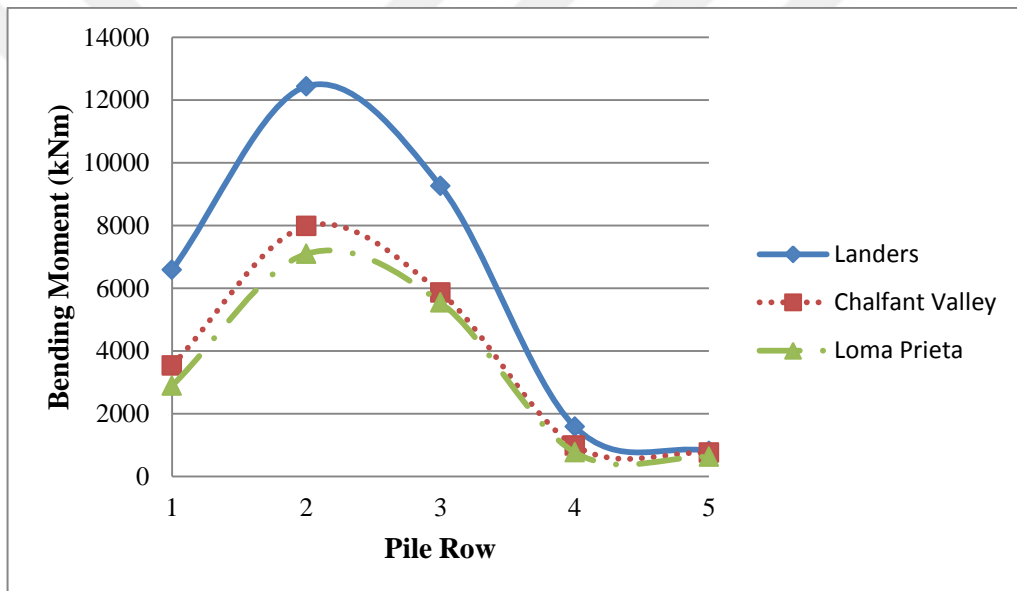


Figure 4.10 Pile Bending Moments.

CHAPTER 5

CONCLUSIONS

5.1 Limit Equilibrium Analyses

The slope instability observed at a site in western part of the Black Sea region of Turkey was analyzed by both limit equilibrium and finite element methods. The steps during the study can be summarized as follows:

- The slip surfaces were determined on six different cross sections based on inclinometer readings. The inclinometer readings revealed a non-circular failure for the investigated sections.
- The shear strength parameters of the sliding soil mass were determined by back analysis of the investigated sections by limit equilibrium solutions. Janbu corrected method was used in back analysis since it is known to give better results for non-circular slip surfaces.
- The necessary number and location of piles to satisfy the safety requirements according to the design guide of “T.C. General Directorate of Highways” were determined based on pseudo-static solutions.
- A horizontal seismic coefficient of $k_h = 0.2$ was used since the investigated site was located in the first degree (most active) seismic region according to Turkish Earthquake Code.
- Under seismic loading the analyses revealed that, five rows of piles having a diameter of $D = 1.2$ m and length of $L = 40$ m placed at $s = 1.5$ m center-to-center spacing were needed to meet $FOS \geq 1.10$ condition by pseudo-static analysis.

5.2 Finite Element Analyses

- After limit equilibrium analyses, the section at the middle of landslide area which also had the thickest sliding mass (Section 4-4) was modeled in plane-strain in Plaxis software.
- The effect of earthquake characteristics were investigated through real time dynamic analyses.
- The records of Landers, Chalfant Valley and Loma Prieta earthquakes were selected to be used in the dynamic analysis.
- The records were selected in a way that the predominant frequency of the applied motion was approximately $f_n = 1, 2$ or 4Hz .
- The ground motion record of Landers earthquake was time scaled to make the $f_n = 1\text{Hz}$ by a time scale of $t_s = 0.75$.
- The motion data were acquired from the ground motion database of the “Pacific Earthquake Engineering Research Center, PEER”. These data were originally filtered and baseline corrected. So, no other modification was applied to the original data.
- The earthquake records were all scaled to give a maximum horizontal acceleration of $a_{\max} = 0.2g$.
- In finite element analyses, the initial case was modeled by gravity loading rather than “Ko procedure” since the ground is inclined. After this stage the piles were constructed and then the related earthquake record was applied to the model as time-history. This procedure was repeated for all analyses.

5.3 Discussions and Conclusions

The main findings of the study according to the performed analyses can be summarized as follows:

- The axial forces calculated for different earthquake records were close to each other for all five rows of piles.
- The maximum change in axial force due to earthquake record for the same row of pile changed between 12% - 39%. Moreover, the axial forces were very high at the first row as compared to other rows.

- The shear forces calculated for Chalfant Valley and Loma Prieta earthquakes were relatively close to each other as compared to the values obtained for Landers earthquake. The minimum values were obtained for Loma Prieta earthquake which has the highest predominant frequency and correspondingly the least dynamic displacements.
- The difference between minimum and maximum values was more critical for shear forces as compared to the axial forces which ranged between 31% - 143% with most of it in the 30% - 50% range.
- This fact revealed that, the shear forces calculated for piles may vary significantly depending on the earthquake data used, which will change the design significantly.
- Similar to the case in shear forces, bending moments calculated for Chalfant Valley and Loma Prieta earthquakes were relatively close to each other as compared to the values obtained for Landers earthquake.
- This fact is attributed to the relatively small displacements of Loma Prieta earthquake due to its higher frequency content. However, the differences in bending moments for different earthquake records were much critical as compared to the axial and shear forces which may lead to significant changes in the design. The percent change range was between 29% - 127% with most of them in the 70% - 100% band.

Based on these findings, it is concluded that the earthquake characteristics significantly affect the analysis results. A dynamic analysis procedure based solely on the magnitude of maximum horizontal acceleration may lead to significant errors in detailing of structural members. A conservative solution may significantly increase the construction costs while an unconservative solution would treat the stability of the slope during an earthquake.

REFERENCES

- Abramson, L. W., Lee, T. S., Sharma, S., Boyce, G. M. (2002). Slope stability and stabilization methods, 2nd Edition, published by John Willey & Sons, Inc.
- Albataineh, N. (2006). Slope stability analysis using 2D and 3D methods, *MSc Thesis*, University of Akron.
- Anderson, M. G. and Richards, K. S. (1987). Modeling slope stability: the complimentary nature of geotechnical and geomorphological approaches, *Slope Stability: Geotechnical Engineering and Geomorphology*. John Wiley and Sons. 1-9.
- Azzouz, A.S., Baligh, M.M. and Ladd, C.C. (1981). Three-dimensional stability analyses of four embankment failures, *In Proceedings of the 10th International Conference on Soil Mechanics and Foundation Engineering*, **3**, 343-346, Stockholm.
- Bishop, A. W. (1955). The use of the slip circle in the stability analysis of slopes, *Geotechnique*, **5**, 7-17.
- Bouckovalas, G. D. and Papadimitriou, A. G. (2005). Numerical evaluation of slope topography effects on seismic ground motion, *Soil Dynamics and Earthquake Engineering*, **25** (7), 547-558.
- Brinkgreve, R. B. J. (2002). Plaxis version 8, Dynamic manual, Delft University of Technology and Plaxis b. v., The Netherlands
- Chandler, R J. (1977). Back analysis techniques for slope stabilization works: a case record, *Geotechnique*, **27** (4), 479-495.
- Cho, K.H. (2002). Deterministic and probabilistic analysis of rock slope stability under earthquake loading conditions, *PhD dissertation*, Purdue University.
- Chopra, A. K. (2011). Dynamics of structures: theory and applications to earthquake engineering, 4th Edition, International Series in Civil Engineering and Engineering Mechanics, Prentice Hall.

Chowdhury, I. and Dasgupta, S. P. (2008). Dynamics of structure and foundation-a unified approach: 2. applications, CRC Press.

Chowdhury, R., Zhang, S. and Flentje, P. (2004). Reliability updating and geotechnical back-analysis. Proc. Advances in Geotechnical Engineering: *The Skempton Conference*, R. J. Jardine, D. M. Potts, and K. G. Higgins, eds., Thomas Telford, London.

Chugh, A. K. (1986). Variable interslice force inclination in slope stability analysis, *Soils and Foundation*, Japanese Society of SMFE, **26** (1), 115-121.

Cornforth, D. H. (2005). Landslides in practice. Investigation, analysis, and remedial/preventative options in soils, John Wiley & Sons Inc. Hoboken New Jersey.

Das, B. M. and Ramana, G. V. (2011). Principles of soil dynamics, Cengage Learning, 2nd Edition, Printed in the United States of America.

Deschamps, R. and Yankey, G. (2006). Limitations in the back-analysis of strength from failures, *Journal of geotechnical and geoenvironmental engineering*, **132** (4), 532-536.

Duncan, J. M. and Stark, T. D. (1992). Soil strengths from back analysis of slope failures, In *Stability and Performance of Slopes and Embankments II*, 890-904, ASCE.

Duncan, J. M., Wright, S. G. and Brandon, T. L. (2014). Soil strength and slope stability, 2nd Edition, John Wiley & Sons.

Fang, H. Y. (1991). Foundation engineering handbook, 2nd Edition, Springer Science & Business Media, New York.

Fellenius, W. (1936). Calculation of the stability of earth dams. In Transactions of the 2nd congress on large dams, Washington DC, **4**, 445-463. International Commission on Large Dams (ICOLD) Paris.

Gilbert, R. B., Wright, S. G. and Liedtke, E. (1998). Uncertainty in back-analysis of slopes: Kettleman Hills case history, *Journal of Geotechnical and Geoenvironmental engineering*, **124** (12), 1167–1176.

Griffiths, D. V. and Lane, P. A. (1999). Slope stability analysis by finite elements, *Geotechnique*, **49** (3), 387-403.

Highland, L. (2004). Landslide types and processes (No. 2004-3072).

Hynes-Griffin, M. E. and Franklin, A. G. (1984). Rationalizing the seismic coefficient method, (No. WES/MP/GL-84-13). *Army Engineer Waterways Experiment Station Vicksburg MS*, Geotechnical Lab.

Janbu, N. (1959). Stability analysis of slopes with dimensionless parameters, Harvard University, Division of Engineering and Applied Physics.

Janbu, N. (1973). Slope stability computations. Embankment Dam Engineering, Casagrande Volume, 47-86.

Jiang, J. C. and Yamagami, T. (2008). A new back analysis of strength parameters from single slips, *Computers and Geotechnics*, **35** (2), 286-291.

Jibson, R. W. (2011). Methods for assessing the stability of slopes during earthquakes—a retrospective, *Engineering Geology*, **122** (1), 43-50.

Koo, R. C. H., Pappin, J. W., Rule, D. C., Wallace, M. I., and Yim, I. P. H. Dynamic Analyses of slopes in Hong Kong,

<http://www.aees.org.au/wp-content/uploads/2013/11/42-PAPPIN Jack.pdf>.

Kramer, S. L. (1996). Geotechnical earthquake engineering, Prentice Hall, Inc., Upper Saddle River, New Jersey 07458.

Leonards, G. A. (1982). Investigation of failures, *Journal of the Geotechnical Engineering Division*, **108** (2), 185-246.

Leroueil, S. and Tavenas, F. (1981). Pitfalls of back-analysis, In Proc., *10th Int. Conf. on Soil Mechanics and Foundation Engineering*, **1**, 185-190. Stockholm.

Lowe, J. and Karafiath, L. (1960). Stability of earth dam upon drawdown, Proceedings of, *first Pan American Conference on Soil Mechanics and Foundation Engineering*, Mexico City, **552**, 537-552.

Luckman, P. G., Der Kiureghian, A. and Sitar, N. (1987). Use of stochastic stability analysis for Bayesian back calculation of pore pressures acting in a cut at failure, *Proc., 5th Int. Conf. on Application of Statistics and Probability in Soil and Struct. Eng.*, 922-929.

Marcuson III, W. F. and Franklin, A. G. (1983). Seismic design, analysis, and remedial measures to improve stability of existing earth dams, (No. WES/MP/GL 83-23). *Army Engineer Waterways Experiment Station vicksburg Miss*, Geotechnical Lab.

Melo, C. and Sharma, S. (2004). Seismic coefficients for pseudo-static slope analysis, *In 13th World Conference on Earthquake Engineering*, 369-383 Vancouver, Canada.

Morgenstern, N. R. and Price, V. E. (1965). The analysis of the stability of general slip surfaces, *Geotechnique*, **15** (1), 79-93.

Newmark, N. M. (1965). Effects of earthquakes on dams and embankments, *Geotechnique*, **15** (2), 139-160.

Ng, S. M., Ismail, M. A. M. and Abustan, I. (2014). Back analysis of slope failure using finite element with point estimate method (FEM-PEM), *Journal of Civil Engineering Research*, **4** (3A), 31-35.

Numata, M. (1960). Earthquake-resistant design for civil engineering structures, Earth-Structures and Foundations in Japan, *Report, Japan Soc. of Civ. Engrs.*, Tokyo, **4**, 37-66.

Ozkan, M. Y. (1998). A review of considerations on seismic safety of embankments and earth and rock-fill dams, *Soil Dynamics and Earthquake Engineering*, **17** (7), 439-458.

Poulos, H. G. (1995). Design of reinforcing piles to increase slope stability, *Canadian Geotechnical Journal*, **32** (5), 808-818.

RocScience. (2004). A New era in slope stability analysis: shear strength reduction finite element technique. *RocNews*, 1-10.

- Sarma, S. K. (1973). Stability analysis of embankments and slopes, *Geotechnique*, **23** (3), 423-33.
- Seed, H. B. (1979). Considerations in the earthquake-resistant design of earth and rockfill dams, *Geotechnique*, **29** (3), 215-263.
- Seed, H. B. and Goodman, R. E. (1964). Earthquake stability of slopes of cohesionless soils, *Journal of the Soil Mechanics and Foundations Division*, **90** (6), 43-74.
- Seed, H. B. and Martin, G. R. (1966). The seismic coefficient in earth dam design, *Journal of the Soil Mechanics and Foundations Division*, **92** (3), 25-58.
- Sica, S., Pagano, L. and Modaressi, A. (2008). Influence of past loading history on the seismic response of earth dams, *Computers and Geotechnics*, **35** (1), 61-85.
- Sigaran-Loria C, Kaynia AM and Hack R (2007) Soil stability under earthquakes: a sensitivity analysis. In: Proceedings of the 4th international conference on earthquake geotechnical engineering, Thessaloniki, Greece.
- Siyahi, B. and Arslan, H. (2008). Nonlinear dynamic finite element simulation of Alibey earth dam, *Environmental geology*, **54** (1), 77-85.
- Skempton, A. W. (1964). Long-term stability of clay slopes, *Geotechnique*, **14** (2), 77-102.
- Skempton, A. W. (1985). Residual strength of clays in landslides, folded strata and the laboratory, *Geotechnique*, **35** (1), 3-18.
- Spencer, E. (1967). A method of analysis of the stability of embankments assuming parallel inter-slice forces, *Geotechnique*, **17** (1), 11-26.
- Stark, T. D., Eid, H. T. (1998). Performance of three-dimensional slope stability methods in practice, *Journal of Geotechnical and Geoenvironmental engineering*, **124** (11), 1049-1060.
- Tang, W.H., Stark, T.D. and Angulo, M. (1998). Reliability in back analysis of slope failures, *Soils and Foundations*, **39** (5), 73-80.

TEC (2007). Specification for structures to be built in disaster areas. Ministry of Public Works and Settlement Government of Republic of Turkey.

Terzaghi, K. (1950). Mechanisms of landslides, *engineering geology* (Berdey) volume. Geological Society of America.

Tiwari, B., Brandon, T. L., Marui, H. and Tuladhar, G. R. (2005). Comparison of residual shear strengths from back analysis and ring shear tests on undisturbed and remolded specimens, *Journal of Geotechnical and Geoenvironmental engineering*, **131** (9), 1071–1079.

US Army Corps of Engineers (2003). Engineering and design: slope stability, Engineer Manual 1110-2-1902.

Wang, L., Hwang, J. H., Luo, Z., Juang, C. H. and Xiao, J. (2013). Probabilistic back analysis of slope failure—a case study in Taiwan, *Computers and Geotechnics*, **51**, 12-23.

Wesley, L. D. and Leelaratnam, V. (2001). Shear strength parameters from back-analysis of single slips, *Geotechnique*, **51** (4), 373–374.

Whitman, R. V. and Bailey, W. A. (1967). Use of computers for slope stability analysis, *Journal of Soil Mechanics and Foundations Div.*, **93** (4), 475-498.

Xueliang, J., Yongquan, Y. and Hui, Y. (2015) Seismic response and stability analysis of rock slope with underground caverns, *Electronic Journal of Geotechnical Engineering*, **20** (24), 11847-11860.

Zhang, J., Tang, W. H. and Zhang, L. M. (2010). Efficient probabilistic back-analysis of slope stability model parameters, *Journal of geotechnical and geoenvironmental engineering*, **136** (1), 99-109.

Zhou, G. Y. and Zuo, X. (2014). Finite element method analysis on slope stability under seismic dynamic, *Green Building, Materials and Civil Engineering*, 279-285.

APPENDICES

Appendix A Pile Axial Force Envelope Diagrams

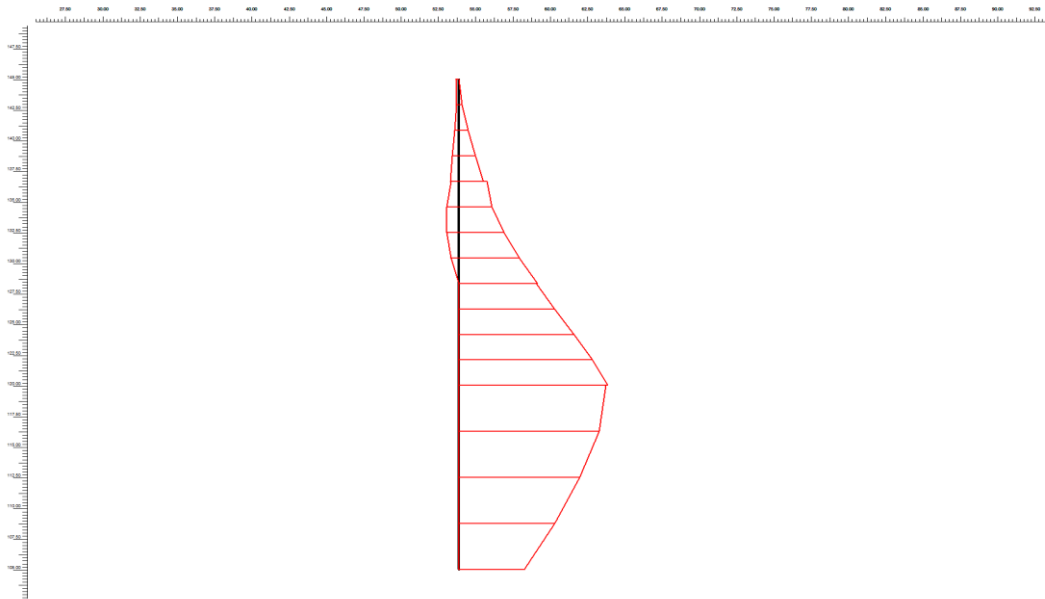


Figure A.1 Axial force diagram of Landers EQ for pile 1 ($N = 5230$ kN/m).

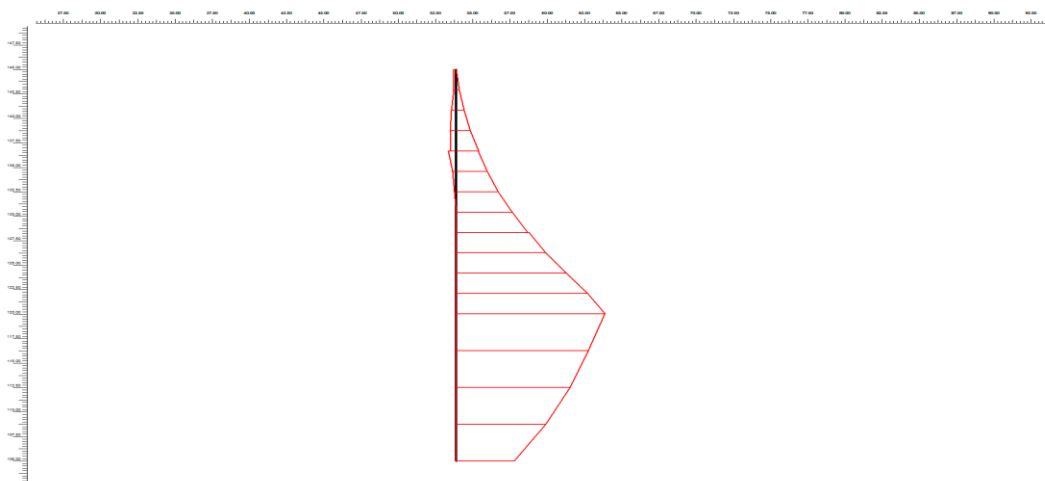


Figure A.2 Axial force diagram of C. Valley EQ for pile 1 ($N = 4630$ kN/m).

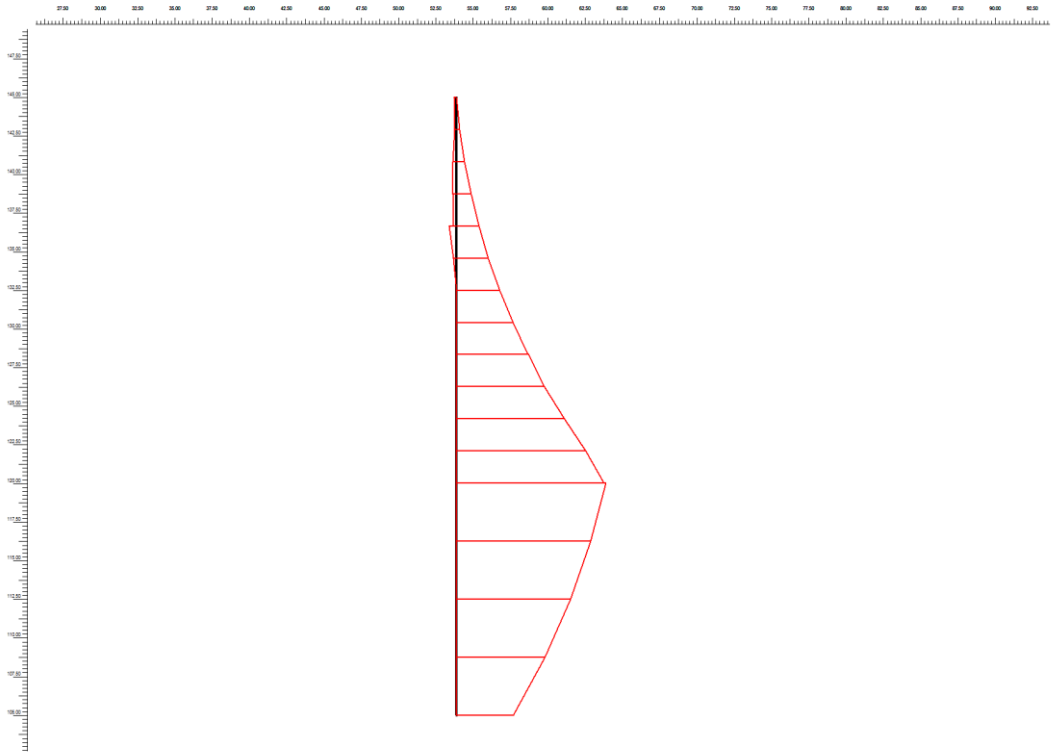


Figure A.3 Axial force diagram of L. Prieta EQ for pile 1 ($N = 4550 \text{ kN/m}$).

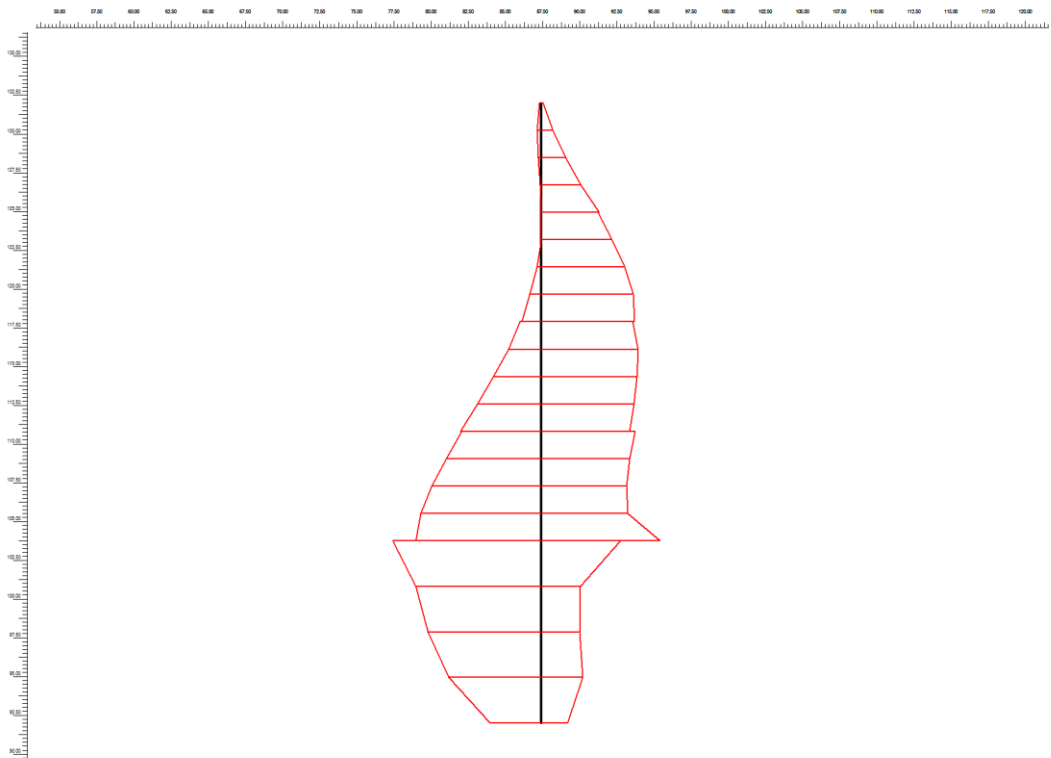


Figure A.4 Axial force diagram of Landers EQ for pile 2 ($N = 1180 \text{ kN/m}$).

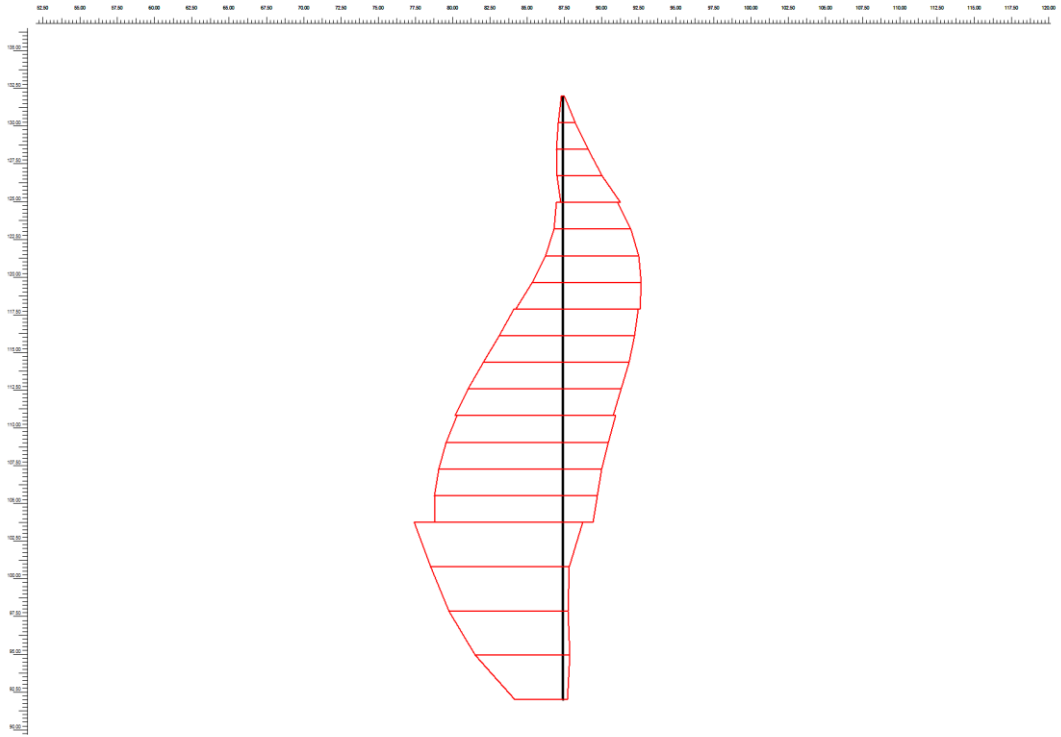


Figure A.5 Axial force diagram of C. Valley EQ for pile 2 ($N = 1090$ kN/m).

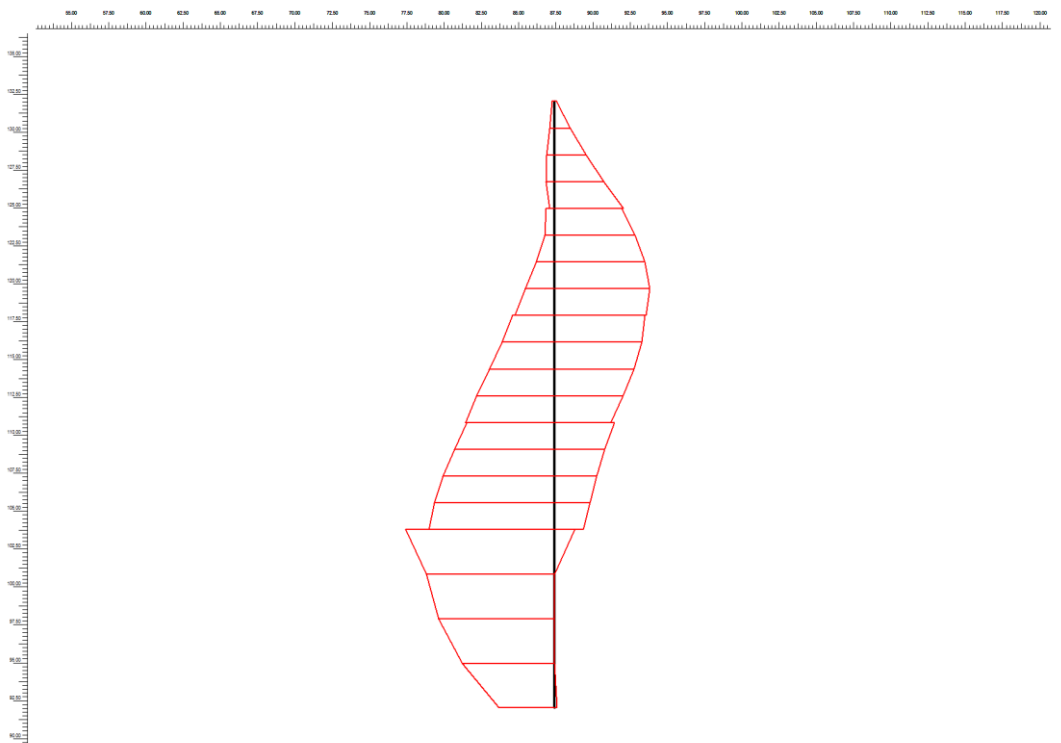


Figure A.6 Axial force diagram of L. Prieta EQ for pile 2 ($N = 848.98$ kN/m).

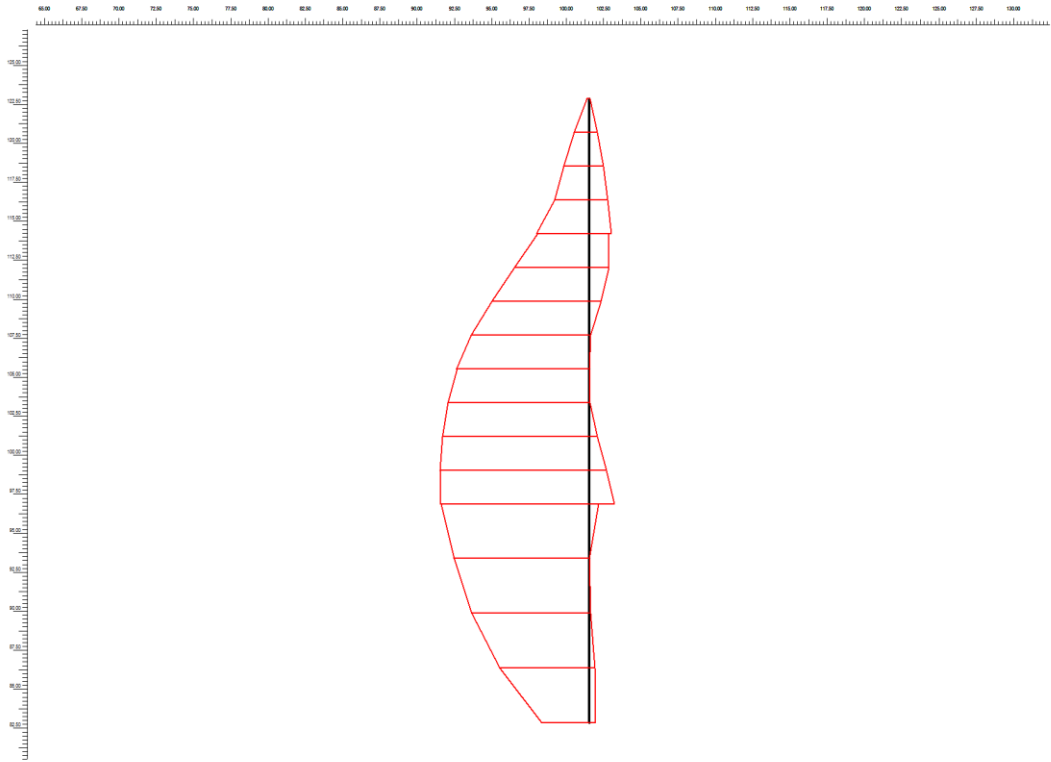


Figure A.7 Axial force diagram of Landers EQ for pile 3 ($N = 1820 \text{ kN/m}$).

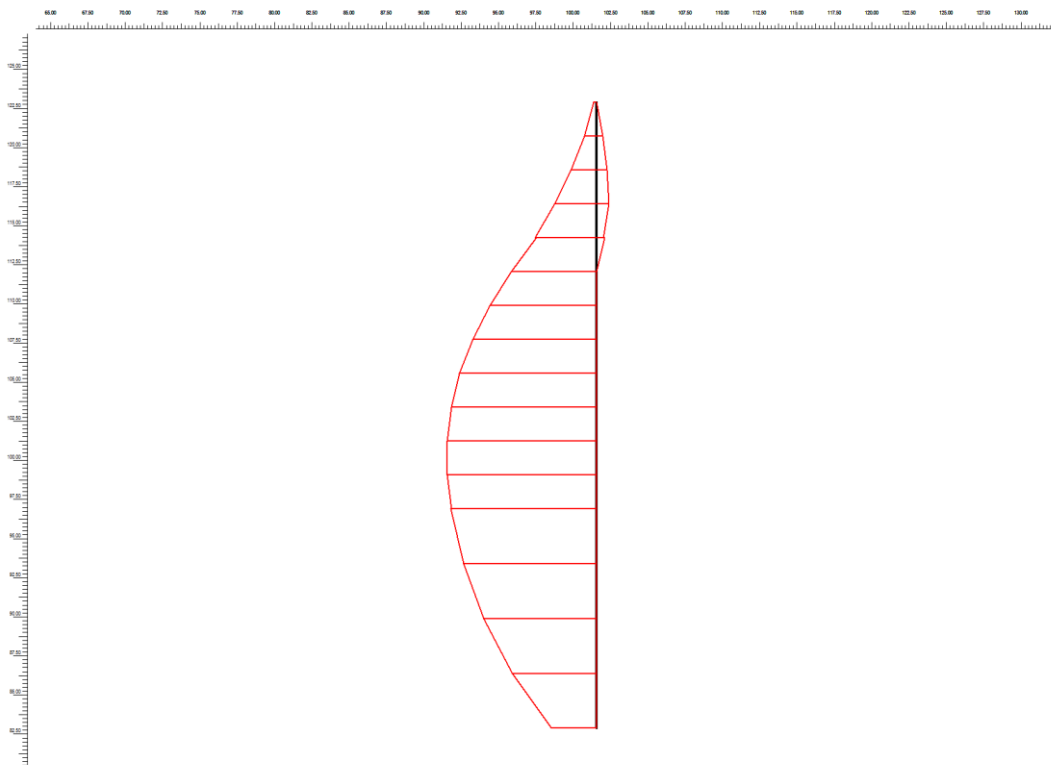


Figure A.8 Axial force diagram of C. Valley EQ for pile 3 ($N = 1780 \text{ kN/m}$).

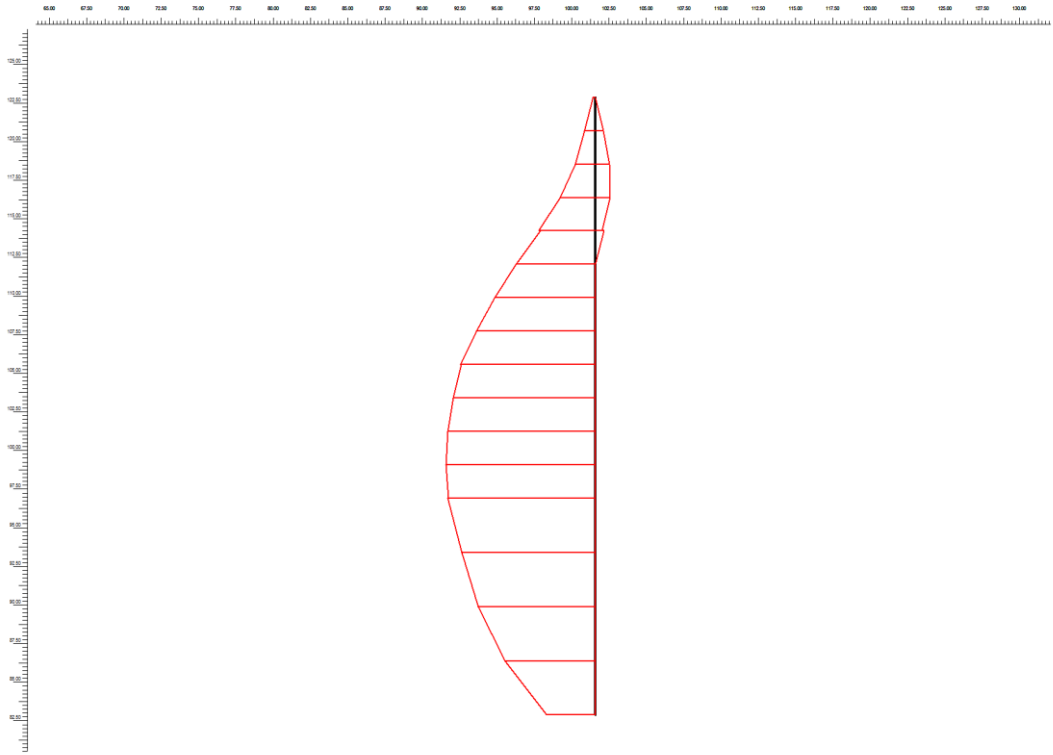


Figure A.9 Axial force diagram of L. Prieta EQ for pile 3 ($N = 1630 \text{ kN/m}$).

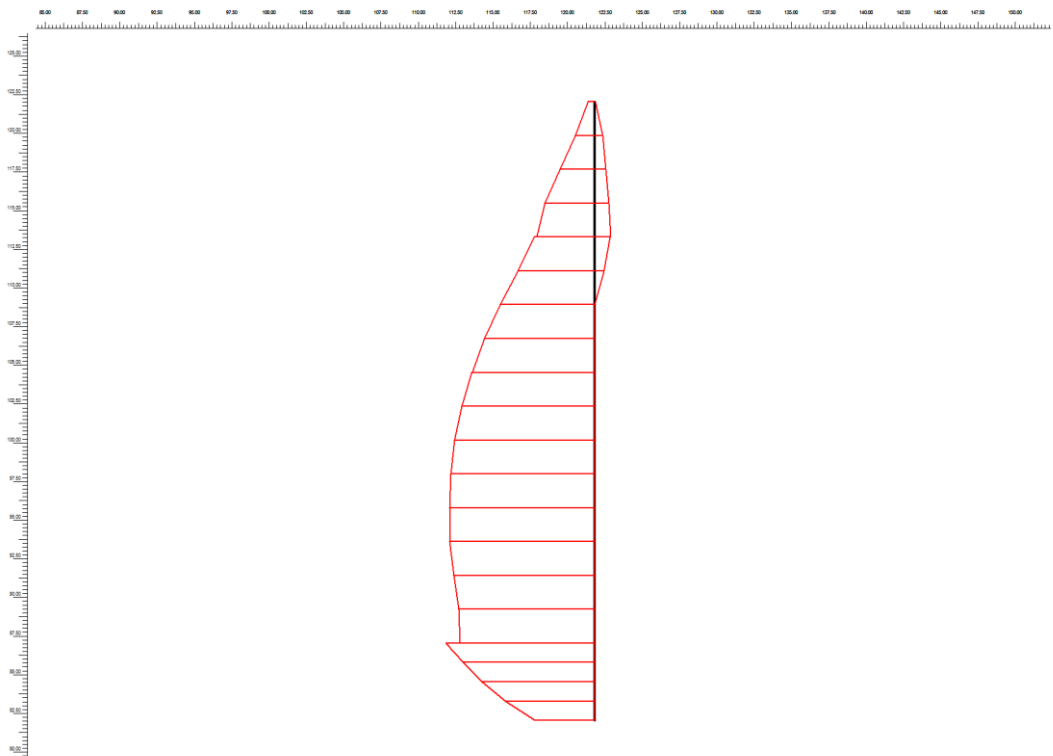


Figure A.10 Axial force diagram of Landers EQ for pile 4 ($N = 1610 \text{ kN/m}$).

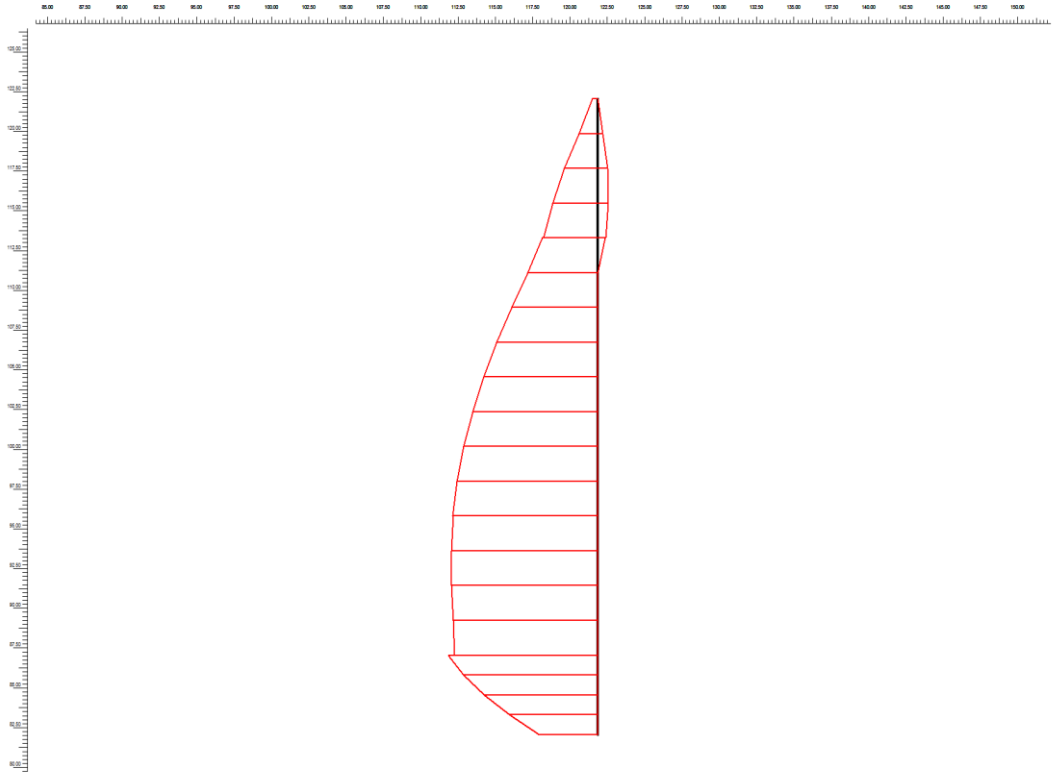


Figure A.11 Axial force diagram of C. Valley EQ for pile 4 ($N = 1450 \text{ kN/m}$).

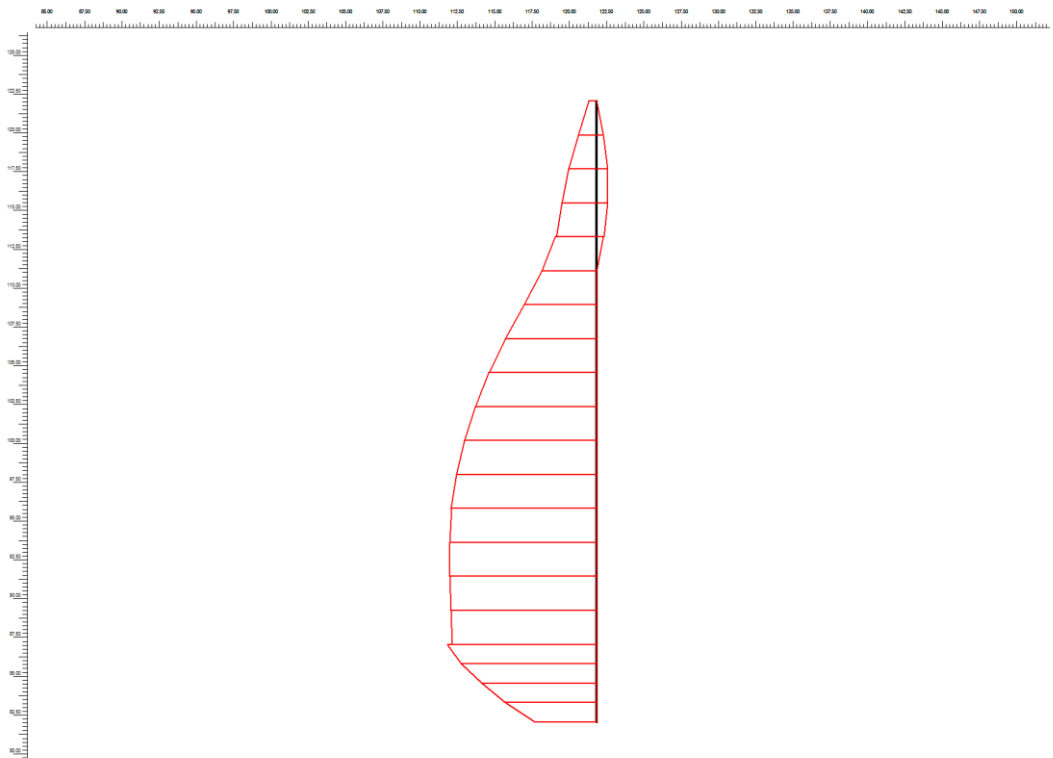


Figure A.12 Axial force diagram of L. Prieta EQ for pile 4 ($N = 1180 \text{ kN/m}$).

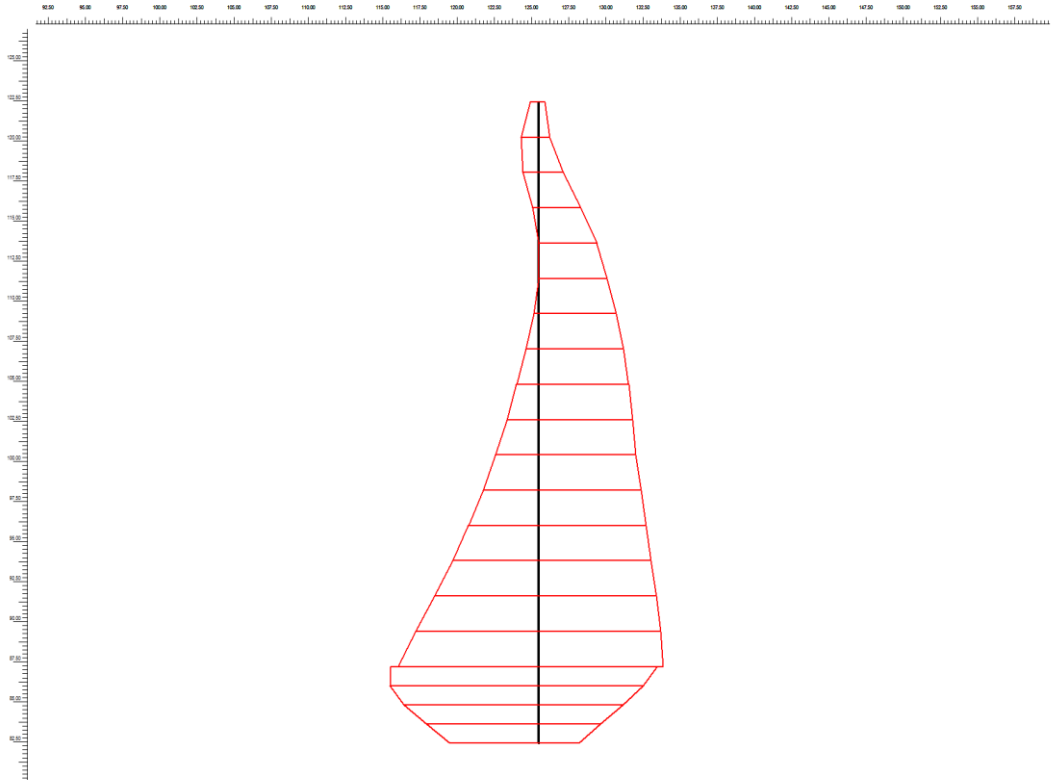


Figure A.13 Axial force diagram of Landers EQ for pile 5 ($N = 1450 \text{ kN/m}$).

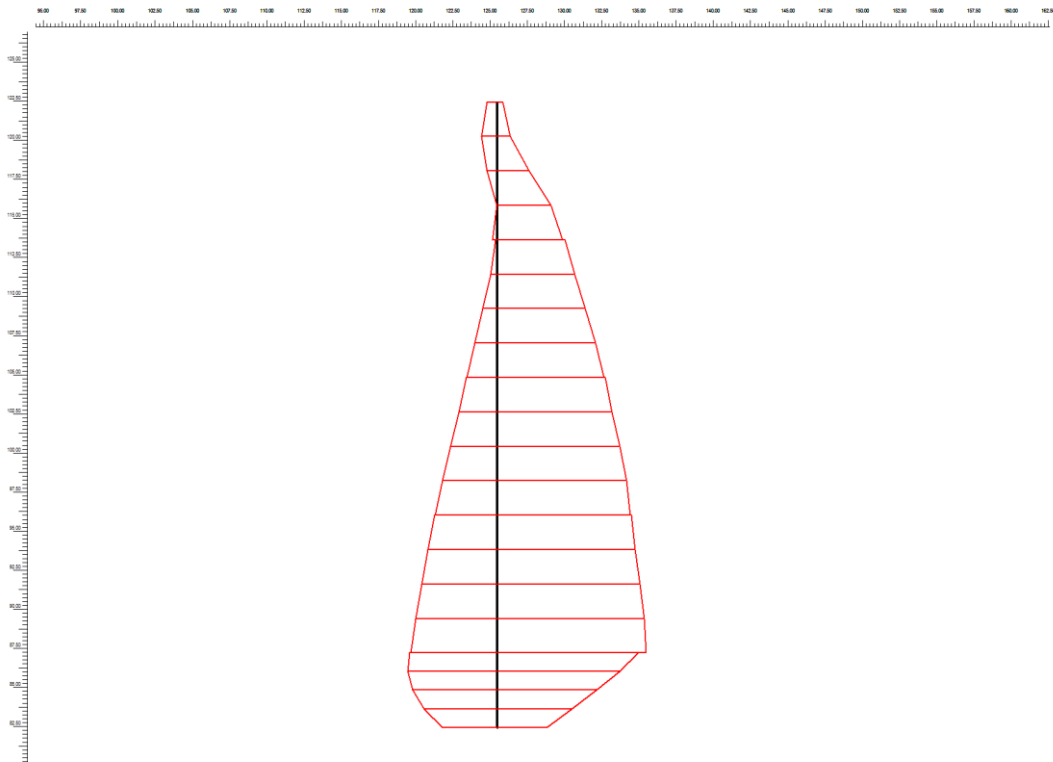


Figure A.14 Axial force diagram of C. Valley EQ for pile 5 ($N = 1270 \text{ kN/m}$).

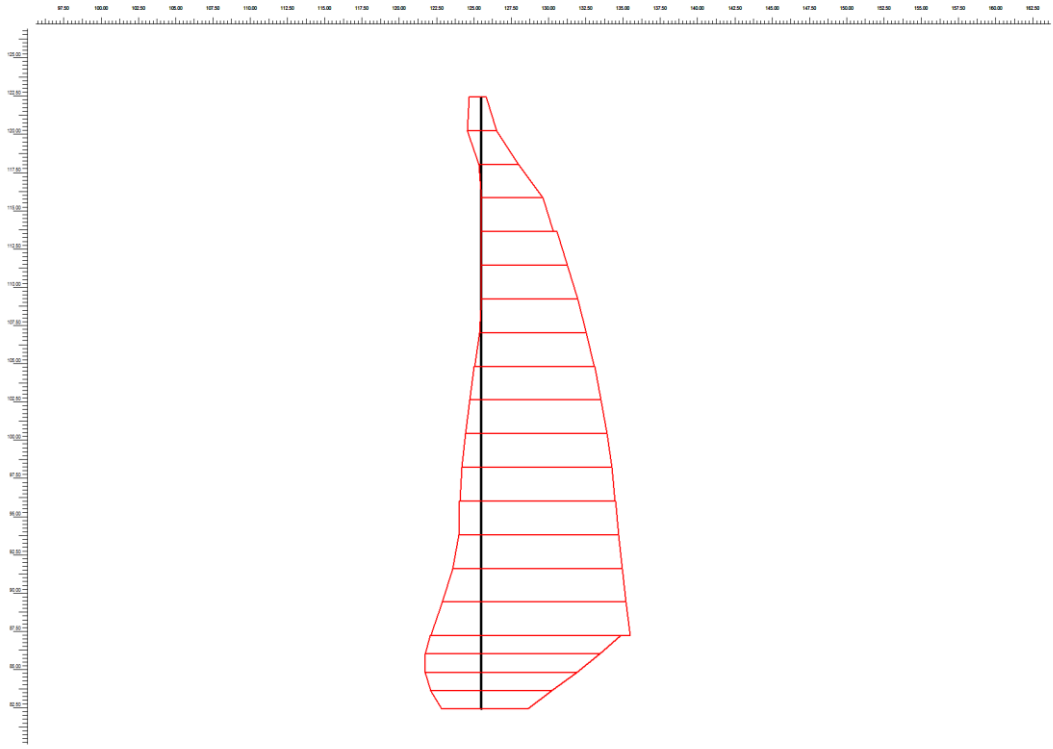


Figure A.15 Axial force diagram of L. Prieta EQ for pile 5 ($N = 1070 \text{ kN/m}$).

Appendix B Pile Shear Force Envelope Diagrams

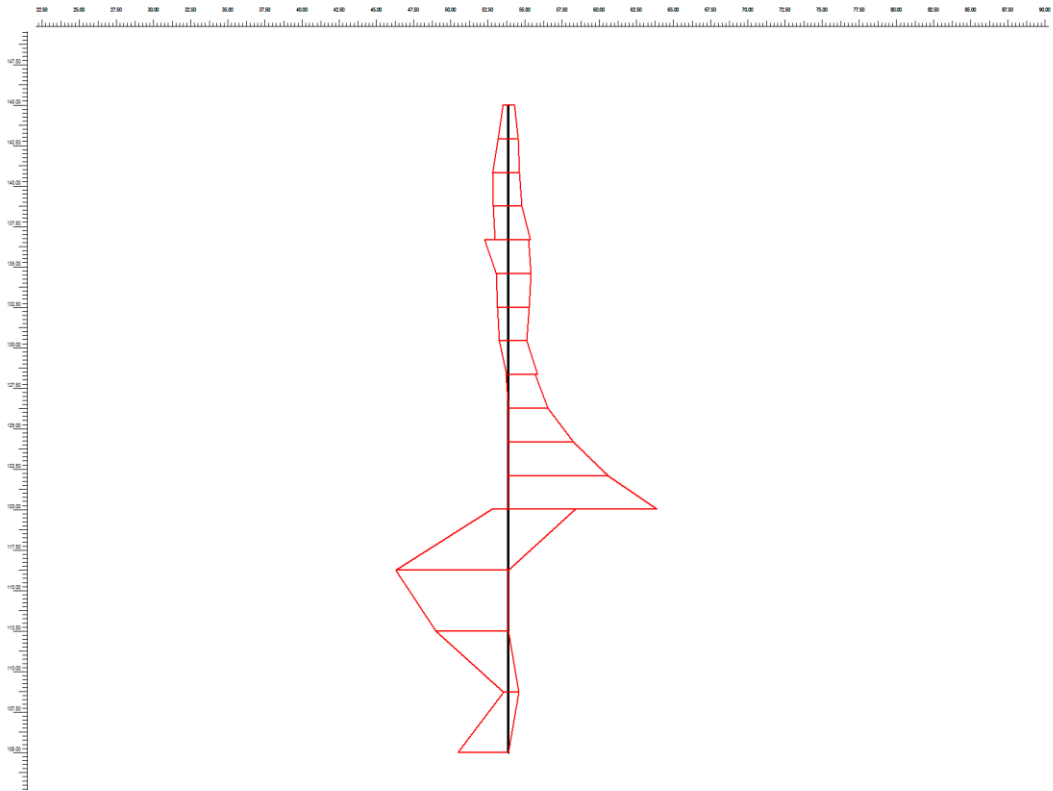


Figure B.1 Shear force diag. of Landers EQ for pile 1 ($V = 914.02$ kN/m).

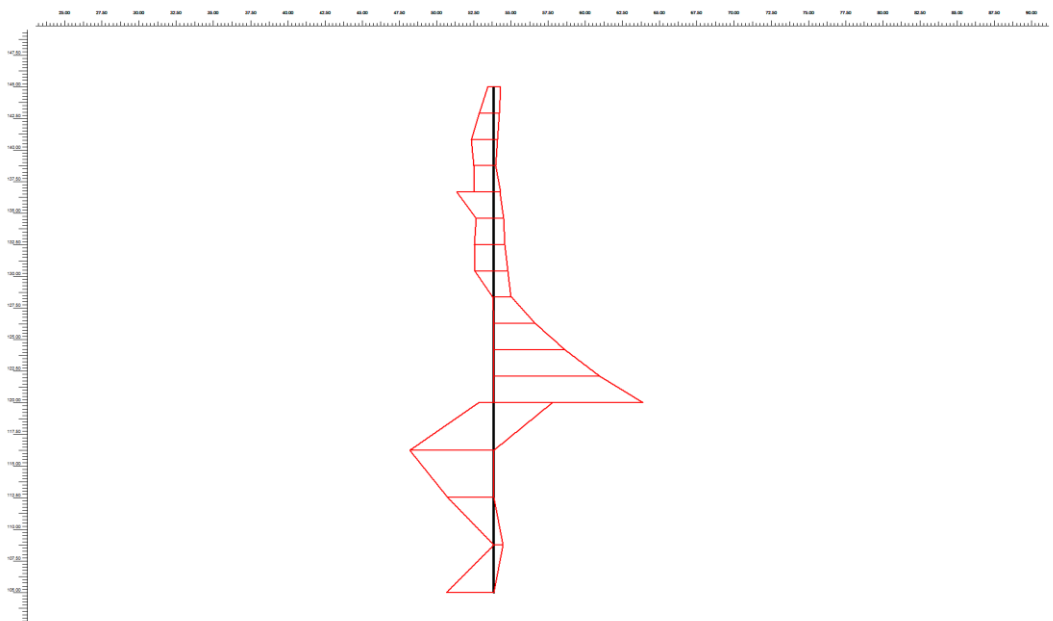


Figure B.2 Shear force diag. of C. Valley EQ for pile 1 ($V = 652.37$ kN/m).

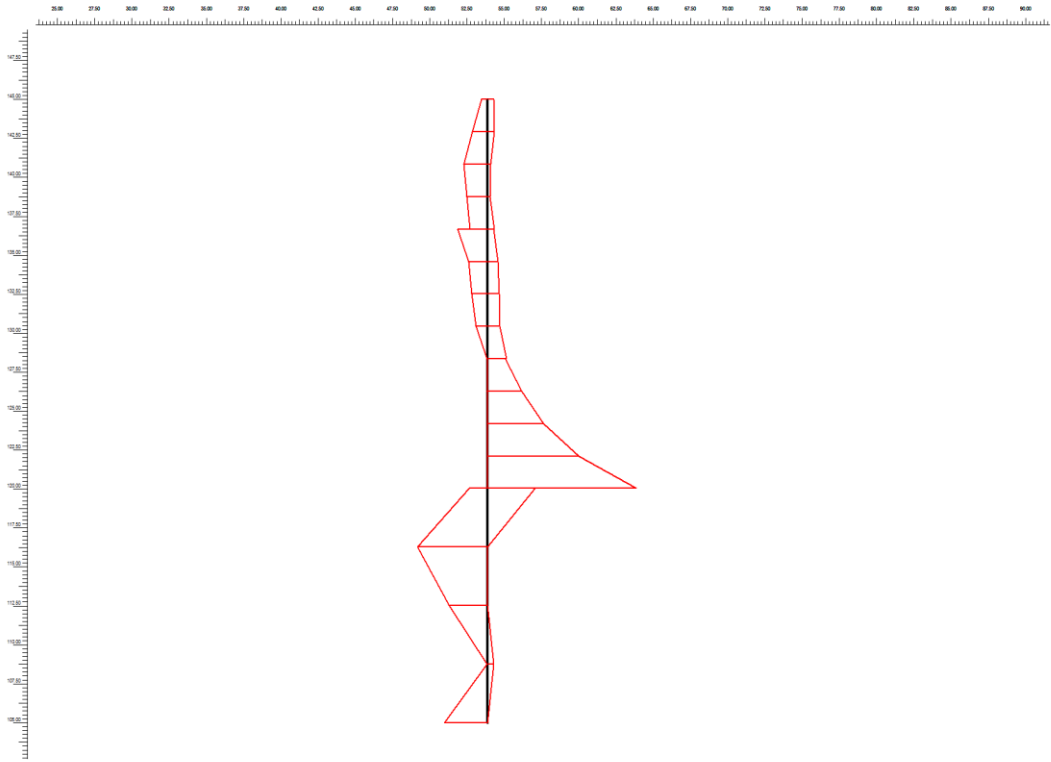


Figure B.3 Shear force diag. of L.Prieta Valley EQ for pile 1 ($V = 621.01$ kN/m).

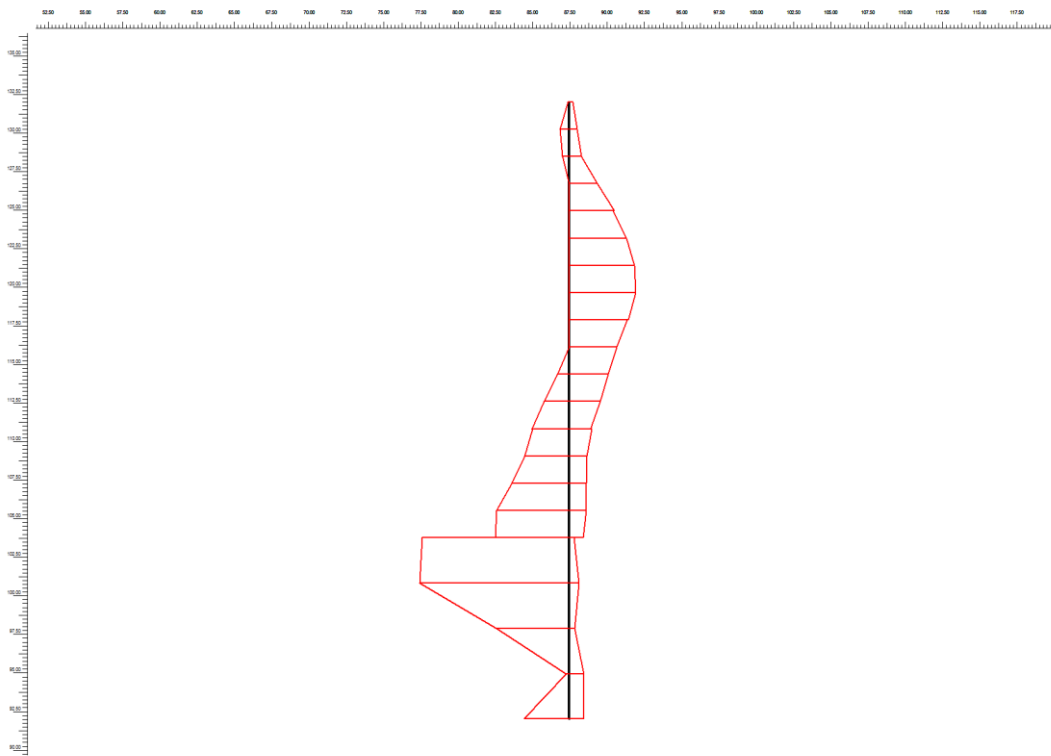


Figure B.4 Shear force diag. of Landers EQ for pile 2 ($V = 1600$ kN/m).

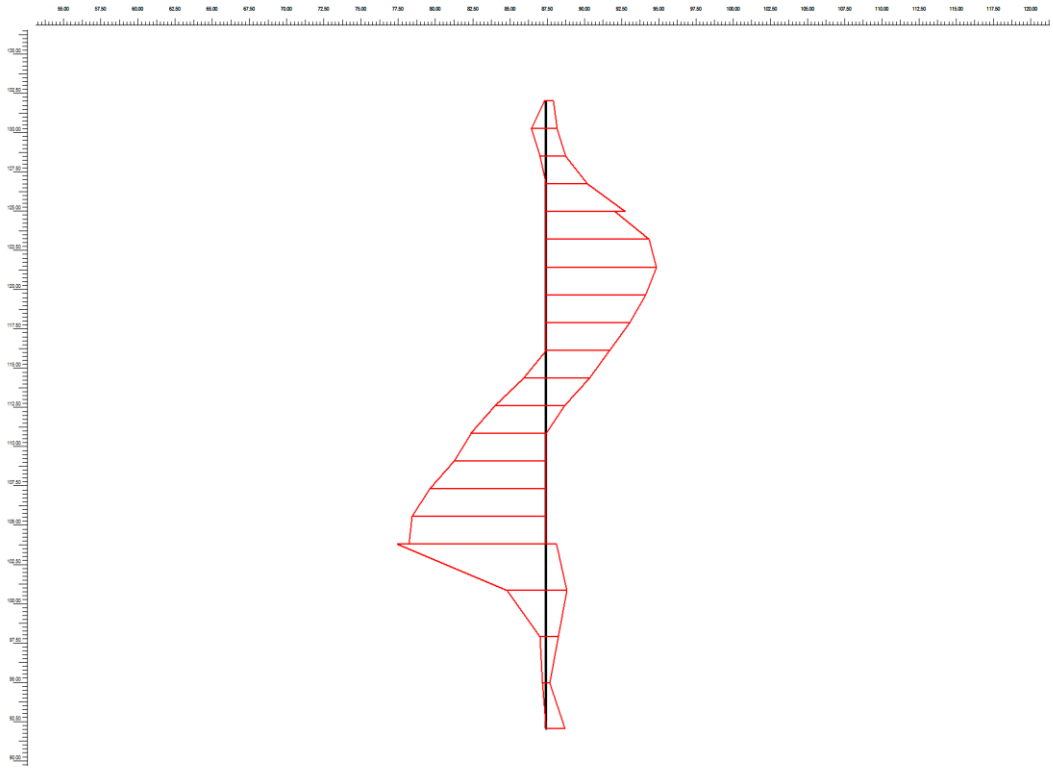


Figure B.5 Shear force diag. of C. Valley EQ for pile 2 ($V = 776.08$ kN/m).

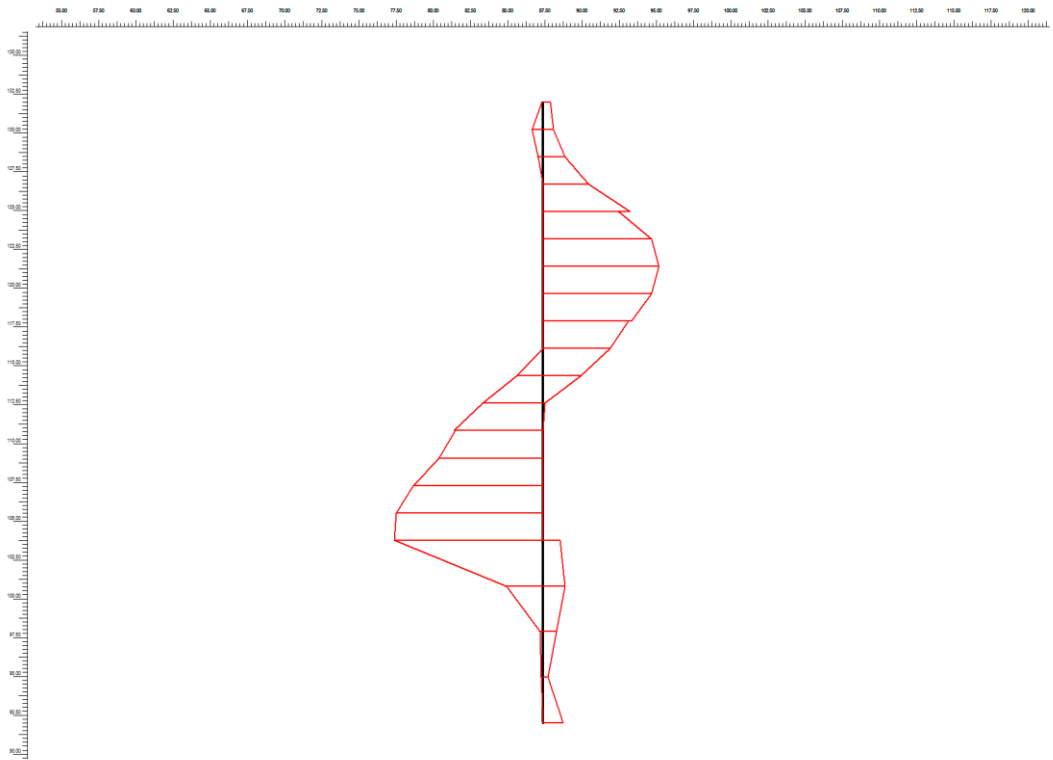


Figure B.6 Shear force diag. of L.Prieta Valley EQ for pile 2 ($V = 657.92$ kN/m).

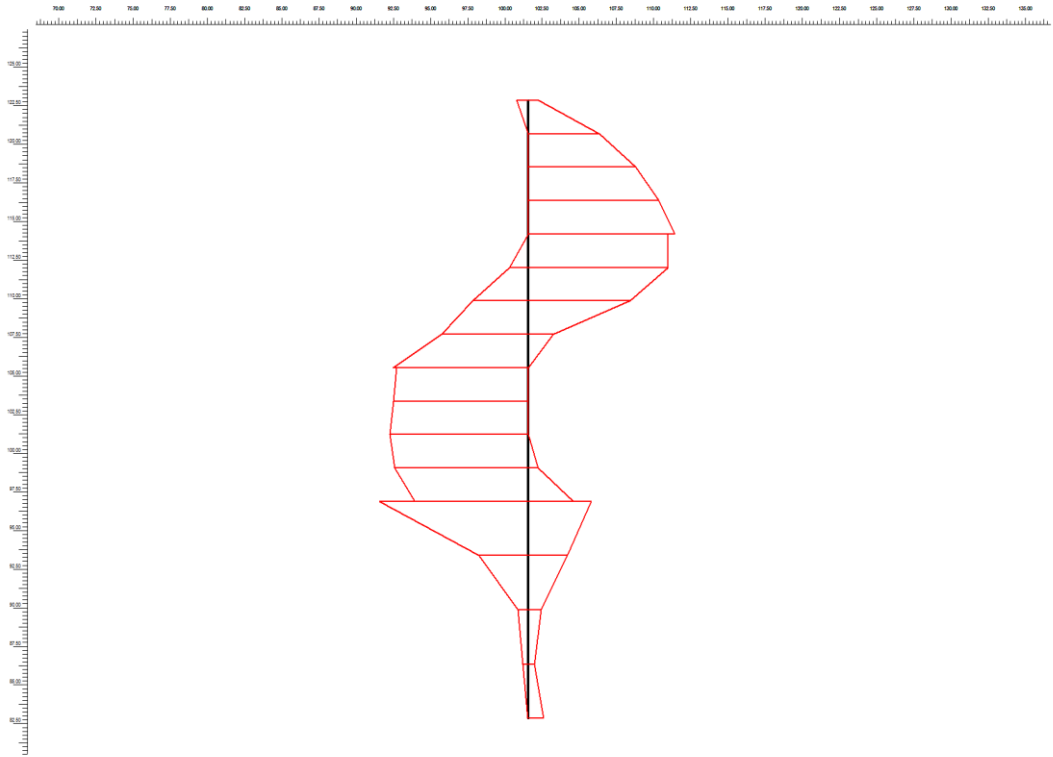


Figure B.7 Shear force diag. of Landers EQ for pile 3 ($V = 670.49$ kN/m).

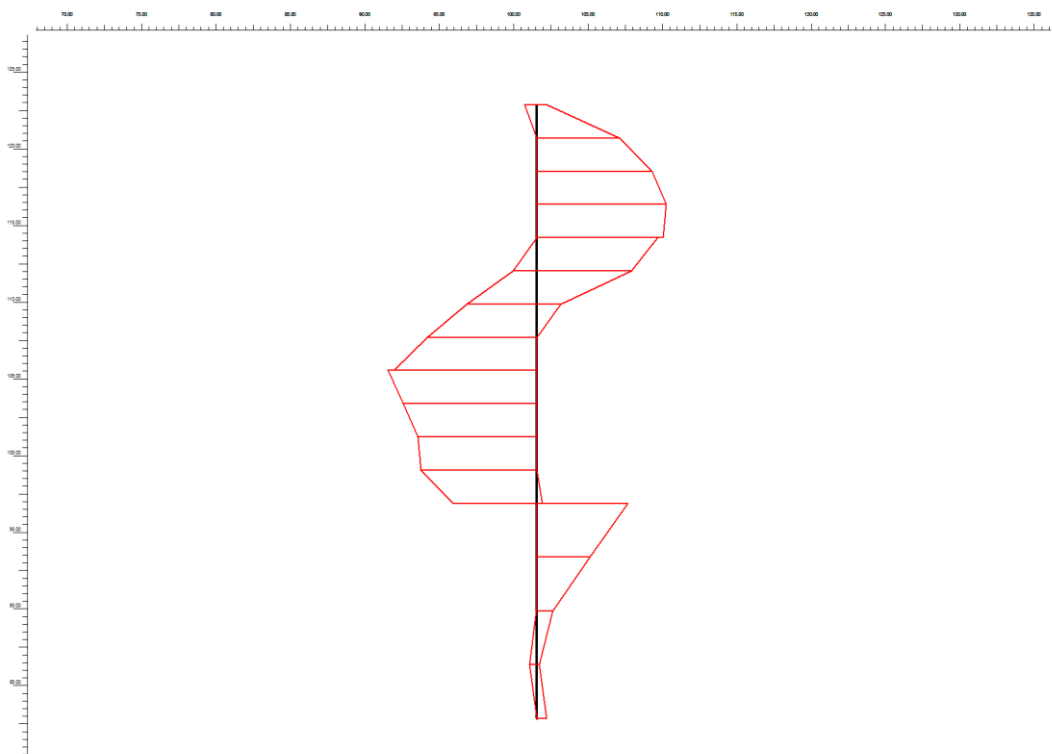


Figure B.8 Shear force diag. of C. Valley EQ for pile 3 ($V = 530.95$ kN/m).

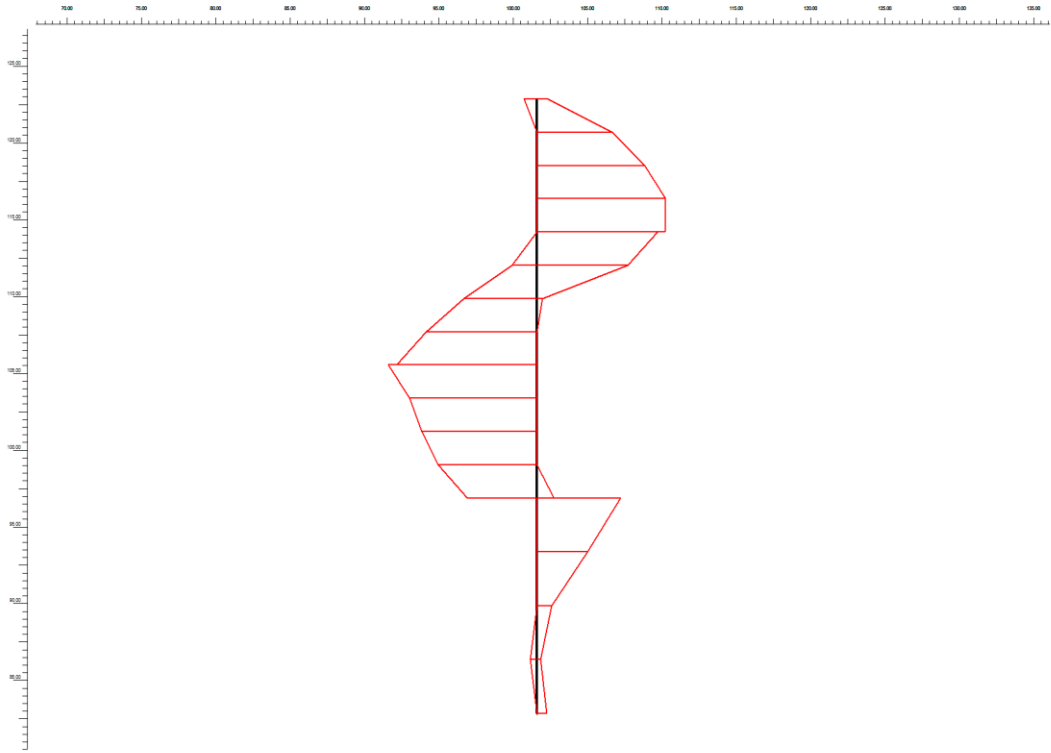


Figure B.9 Shear force diag. of L. Prieta Valley EQ for pile 3 ($V = 510.34$ kN/m).

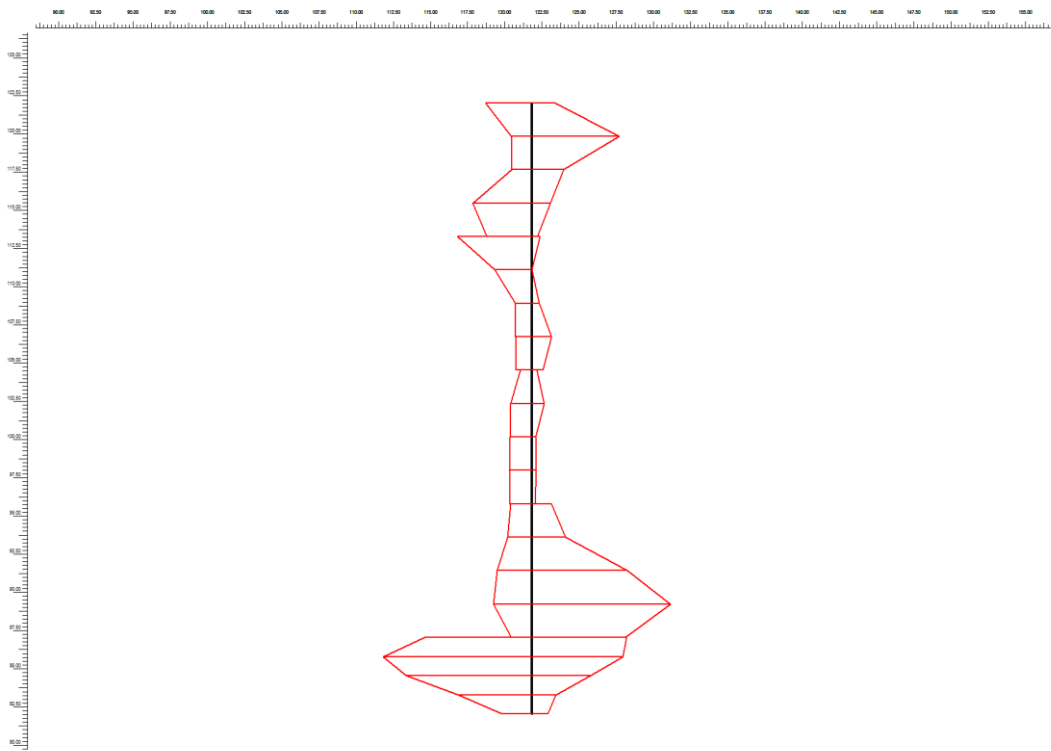


Figure B.10 Shear force diag. of Landers EQ for pile 4 ($V = 295.97$ kN/m).

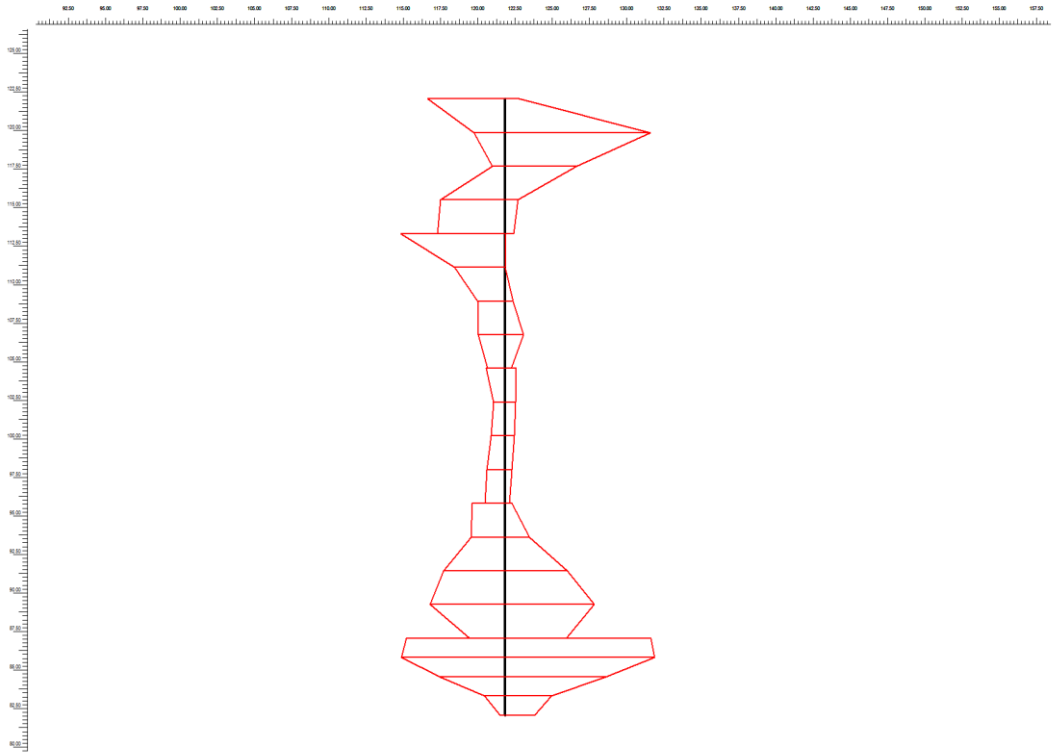


Figure B.11 Shear force diag. of C.Valley EQ for pile 4 ($V = 206.54$ kN/m).

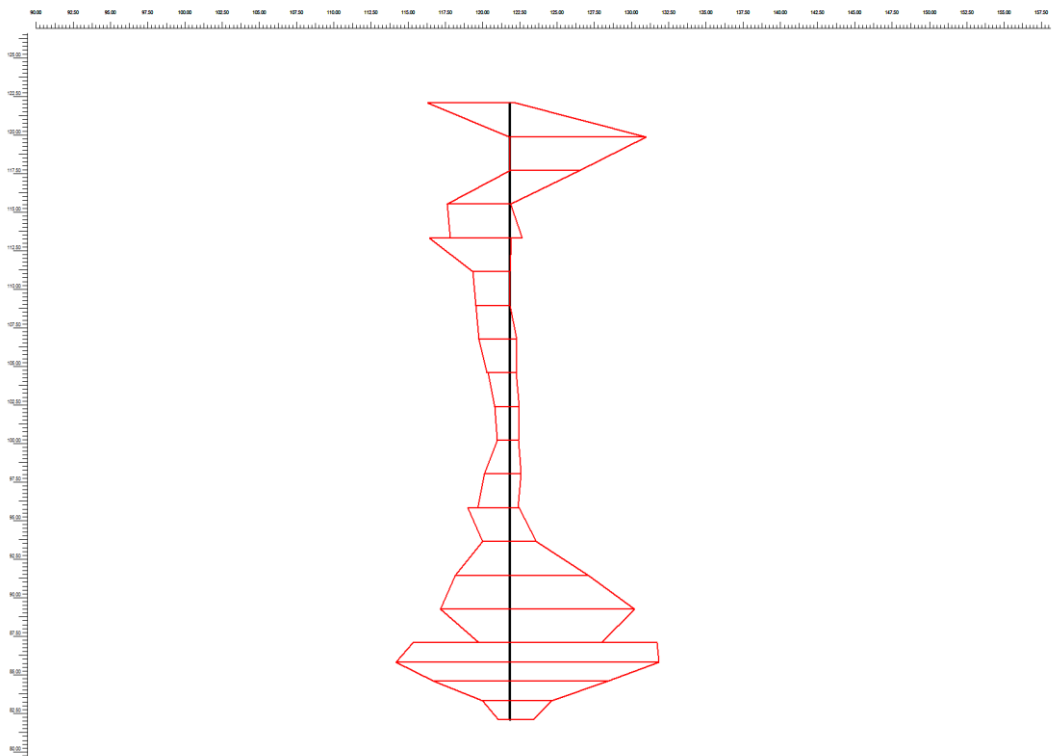


Figure B.12 Shear force diag. of L.Prieta Valley EQ for pile 4 ($V = 165.4$ kN/m).

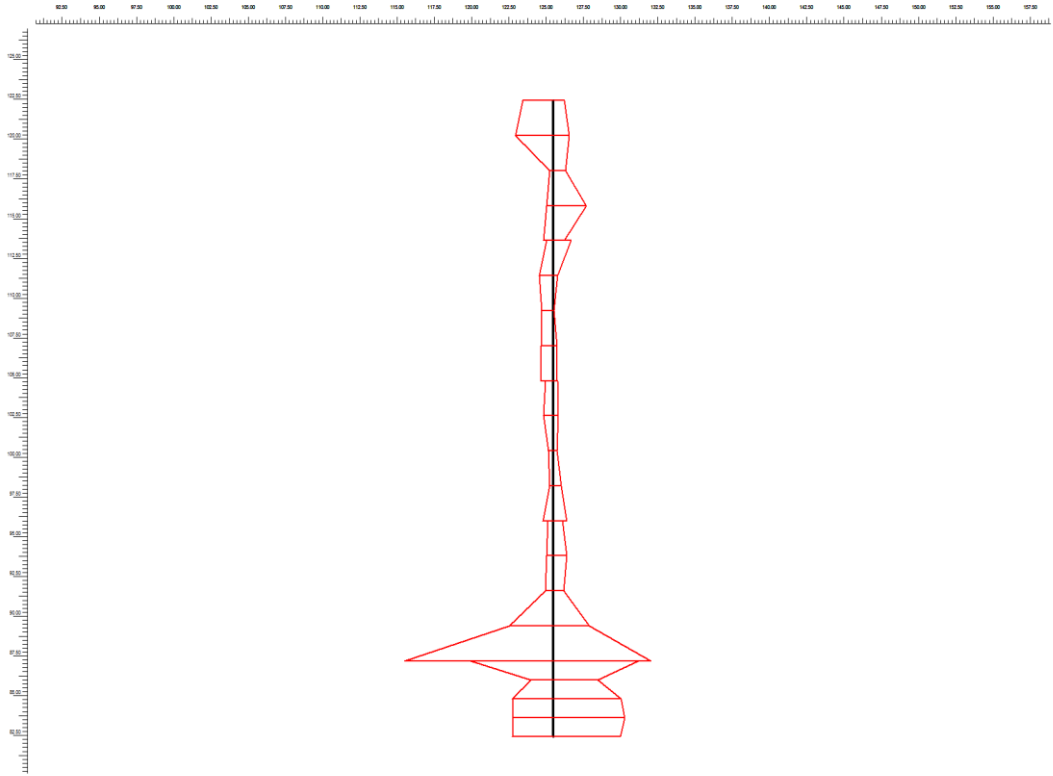


Figure B.13 Shear force diag. of Landers EQ for pile 5 ($V = 357.46 \text{ kN/m}$).

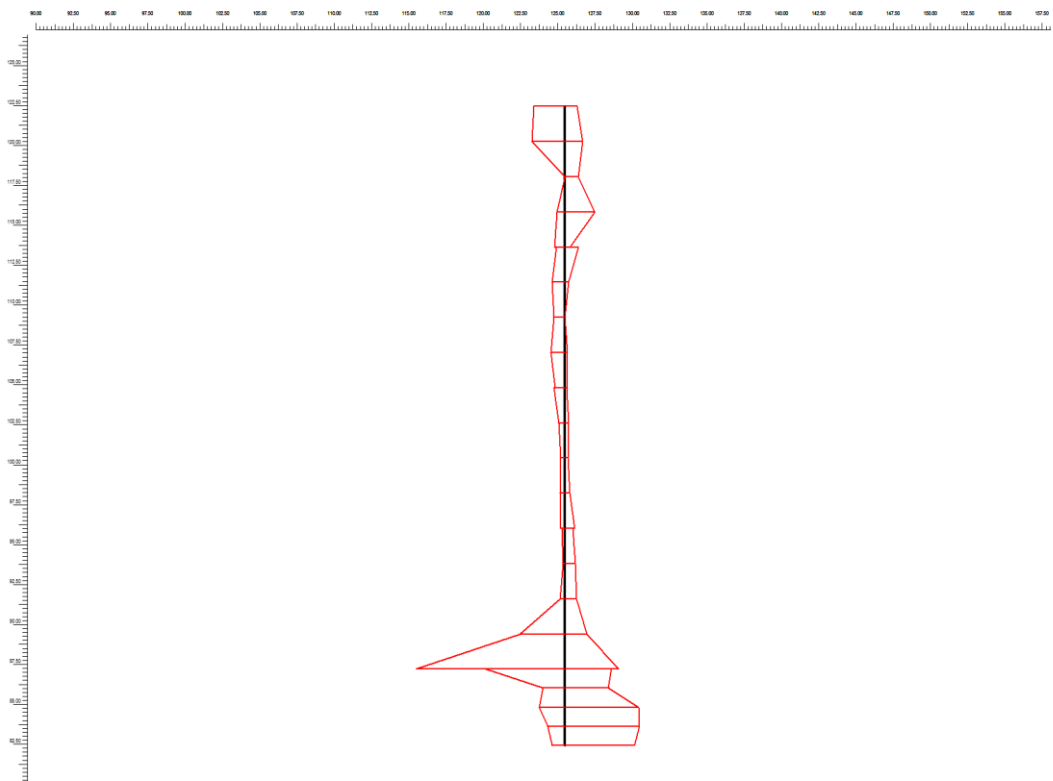


Figure B.14 Shear force diag. of C. Valley EQ for pile 5 ($V = 311.53 \text{ kN/m}$).

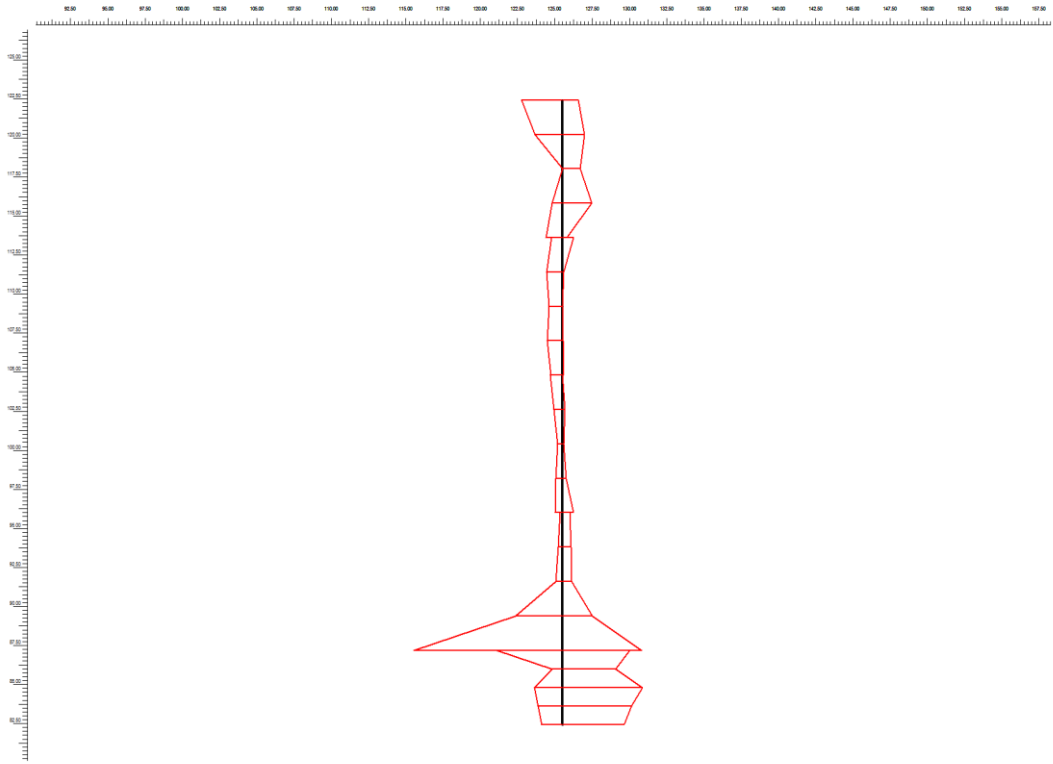


Figure B.15 Shear force diag. of L. Prieta Valley EQ for pile 5 ($V = 242.3$ kN/m).

Appendix C Pile Bending Moment Envelope Diagrams

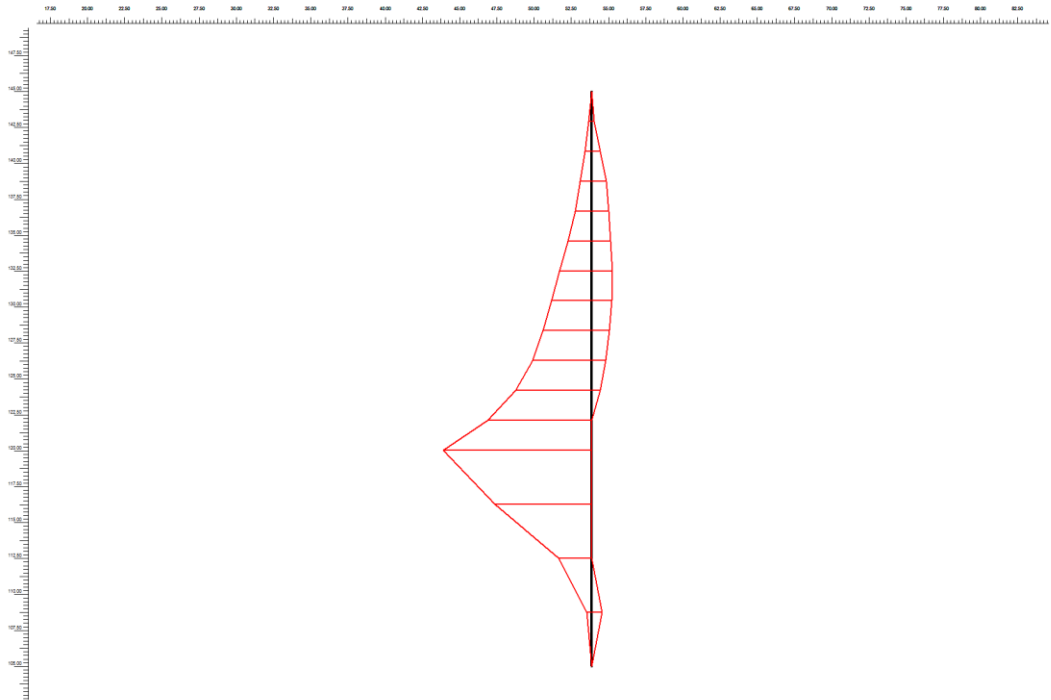


Figure C.1 Bending moment diag. of Landers EQ for pile 1 ($M = 4390$ kNm/m).

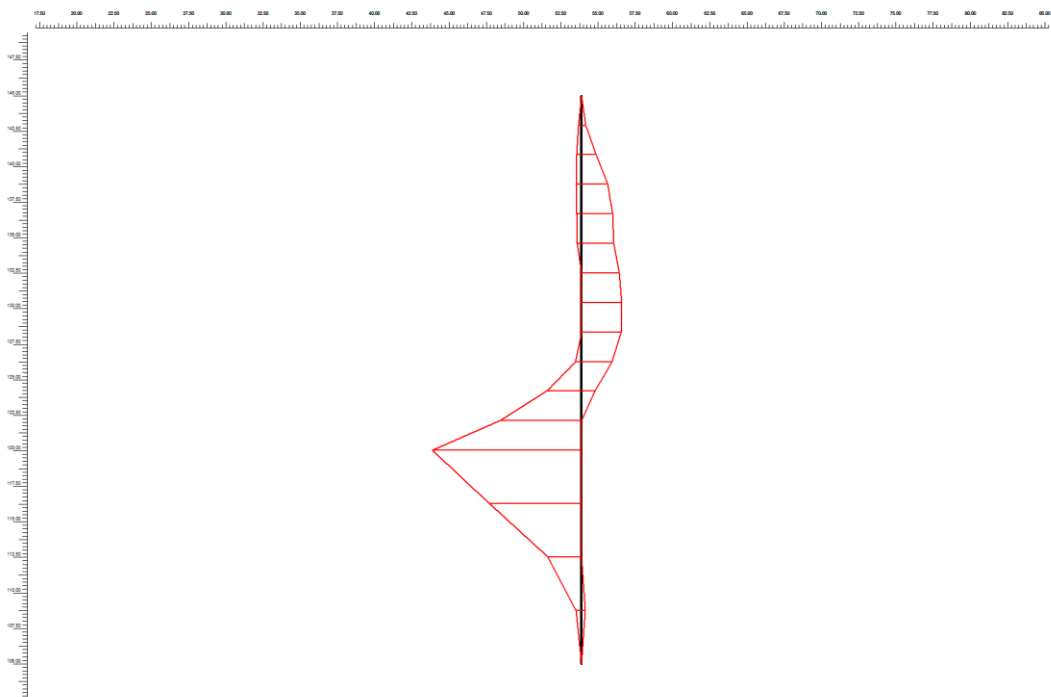


Figure C.2 Bending moment diag. of C. Valley EQ for pile 1 ($M = 2360$ kNm/m).

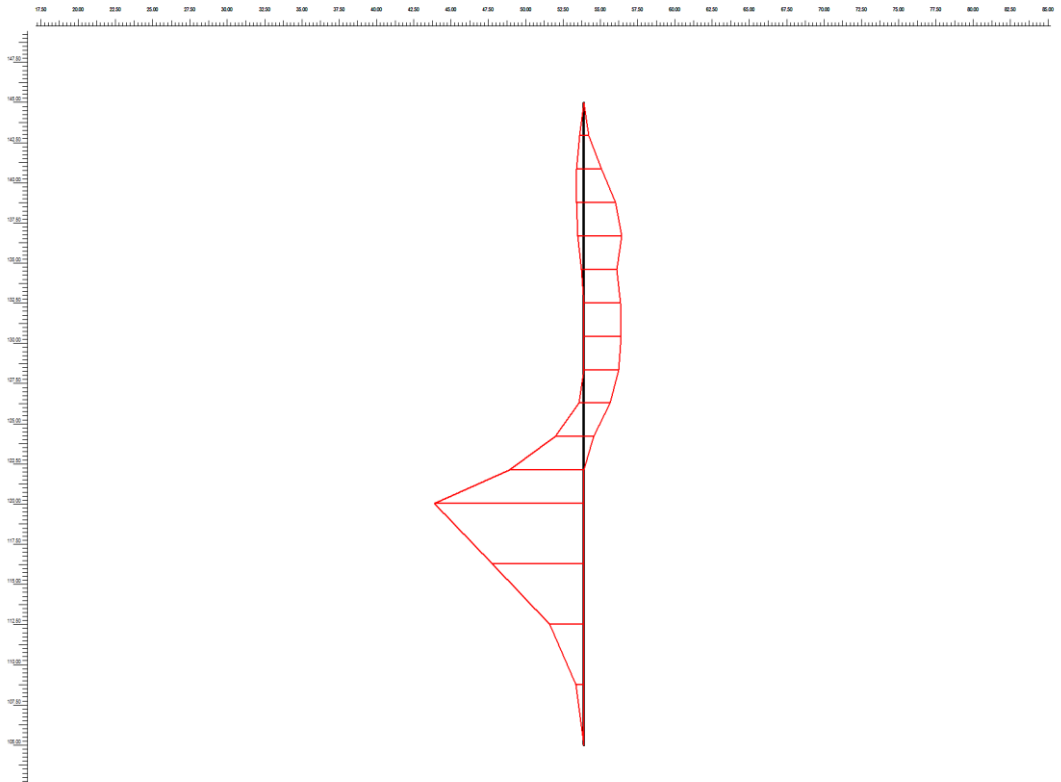


Figure C.3 Bending moment diag. of L. Prieta EQ for pile 1 ($M = 1930$ kNm/m).

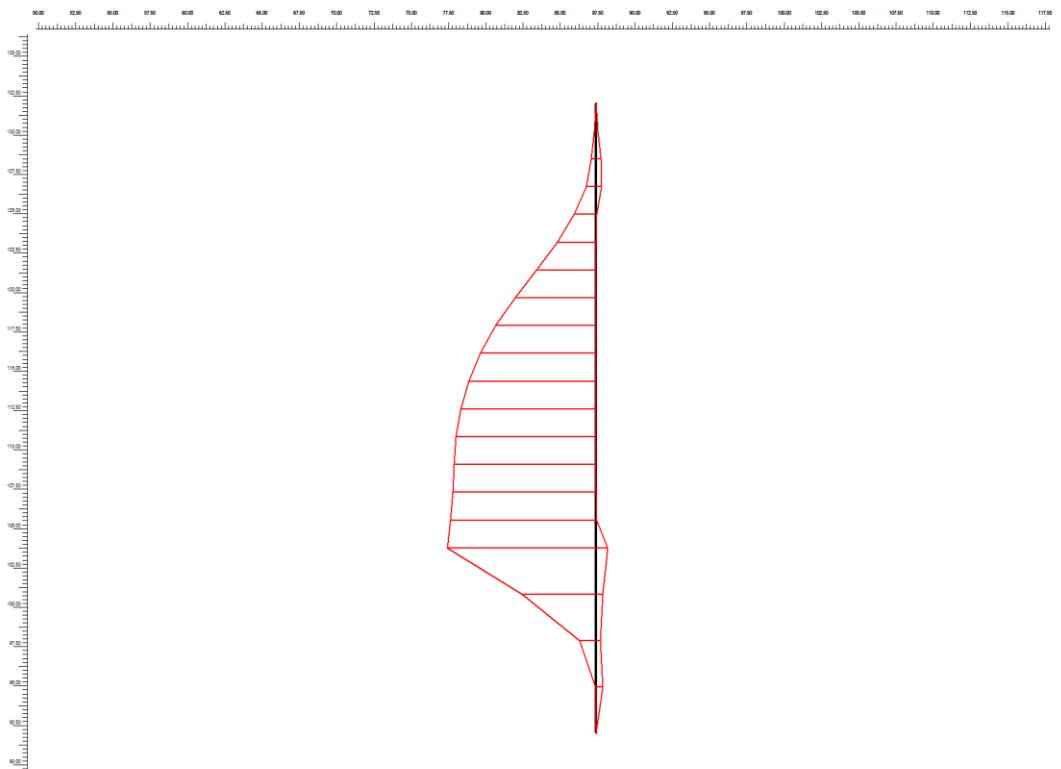


Figure C.4 Bending moment diag. of Landers EQ for pile 2 ($M = 8290$ kNm/m).

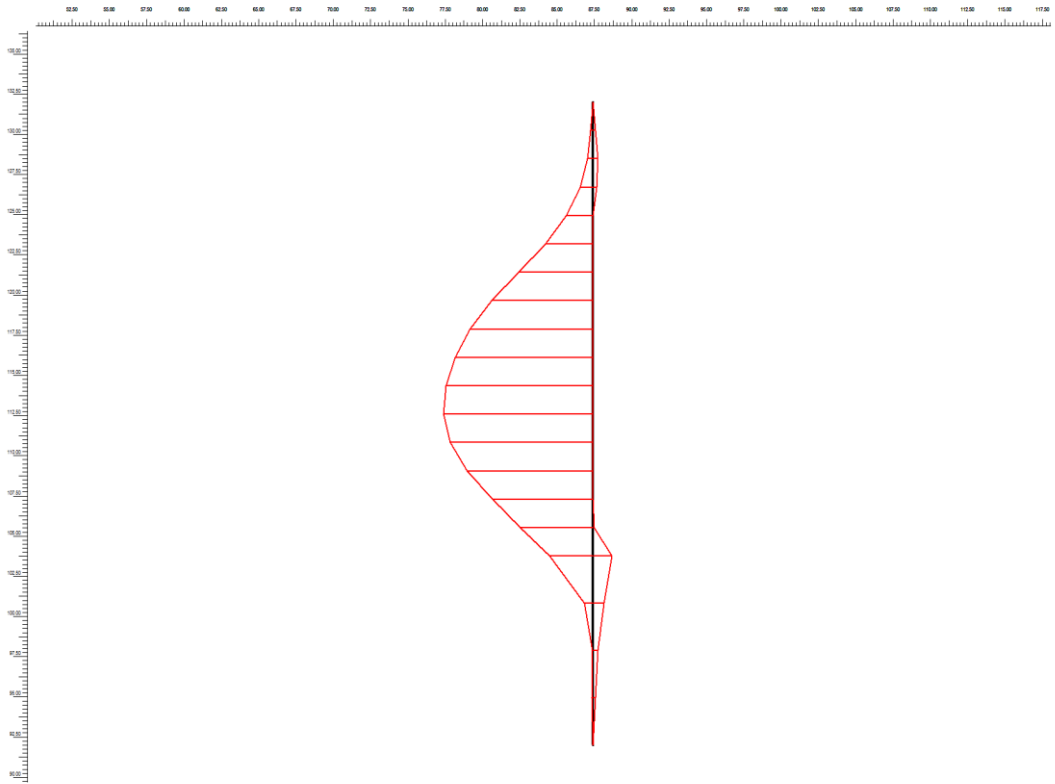


Figure C.5 Bending moment diag. of C. Valley EQ for pile 2 ($M = 5320 \text{ kNm/m}$).

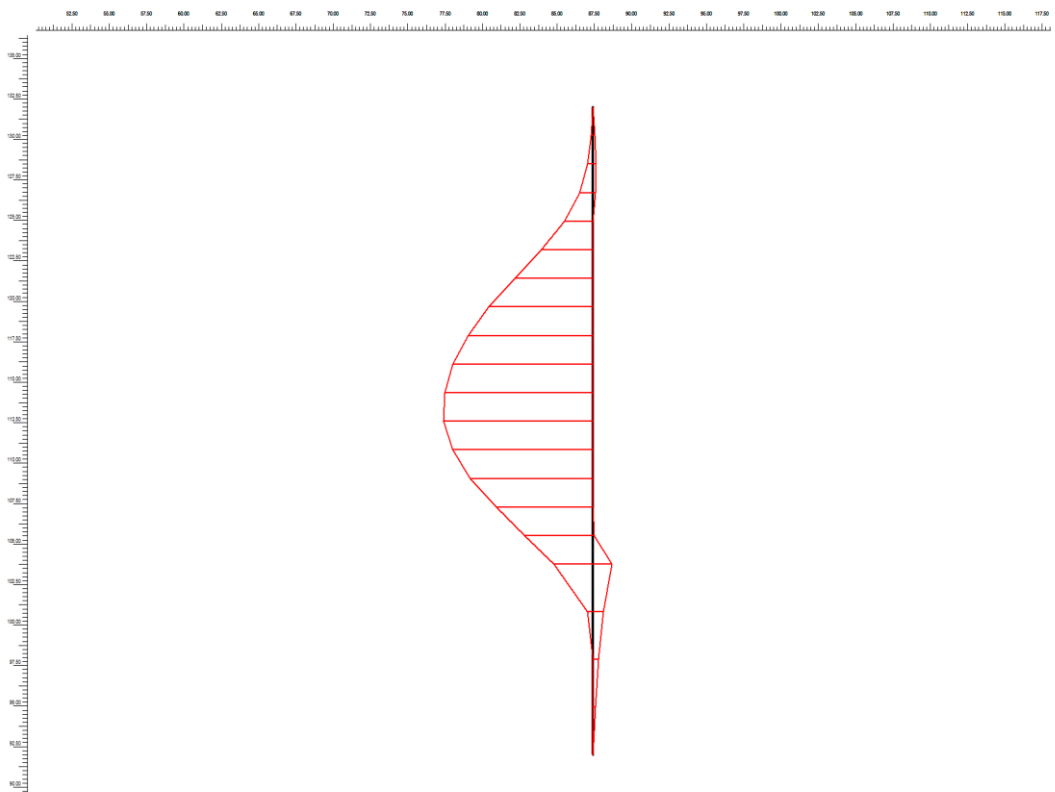


Figure C.6 Bending moment diag. of L.Prieta EQ for pile 2 ($M = 4730 \text{ kNm/m}$).

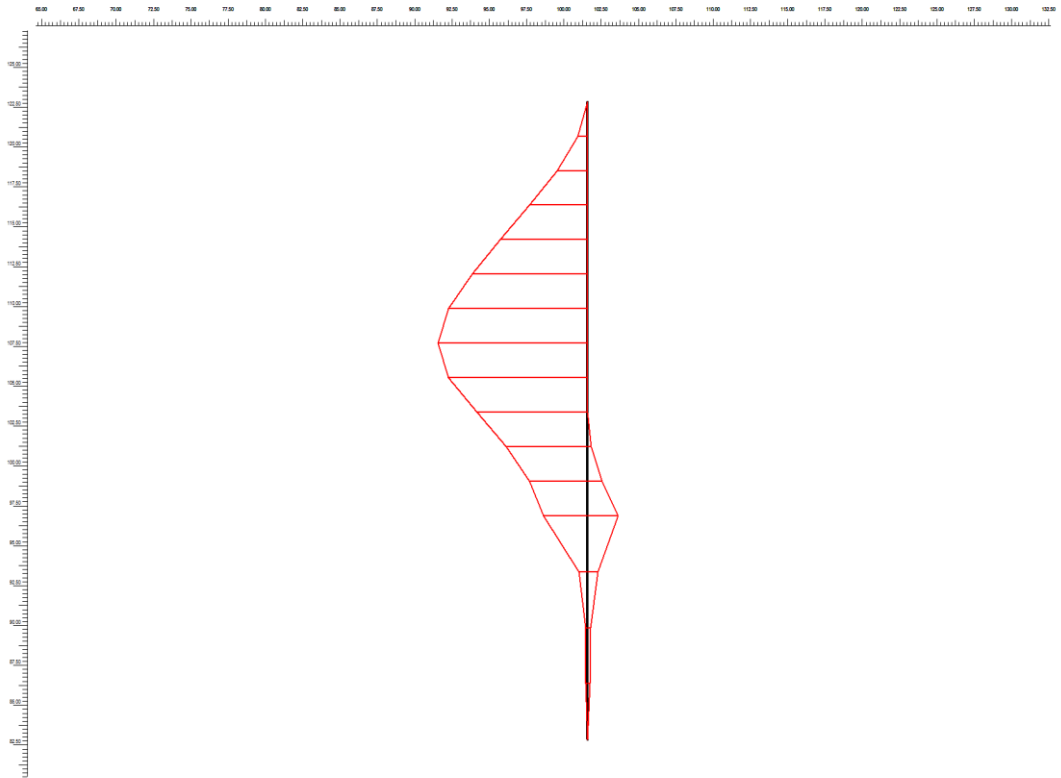


Figure C.7 Bending moment diag. of Landers EQ for pile 3 ($M = 6170 \text{ kNm/m}$).

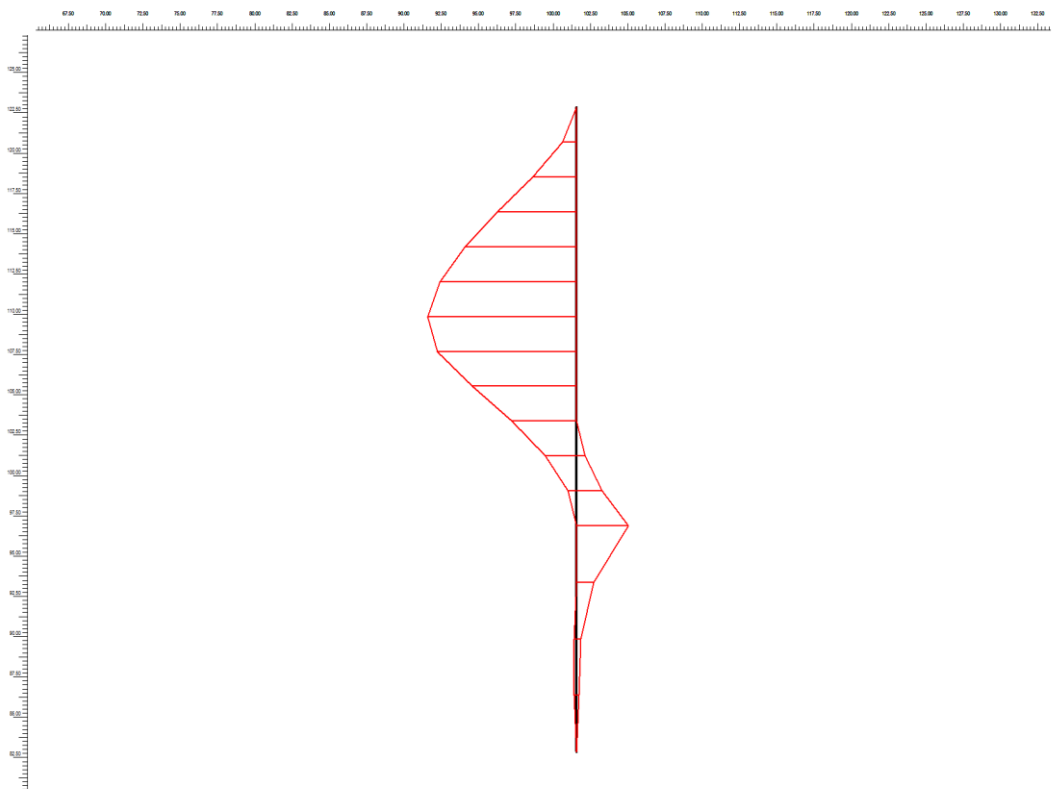


Figure C.8 Bending moment diag. of C. Valley EQ for pile 3 ($M = 3910 \text{ kNm/m}$).

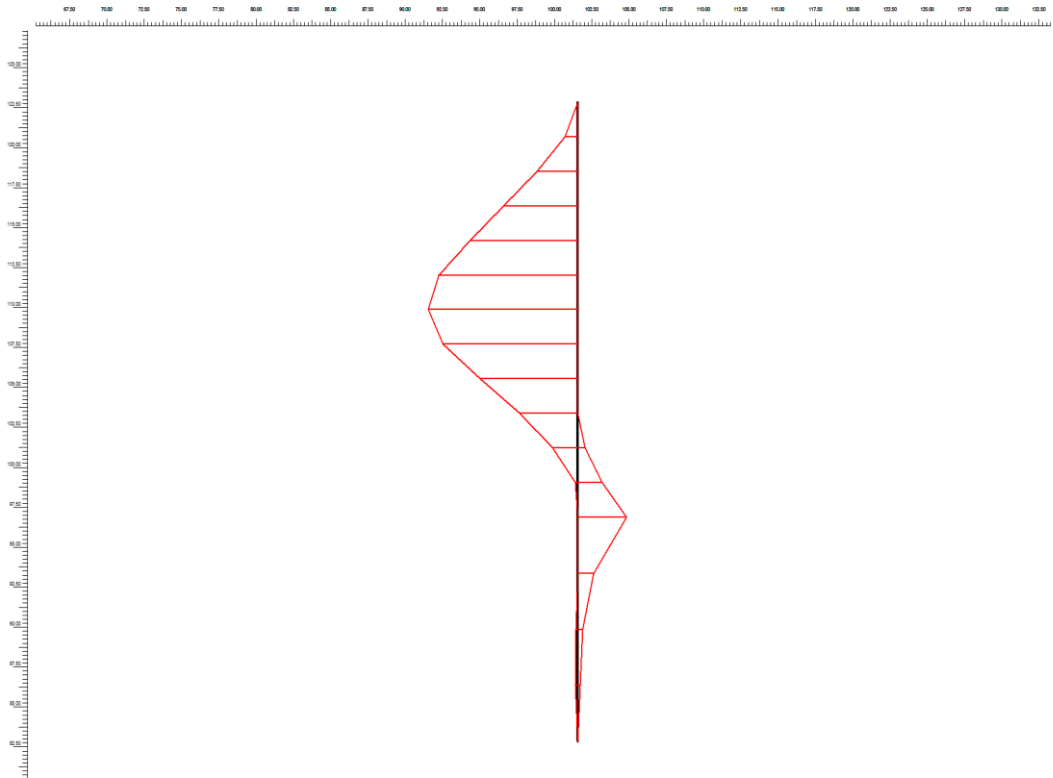


Figure C.9 Bending moment diag. of L. Prieta EQ for pile 3 ($M= 3700 \text{ kNm/m}$).

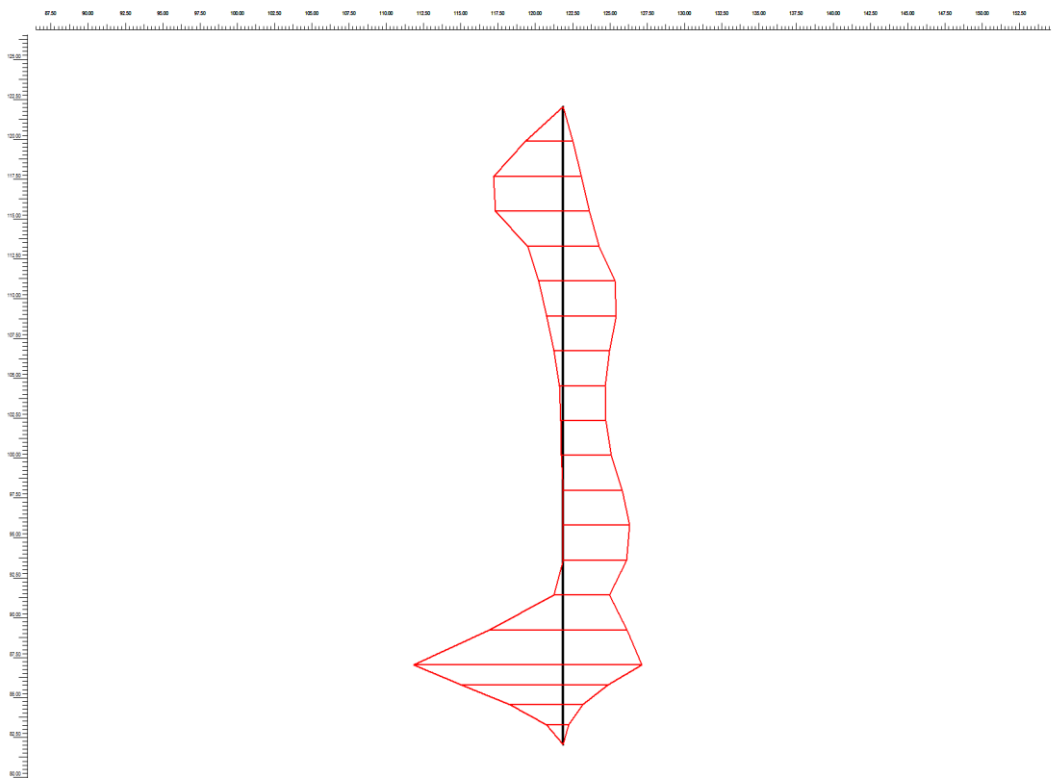


Figure C.10 Bending moment diag. of Landers EQ for pile 4 ($M = 1060 \text{ kNm/m}$).

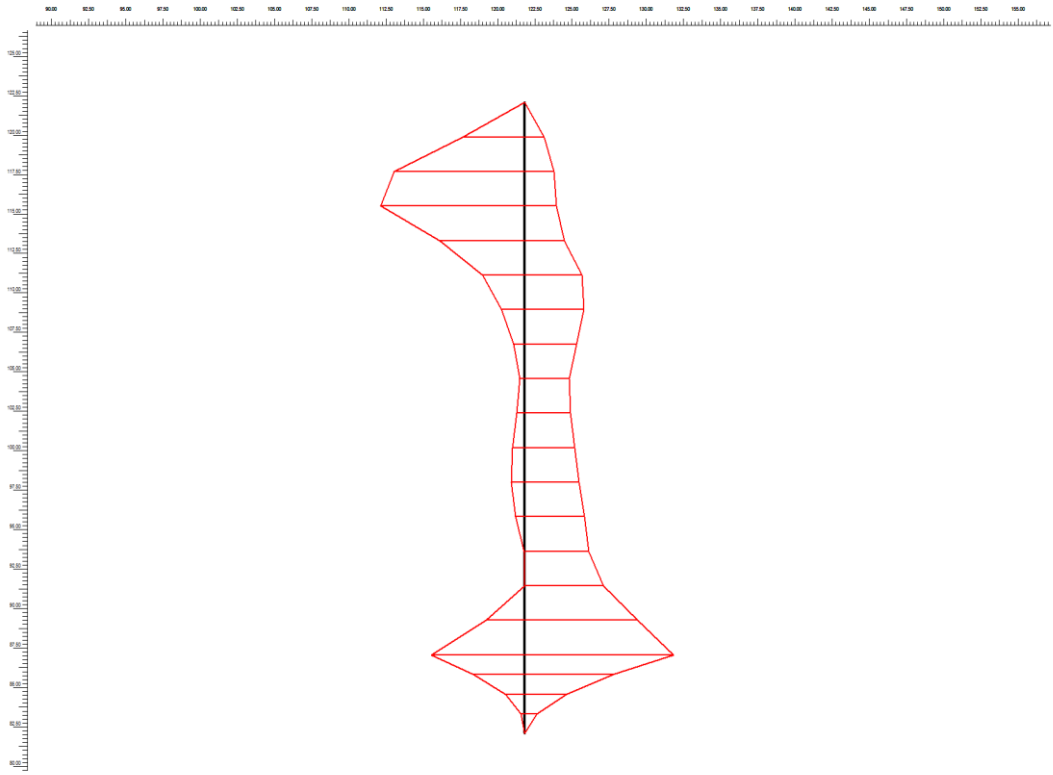


Figure C.11 Bending moment diag. of C.Valley EQ for pile 4 ($M = 660 \text{ kNm/m}$).

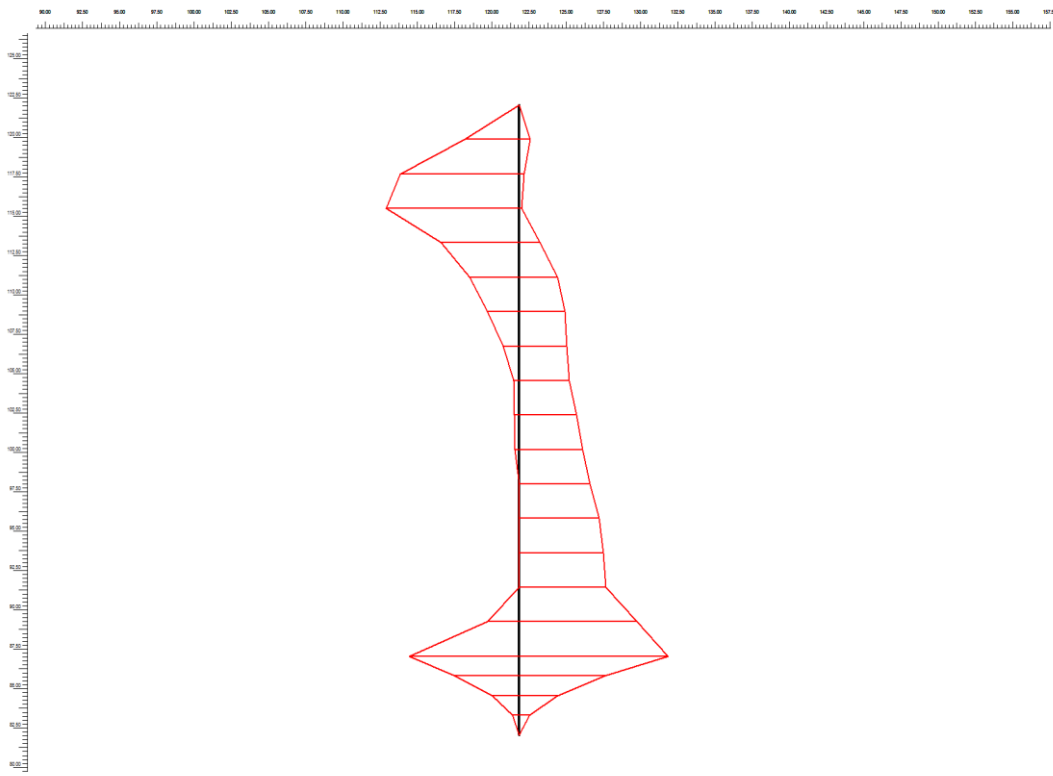


Figure C.12 Bending moment diag. of L. Prieta EQ for pile 4 ($M = 515.4 \text{ kNm/m}$).

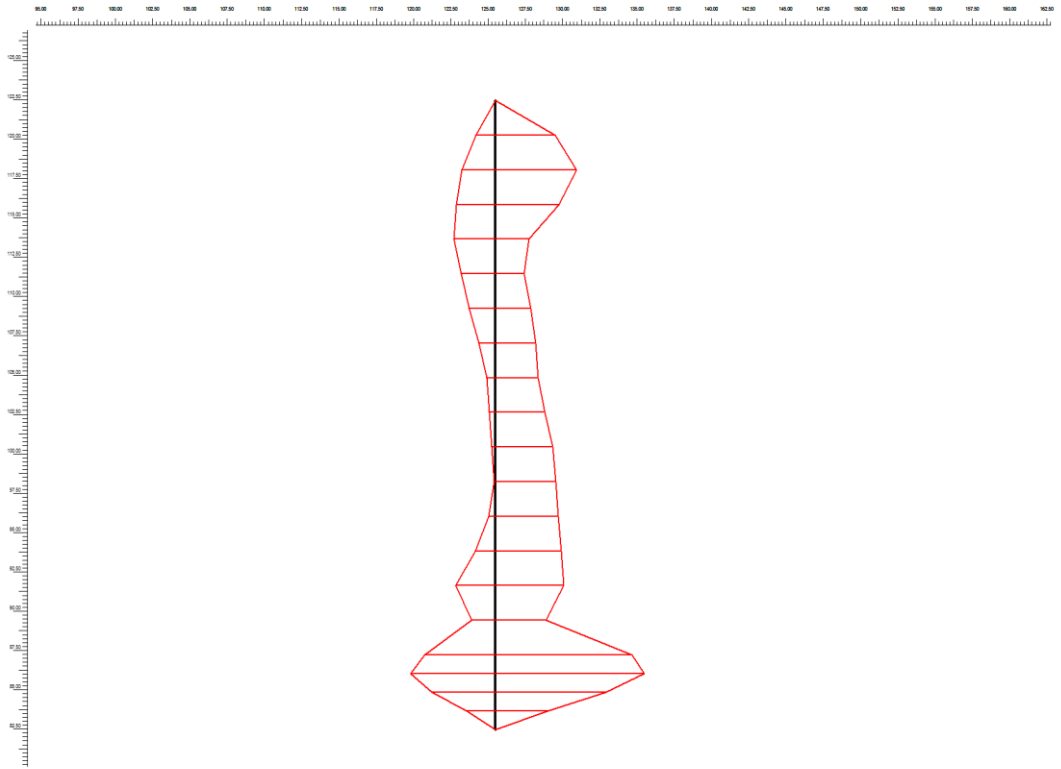


Figure C.13 Bending moment diag. of Landers EQ for pile 5 ($M = 542.5 \text{ kNm/m}$).

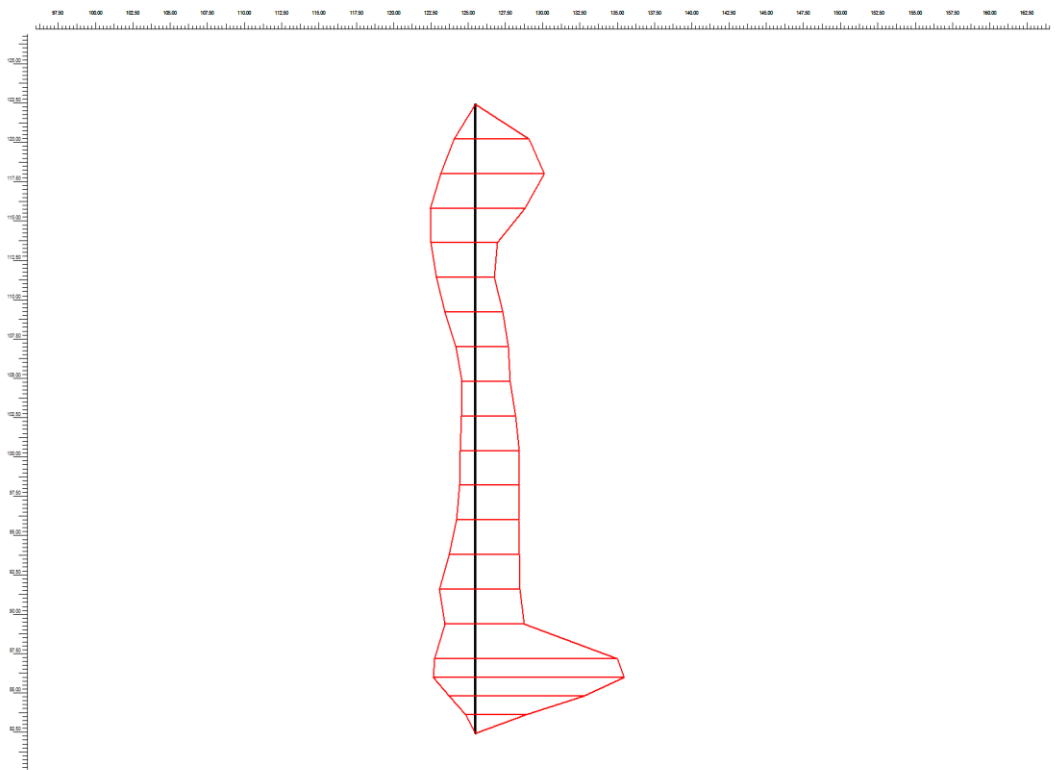


Figure C.14 Bending moment diag. of C.Valley EQ for pile 5 ($M = 507 \text{ kNm/m}$).

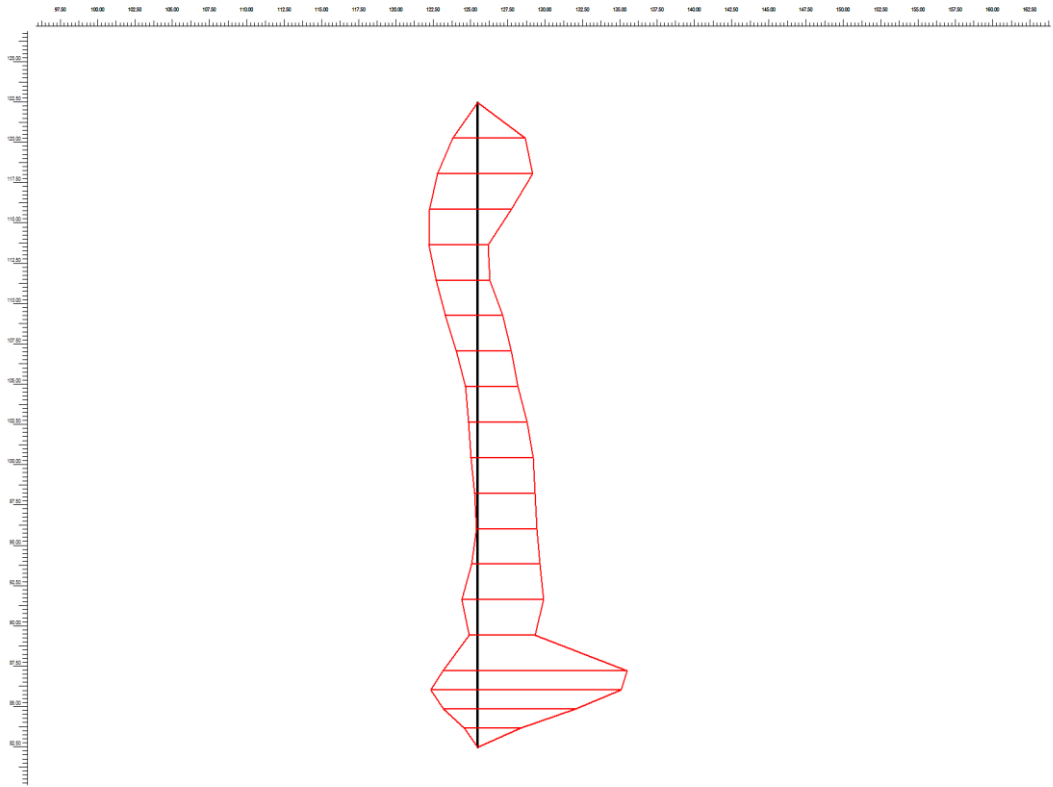


Figure C.15 Bending moment diag. of L.Prieta EQ for pile 5 ($M = 421.2 \text{ kNm/m}$).